Vacuum membrane stripping of wastewater for the production of ammonia fuel gas for solid oxide fuel cells.

From synthetic to real wastewater

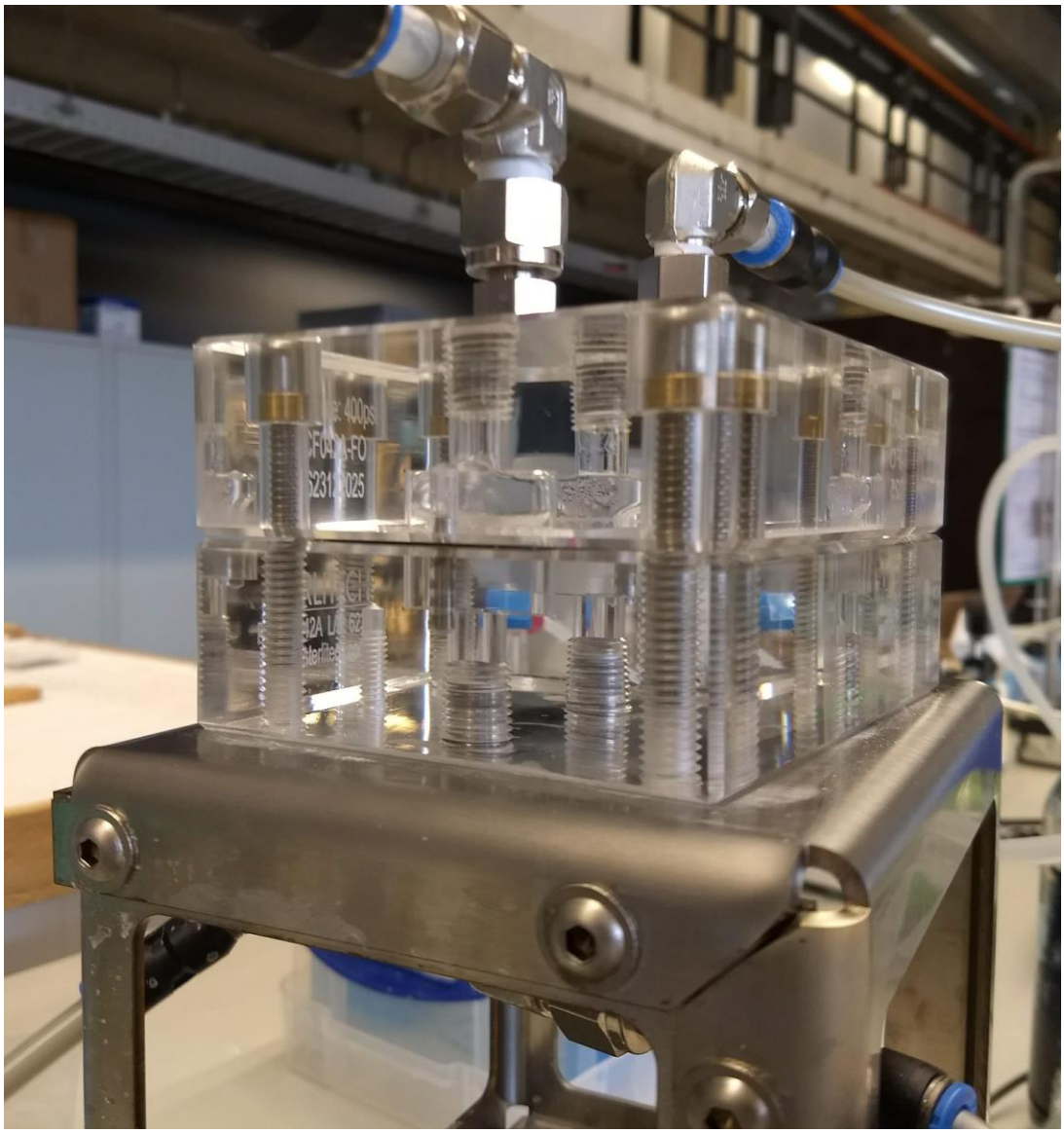

TU Delft

Lotte Kattenberg
4218981

Vacuum membrane stripping of wastewater for the production of ammonia fuel gas for solid oxide fuel cells.

From synthetic to real wastewater

By

Lotte Kattenberg

in partial fulfilment of the requirements for the degree of

Master of Science

in Civil Engineering

at the Delft University of Technology,

to be defended publicly on November 20, 2018 at 14:00 PM.

Supervisor:	Ir. Niels van Linden	TU Delft, Department of Sanitary Engineering
Thesis committee:	Prof. Dr. Ir. Jules van Lier	TU Delft, Department of Sanitary Engineering
	Dr. Ir. Henri Spanjers	TU Delft, Department of Sanitary Engineering
	Prof. Dr. Ir. Ernst J.R. Sudhölter	TU Delft, Department of Chemical Engineering
	Mr. Richard de Oude	Croda Nederland

This thesis is confidential and cannot be made public until November 20, 2019

An electronic version of this thesis is available at http://repository.tudelft.nl/.

TU Delft

Abstract

In today's industry ammonia is produced on a large scale, and is used in the production of fertilisers, cleaning products and much more. Eventually the ammonia enters our wastewater, either directly or through urine. This is then removed with conventional nitrifying-denitrifying treatment or with Anammox. That process consumes energy and does not recover the ammonia.

Therefore, the goal of the 'From Pollutant to Power' project, of which this thesis is a part, is to achieve a paradigm shift for ammonia to become an energy resource instead of a wastewater pollutant. The objective of the project is to recover ammonia and use it in a solid oxide fuel cell (SOFC) to produce energy. To do this, a vapour with at least a mass percentage of ammonia ($m\%NH_3$) of 5% is needed. The energy produced with the SOFC can then be used to cover the energy need for the extraction of ammonia. The SOFC can produce 4.2MJ·kg-N^{-1} of thermal energy and 8.4 MJ·kg-N^{-1} of electrical energy.

This study examines the use of vacuum membrane stripping (VMS) to strip ammonia from wastewater. The research objective is to go from using VMS to recover ammonia from synthetic wastewater to strip ammonia from real wastewater, in order to produce ammonia fuel for a SOFC. To accomplish this, some knowledge gaps need to be filled. First, methods need to be found that concentrate the permeate more than previously possible with the VMS to reach the desired $m\%NH_3$ in the permeate. Therefore, the effect of the cross-flow of the feed side was investigated and how to concentrate the permeate vapour with the help of condensation. Next, the effect of contaminants on the VMS process was examined by looking at the effect of salts in the wastewater and testing with real industrial ammonia-rich wastewater from amide production, which contains some organics. The final issue to consider was whether this process would be feasible in terms of energy; therefore, an energy balance was made.

Multiple experimental tests were conducted with VMS to investigate the knowledge gaps mentioned above. The selected test conditions were a minimum pH of 10 to exclude CO_2 gas transfer, and to ensure the total ammonia nitrogen (TAN) in the water was in the form of ammonia and not ammonium. For the experiments, feed solutions of ammonium hydroxide and ammonium bicarbonate were selected with a concentration of 1.5, 12 and 20 gTAN·L^{-1} with a temperature of 35°C. For the cross-flow experiments, the initial test was carried out with the Reynolds numbers 200, 300, 400, 500 and 600. From this initial test it was concluded that a Reynolds number of 200 is laminar and 500 is turbulent, and those values were used in the rest of the experiments. For the experiments with condensation, a condensation tube with cooling water of 5-10°C, 15-20°C and 25-30°C was added to the setup. Next, the composition of the industrial wastewater was investigated. In the end, the results from the different experiments were used to make an energy balance.

The results of the experiments with VMS show that turbulent flow is preferred above laminar flow, due to the increased ammonia flux and the ammonia selectivity of the membrane, which both provide a higher concentration of ammonia and more permeate. Salt (high ionic strength) will lower the ammonia flux through the membrane and the selectivity of the membrane. The condensation experiment was successful and adding a subsequent condensation step will concentrate the ammonia in the permeate vapour. Moreover, this condensation step will make it possible to recover some of the energy lost in the VMS. The experiment with the real wastewater was however not successful. The membrane fouled badly due to the organics in the water, where organics acted as surfactants and decreased the hydrophobicity of the membranes. The energy balance shows that the system would be energetically beneficial in terms of electrical energy with a concentration above 12 gTAN·L^{-1} in the solution for both ammonium hydroxide and ammonium bicarbonate, and that a concentration around

100 $gTAN \cdot L^{-1}$ from ammonium hydroxide is needed to make it energy efficient in terms of thermal energy.

More investigation is needed to be able to use real wastewater in a VMS module. For the wastewater tested in this study, stripping with VMS is not an alternative. This does not mean that other wastewater cannot be used in the VMS, therefore, other industrial wastewaters, reject water and urine should be investigated. Another possibility could be to review other stripping methods for wastewaters with relatively high contents of organics.

Acknowledgements

To be able to finish my master thesis in civil engineering with a specialisation in sanitary engineering at TU Delft I received a lot of help from different people. I would hereby like to thank a few of them.

Firstly, I want to thank Ir. Niels van Linden for giving me the opportunity to do this thesis and for his daily guidance through the struggles I encountered. He was a great source of information and was always open for a discussion on how things could be done.

Next, I want to thank Mr. Richard de Oude for being enabling me to use the wastewater from the amide production of Croda in my research, for giving me an interesting tour of the Croda Netherland, and for the useful information about the background of the water. I am also grateful that he was willing to take a position in my graduation committee and give feedback during the process.

I also want to thank the rest of my committee, Prof. Dr. Ir. Jules van Lier, Dr. Ir. Henri Spanjers, and Prof. Dr. Ir. Ernst J.R. Sudhölter for giving feedback on the thesis process at the kick off, midterm and greenlight moments. Their critical comments and suggestion helped form this thesis.

To my fellow master students Yundan and Giacomo, thanks for being there to discuss results and literature during my thesis, and for making it a bit easier by being willing to share equipment and knowledge.

Finally, I want to thank everyone that supported me during my thesis by being there for me when I needed support or to take my mind off things. Especially thanks to Nadia and Marieke for making the writing a bit easier with their presence, and for being willing to hear me out when I needed a second opinion.

Table of content

Abbreviation and symbols

δ	Membrane thickness
%cond	Percentage condensed
(aq)	Aqueous state
(g)	Gasous state
(l)	Liquid state
[i]	Activity
μ	Dynamic viscosity
A_{flask}	Surface area flask
A_m	Membrane area
amm	Ammonia
AmmBi	Ammonia bicarbonate
AmmH	Ammonia hydroxide
b	Relative change in vapour pressure compared to concentration
C_0	Initial concentration
Cd	Concentration contaminant
C_f	Concentration feed bulk
CF	Concentration factor
C_m	Concentration membrane
CO_2	Carbon dioxide
CO_3^{2-}	Carbonate
COD	Chemical oxygen demand
C_t	Concentration at time t
d	Characteristic length
d_h	Hydraulic diameter
ED	Electro dialysis
E_r	Energy feed pump
E_{va}	Energy vacuum pump
F	Filtered
g	Gravitational constant
H^+	Hydrogen ion
H_2	Molecular Hydrogen
H_2CO_3	Carbonic acid
H_2O	Water
H_3O^+	Hydronium
HCO_3	Bicarbonate
H_v	Latent heat
I	Dimensionless ionic strength
i	Component i
J	Flux
J_T	Flux total
K	Equilibrium constant
K_f	Mass transport coefficient in feed
K_m	Mass transport coefficient of the membrane
K_{ov}	Overall mass transfer coefficient
K_p	Mass transport coefficient in permeate

K_w	Equilibrium constant water
M	Molecular weight
m%	Mass percentage
$mass_{cond}$	Mass condensed
m_i	Molality
m_i^0	Standard state molality
N	Nitrogen
N_2	Molecular nitrogen
NaCl	Sodium chloride
NaOH	Sodium hydroxide
NH3	Ammonia
Nu	Nusselt number
O_2	Molecular Oxygen
OH^-	Hydroxide
Patm	Atmospheric pressure
PES	Polyethersulfone
P_f	Partial pressure in the bulk of the feed
P_{mf}	Partial pressure at the liquid feed/membrane interface
P_{mp}	Partial pressure of component at the permeate membrane surface
P_p	Partial pressure in the bulk of the permeate
Pr	Prandtl number.
P_t	Total Pressure
PVDF	Polyvinylidene difluoride
Q	Flow or Energy
Q_C	Energy freed when water is condensed
Q_T	The total heat transferred from the feed to the permeate
R	Standard gas constant
r	Mean pore radius
Re	Reynolds number
Sc	Schmidt number
Sh	Sherwoods number
SI	Saturation index
s_{mass}	Slope mass
SOFC	Solid oxide fuel cell
$SOFC_E$	Electrical energy SOFC
$SOFC_{Th}$	Thermal energy produced SOFC
T	Temperature
t	Time
TAN	Total ammonia nitrogen
T_f	Temperature in the feed bulk
T_m	Temperature at the membrane
u	Average cross flow velocity
UnF	Unfiltered
V	Volume feed
VMS	Vacuum membrane stripping

w	Water
x	Mole fraction
z_i	Charge number
α	Heat transport coefficient
β	Selectivity
γ_i	Activity coefficient
ΔH_f^{θ}	Standard enthalpy of formation
ΔH^o	Standard enthalpy change
ε	Membrane porosity
λ	Thermal conductivity
ρ	Density
τ	Pore tortuosity
P	Partial pressure

1 Introduction

1.1 Ammonia in wastewaters

Nitrogen is regarded as a pollutant in today's wastewater streams, because it can lead to excessive algae growth and eutrophication in the receiving water bodies. Total ammonia nitrogen (TAN) must therefore be removed from the water streams before releasing them into the environment.

At present this is mostly achieved with the help of biological treatment methods such as conventional nitrification/denitrification processes or Anammox, as seen in Figure 1. These methods convert the ammonium with the help of bacteria. These conventional methods have some disadvantages.

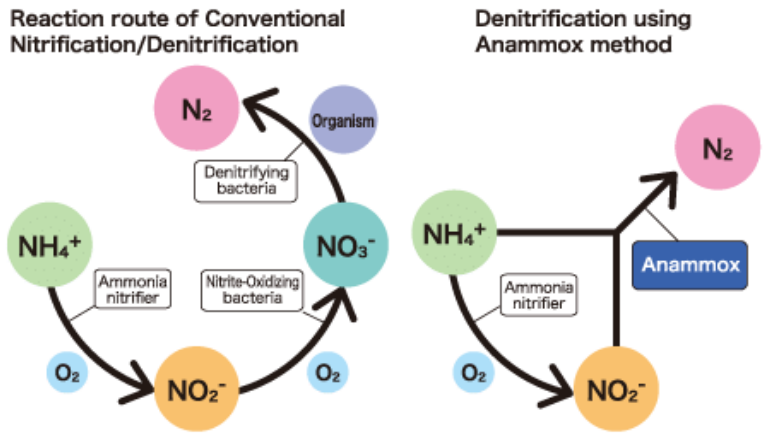

Figure 1 Overview of the Nitrification/Denitrification process and the Annamox process (Aguirre-Sierra, 2017)`

First, the nitrogen is consumed by the bacteria instead of being recovered so that it can be reused. Ammonia is used in many products such as ammonia nitrate fertilisers, cleaning products and many more. Therefore it is artificially produced on a large scale; the total production of ammonia in 2016 was 140 million tonne N (Lambot et al., 2004). Re-using some of the ammonia from wastewater would reduce the need to produce ammonia and thus save energy and resources.

Second, traditional treatment processes use energy to heat the water to temperatures optimal for bacteria, and energy for the aeration of the aerobic tank. Thus, the processes are quite energy intensive. The Annamox process uses less energy, but still has some energy usage (Gu et al., 2017).

Finally, the nitrification/denitrification processes can only remove nitrogen in streams with relatively low nitrogen concentrations and with organics present. If the concentration becomes too high, it is toxic to the bacteria and biological treatment is no longer feasible. The often-used solution is to dilute the water with other wastewaters to make biological treatment possible(Krakat et al., 2017).

1.1.1 Ammonia-rich wastewaters

For high-concentration ammonia wastewaters there are no efficient removal methods, as the conventional methods use a high amount of energy and in some cases are unable to treat the water without diluting it first. These waters are of interest as the main potential sources for ammonia fuel production with VMS. These sources are reject water, urine, and industrial ammonia-rich wastewaters. In this thesis, industrial ammonia-rich wastewaters from the production of amides will be used.

Reject water

Dewatering anaerobically digested sludge creates a wastewater that contains a large amount of nitrogen, because organic nitrogen is degraded and released into the liquid phase as ammonium and ammonia during the anaerobic digestion process. TAN concentrations of reject water differ, but generally range between 1 and 1.5 gTAN·L^{-1}. Alkalinity concentration in reject water is high, and alkalinity primarily appears in the form of bicarbonate. Other characteristics of reject water streams include the presence of salts and suspended solids, some biochemical oxygen demand, and orthophosphates. (Karwowska et al., 2016)

Urine

The amount of TAN in municipal wastewater originates to 80% from urine(Wilsenach & van Loosdrecht, 2003). Although the composition will vary, the properties and overall composition of urine are presented in literature. Urine consists of about 95% water and 5% dissolved solids, with urea and sodium chloride as primary compounds (Wilsenach & van Loosdrecht, 2003). The urea concentration in urine is typically 20 gUrea·L^{-1} and is hydrolysed and decomposed naturally within several days, resulting in a concentration of 4.9 gTAN·L^{-1} average (Jönsson et al., 1997).

Industrial ammonia-rich wastewater from amide production

Industrial ammonia-rich wastewater stems from the production of amides, where fatty acids are mixed with ammonia to produce amides. As seen in Equation 1.

$$Fatty\ acids\ +\ Ammonia \rightarrow Amides + Water \quad (1)$$

The amides are then distilled out of the solution, leaving mostly ammonia and water with some residual organics. The wastewater from this production contains a high ammonia concentration of about 100 gTAN·L^{-1}. The water also has low conductivity and contains some residual organic matter from the production.

1.1.2 From pollutant to power

This thesis is part of the project 'N2kWh- From Pollutant to Power'. The project is a cooperation between the Delft University of Technology, University of Leuven, Bioelectric, Fiaxell, HoST, Inopsys, Royal Haskoning DHV and Waternet(van Linden, 2017). The goal of the project is to create a paradigm shift concerning the removal of nitrogen, moving from nitrogen being regarded as a pollutant to it being viewed as a resource. The TU Delft section of this project strives to accomplish this by using ammonia-rich streams with low chemical oxygen demand (COD) concentration to fuel an SOFC, resulting in the production of electrical and thermal energy.

This electrical and thermal energy can then be used in the production of this same ammonia-rich fuel, thereby making the new system energy neutral or energy positive overall, instead of an energy consumer. To do this, the ammonia must be concentrated and converted into its gaseous form.

The whole process of converting ammonia into power is shown in the scheme in Figure 2. (van Linden, 2017). Depending on the water, the ammonia must first go through some pre-treatment. Then, depending on the ammonia concentration in the original water, the water undergoes a concentration step. This is most likely electrodialysis (ED), which concentrates the ammonia and increases the pH to the required levels. Then the ammonia must be stripped from the wastewater, before it can be fed into the SOFC.

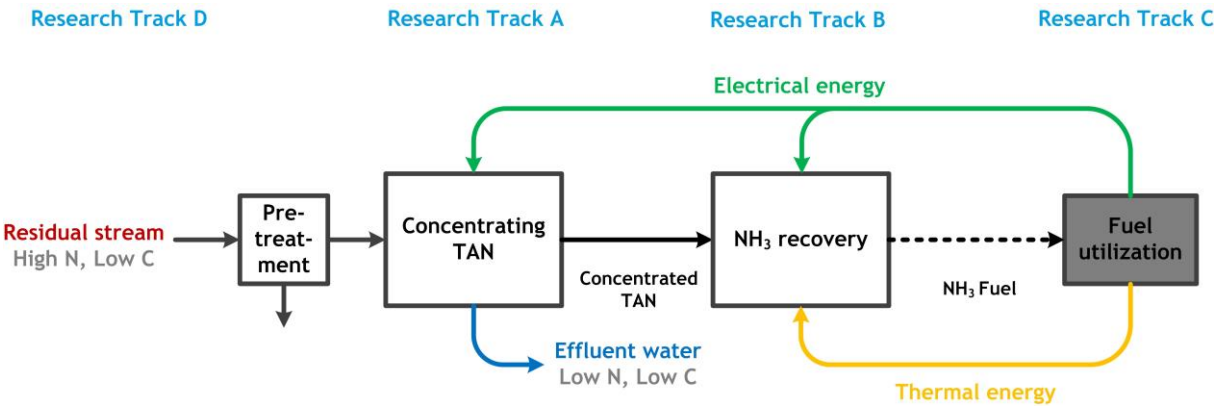

Figure 2 Project overview 'From Pollutant to Power'(van Linden, 2017)

This thesis will look at the ammonia extraction with help of VMS, and how to go from synthetic feed solutions to real wastewater in the VMS.

VMS of ammonia has already been subject to some research. Below the technologies and the previous results in this project of the three steps ED, VMS and the SOFC are discussed.

ED

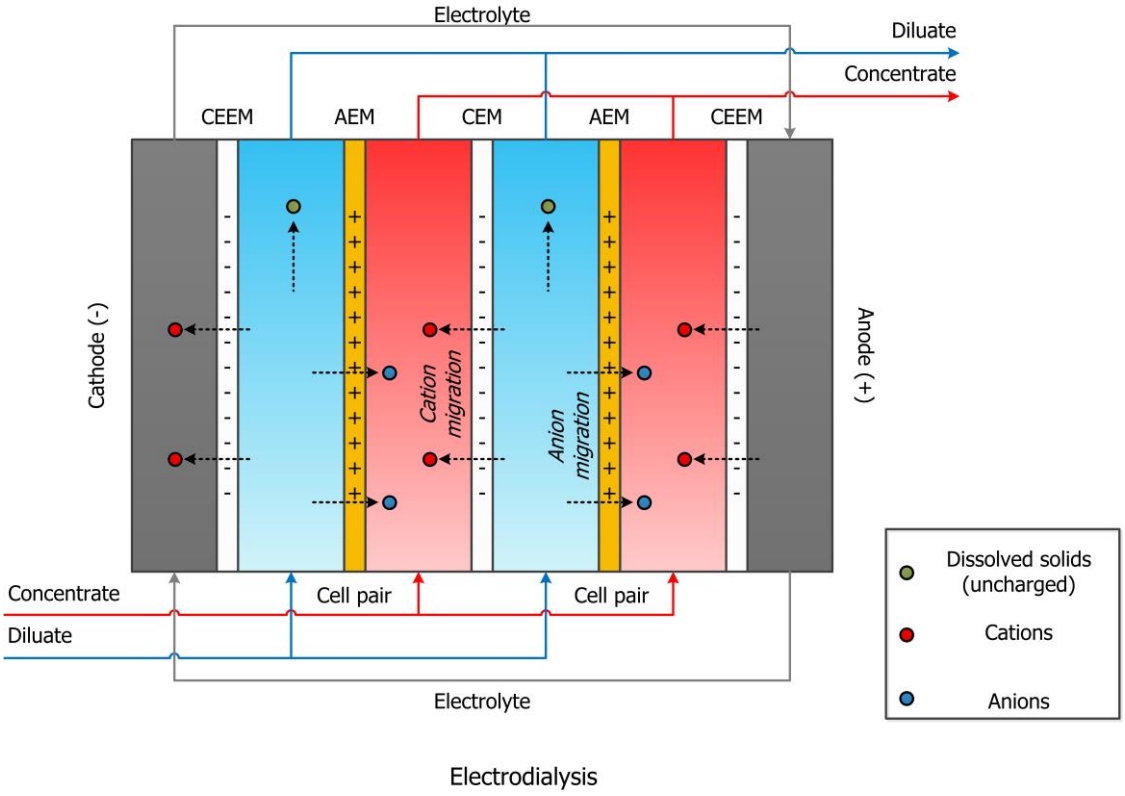

Figure 3 An overview of the stream and reaction in a regular ED module. (Spanjers, 2017)

ED is a membrane process in which ions are transported through a semi-permeable membrane, with help of a driving force of electric potential (see Figure 3). The membranes are either cation-selective or anion-selective, which means that either positive ions or negative ions are able to pass through the membrane. By placing membranes that are alternately cation- or anion-selective in a row, an ion-rich stream (the concentrate) can be derived from the water (the dilute). This can be used to collect the ammonium salt in the concentrate(Mei & Tang, 2018).

One special application is bipolar ED. Where bipolar membranes are used, this type of membrane has a cationic side and an anionic side. When an electric potential is applied to the ED cell, water is actively dissociated between the membranes. OH^- is then produced in the section next to the positively charged membrane and H^+ is produced in the section next to the negatively charged membrane. This results in the production of an acidic and an alkaline stream. Because the regular ion transfer from the dilute is still active, new chemicals can be produced and accumulated in the base and acid stream(Fernandez-Gonzalez et al., 2017). This application can be used to produce ammonia and CO_2 from ammonium bicarbonate solutions.

Previous results from the 'From Pollutant to Power' project

Some tests under the 'From Pollutant to Power' project with both regular ED and bipolar ED examined whether it is possible to concentrate ammonium and to make an alkaline waste stream with concentrated ammonia instead of ammonium. This was successful; a concentration factor of 8 was achieved for regular ED and 4 for bipolar ED. Bipolar ED also enables increase the pH of the ammonia-containing alkaline stream to above 10 without additives. These processes do however need some energy to run. Normal ED needs 3.3 to 6.8 $MJ \cdot kg\text{-}N^{-1}$ depending on the wastewater, and bipolar ED needs 10 $MJ \cdot kg\text{-}N^{-1}$. The objective is, however, to still be able to reduce the energy needed for the bipolar ED process.

VMS

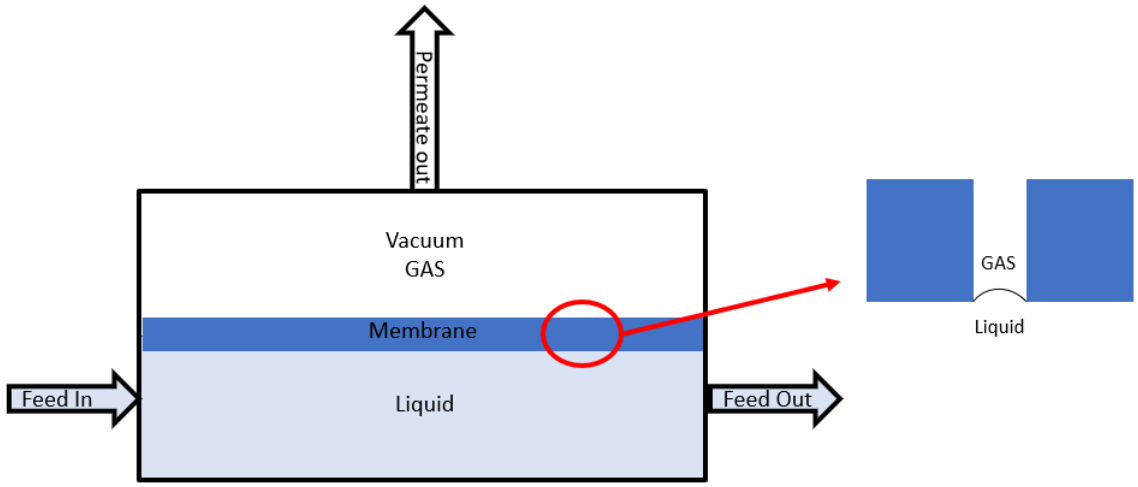

Figure 4 Illustration of a VMS module and the gas liquid interface at the membrane pores.

VMS is a variant of membrane distillation. It is a thermally driven process in which only vapour molecules are transported through porous hydrophobic membranes. On the feed side, the liquid is in direct contact with one side of the membrane, and on the permeate side the gas is in direct contact with the membrane, see Figure 4. The driving force in the vacuum membrane configuration is a vapour pressure difference between the vacuum on the permeate side, achieved with the help of vacuum pumps and the feed liquid.

Previous results from the 'From Pollutant to Power' project

This thesis builds on the work on VMS by E. Martens and N. van Linden under the 'From Pollutant to Power' project, which used synthetic wastewater to determine the influence of feed temperature and ammonia concentration on permeate quantity (flux) and quality (ammonia selectivity). Martens (2017) found that a permeate $m\%NH_3$ between 5 and 10 was obtained at temperatures of 25, 35, and 45°C for feed concentrations of 12 and 20 $gTAN \cdot L^{-1}$.

SOFC

In a fuel cell, electrical and thermal energy is derived directly from the chemical energy of fuel without an intermediate step such as combustion. This means that in general fuel cells have better energy efficiency than other conventional thermomechanical methods. SOFC have also been considered as a promising high-temperature fuel cell technology. A SOFC system operates at extremely high temperatures (600– 1,000°C). In terms of fuel input to electricity output, SOFCs are the most efficient fuel cell electricity generators currently being developed worldwide and create no CO_2 emissions, making them a great technology in the era of global warming (Stambouli & Traversa, 2002).

The operating principles of fuel cells are like those of batteries, meaning that the energy released during chemical reactions is used to generate electricity. A gaseous fuel and an oxidant gas are combined through electrodes and via an ion-conducting electrolyte. In this case, ammonia is cracked and oxidised on the anode side and oxygen is reduced on the cathode side, as demonstrated in Equation 2 and 3 and in Figure 5 (Okanishi et al., 2017).

$$2NH_3(g) \rightarrow N_2(g) + H_2(g) \quad (2)$$

$$H_2(g) + O_2(g) \rightarrow 2H_2O(g) \quad (3)$$

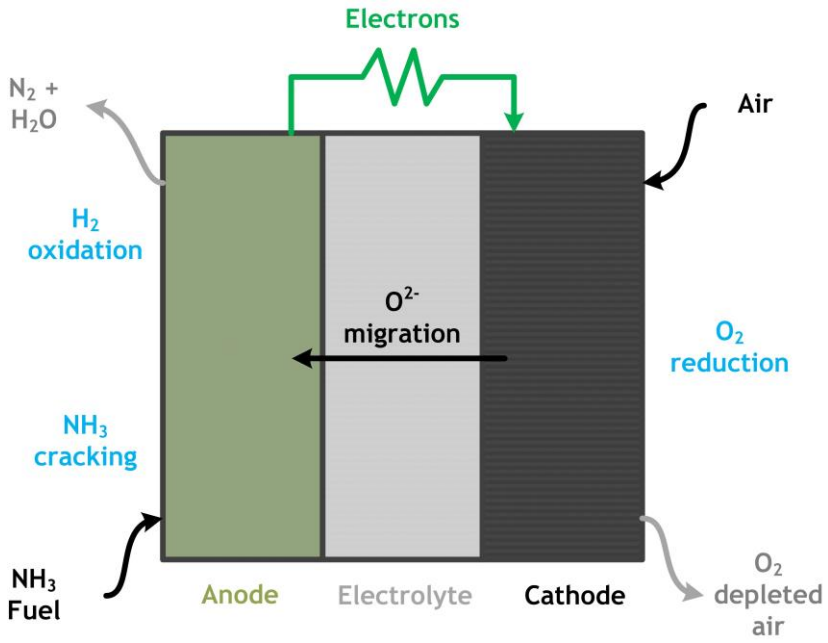

Figure 5 A schematic overview of the SOFC(van Linden, 2017)

Energy of ammonia in an SOFC

Energy Ammonia

To know the energy potential of an SOFC, first the energy potential of ammonia should be known. This can be calculated with the help of the standard enthalpy change of formation (ΔH_f^θ). "The standard enthalpy change of formation of a compound is the enthalpy change when one mole of the compound is forming its elements in their standard state at 198 K and 1 atm pressure" (Atkins & De Paula, 2006). Using Hess's law, the enthalpy of the SOFC can be calculated as seen in Equation 4.

$$\Delta H_f^\theta = \sum \Delta H_f^\theta(products) - \sum \Delta H_f^\theta(reactants) \quad (4)$$

The standard energy of a formation at 298k of the elements found in the reaction in the SOFC (Atkins & De Paula, 2006) is given in Table 1.

Table 1 The enthalpy of formation of the components present in the SOFC.

	Enthalpy of formation [kJ/mol]
NH_3	-46.11
H_20	-285.78
N_2	0
O_2	0
H_2	0

Taking Hess's law (see Equation 4) and the two reactions in the SOFC (see Equation 2 and 3):

$$\Delta H_{f\ 1}^{\theta} = \Delta H_f^{\theta}(N_2) + \Delta H_f^{\theta}(H_2) - 2 \cdot \Delta H_f^{\theta}(NH_3) \tag{5}$$

$$\Delta H_{f\ 2}^{\theta} = \Delta H_f^{\theta}(H_20) - \Delta H_f^{\theta}(H_2) - \Delta H_f^{\theta}(O_2) \tag{6}$$

Filling in the values from Table 1 into Equation 5 and 6 gives:

$$\Delta H_{f\ 1}^{\theta} = 0 + 0 - 2 \cdot (-46.11) \tag{7}$$

$$\Delta H_{f\ 2}^{\theta} = 2 \cdot (-285.78) - 0 - 0 \tag{8}$$

Combining the two energy of formation gives the total energy as seen in Equation 9:

$$\Delta H_{f\ T}^{\theta} = \frac{(2 \cdot 46.11 - 2 \cdot 285.78)}{2} = -239.7 \tag{9}$$

This means that 239.7 KJ·mol^{-1} is the maximum energy potential per mol of ammonia put into the fuel cell. This equal to 14.0 MJ·Kg-N^{-1}.

Energy SOFC

The 239.7 KJ·mol^{-1} freed is not all directly converted to useful energy. According to studies by Stambouli and Treversa (2002), an SOFC can recover 90% of the energy from the ammonia, including heat. The recovered electrical heat is however 45-60%, according to the same study. Another study by Dekker and Rietveld (2005) states a higher electrical recovery of 52-70%. Taking the maximum overlap of the two studies, 60% of the energy in ammonia can be used for electricity production and 30% is converted to useful heat. This gives 8.4 MJ·Kg-N^{-1} of electrical energy and 4.2 MJ·Kg-N^{-1} of thermal energy produced (see Appendix D).

Previous results 'From Pollutant to Power' project

A test conducted in the project showed that m%NH_3 of the feed of the SOFC has to be above 5% to be able to use the SOFC to produce energy. The above-mentioned energy of 8.4 MJ·K-N^{-1} of electrical energy and 4.2 MJ·Kg-N^{-1} of thermal energy is based on what is reached in literature. However, some tests conducted inside the project itself still have to succeed. In the 'Form Pollutant to Power' project with a feed with 5 m%NH_3, only 4.5 MJ·kg-N^{-1} of electrical energy could be produced. However, in this thesis, the 8.4 MJ·K-N^{-1} of electrical energy and 4.2 MJ·Kg-N^{-1} of thermal energy will be used

1.3 Research plan

1.3.1 Problem description

The goal of this thesis was to improve the understanding of the mechanisms of mass transport of water and ammonia in VMS and to build on previous results in this project and move from using synthetic water to real wastewater in the VMS to strip ammonia gas for energy production in an SOFC. However, first some more research was necessary.

Firstly, the mas transport mechanism where researched. This was done by looking at the effect of cross-flow velocity in the VMS and the effect of ionic strength of the feed solution. By increasing the understanding of the VMS the hope is to be able to improve the ammonia fuel made.

Also, the system with only VMS does not concentrate the feed solution of 1-1.5 $gTAN \cdot L^{-1}$ to the required 5%mNH_3 that is needed in SOFC. Consequently, it is not possible to make fuel directly from the lowest-value wastewater that could be interesting to use, namely reject water from aerobic sludge reactors. Hence, it is interesting to look at options to improve the VMS system further.

Another important part of going from synthetic wastewater to actual wastewater is that extra contaminants are added to the water. This can lead to a change in the efficiency of the VMS due to polarisation effects and fouling. The effect of polarisation and fouling will be investigated.

The last thing that needs to be covered before actual wastewater can be used in the VMS is to make the energy balance. In theory, one of the biggest advantages of this system is that it could produce energy. Therefore, it is essential to see if this would also be the case in practice with the actual wastewaters available, and whether this can be achieved based on the results obtained.

1.3.2 State-of-the-art

There is some research on the effect of different conditions on the efficiency of VMS, and on how to optimise the system. Below this research is summarised:

Effect of Temperature

Much research has been conducted on the effects of the temperature of the feed solution on the performance of VMS. It is agreed that increasing the temperature increases the flux of water and ammonia (EL-Bourawi et al., 2007; You et al., 2014) and decreases the overall mass transport coefficient (K_{ov}) (Ding et al. , 2006; He et al., 2018) , but lowers the selectivity of ammonia (Ding et al., 2006; El-Bourawi et al., 2007; He et al., 2018; You et al., 2015; You et al., 2014), which means that a choice must be made between high fluxes and high selectivity. To read more about selectivity, fluxes and the mass transport coefficient see Section 2.3.3.

Research completed earlier in the 'From Pollutant to Power' project suggests that a temperature of about 35°C is optimal for ammonia extraction because the decrease in mass% in the permeate is minimal between 25°C and 35°C, but the total flux increases significantly, as seen in Figure 6 and 7 (Martens, 2017).

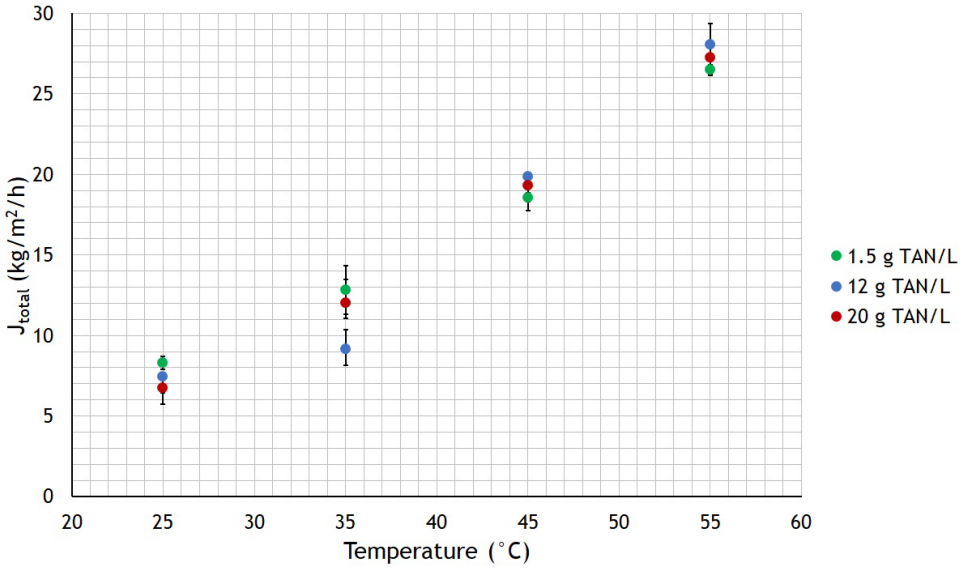

Figure 6 The total flux through the membrane of the VMS at different feed temperatures. (Martens, 2017)

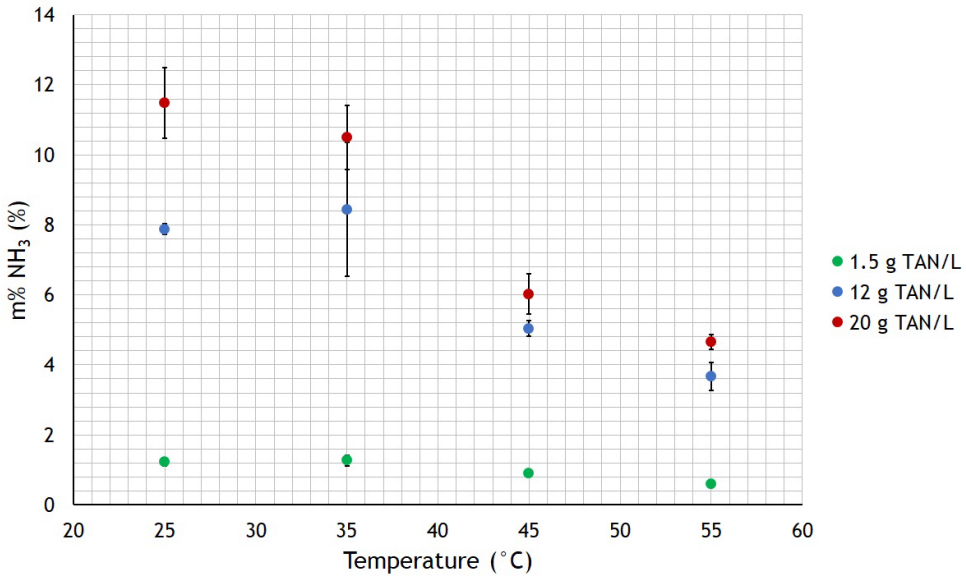

Figure 7 The m%NH_3 at different feed temperatures. (Martens, 2017)

Effect of feed ammonia concentration

Research results have been contradictory when it comes to the effect of feed concentration on K_{ov}, flux and selectivity. The study by El-Bourawi et al. (2007) indicates that the total flux will increase, the study by You et al. (2014) found the total flux to lower with concentration, and the study by He et al. (2018) indicates it to remain the same. The flux of ammonia increases due to a higher driving force as a result of the higher concentration. It appears that concentration has little or no effect on the K_{ov} (El-Bourawi et al., 2007). Mixed results were found on selectivity; the study by El-Bourawi et al. (2006) found it to remain the same, while the study by Ding et al. (2006) found a decrease of selectivity over feed concentration.

This was also previously tested in the 'From Pollutant to Power' project. No significant effect of feed concentration on the total flux was found (see Figure 8). The selectivity of the VMS is, however, higher at a lower concentration, as seen in Figure 9 (Martens, 2017).

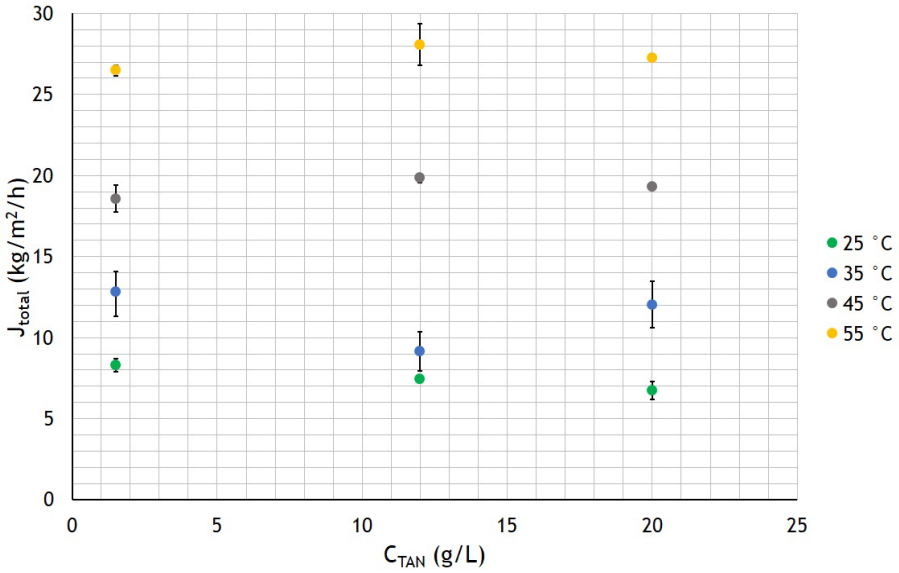

Figure 8 Total flux over concentration TAN in feed solution (Martens, 2017).

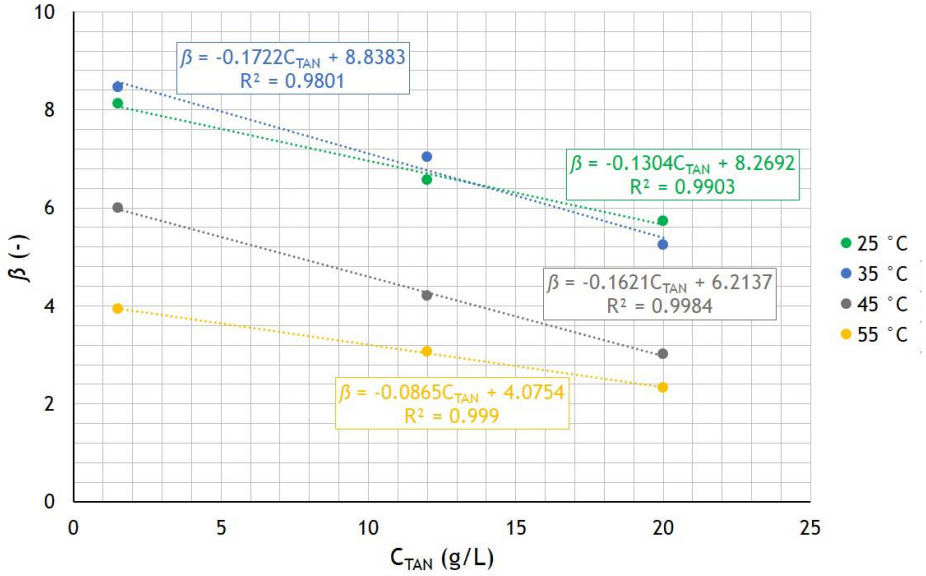

Figure 9 Selectivity over TAN concentrations feed solution (Martens, 2017)

Effect of pH

The pH influences the equilibrium concentration between different species in the water (see Section 2.1). The two most important equilibria to consider for the consideration of the pH in the VMS is the one of TAN in water and the one of total inorganic carbon (TIC) in water. This is because in the VMS the ammonia is stripped while the ammonium remains in the feed, and at low pH, the TAN in the water will be in the form of ammonium. Also, CO_2 competes with the ammonia in passing through the membrane. CO_2 should therefore also be avoided in the feed. In research this is confirmed by evidence that higher pH leads to higher ammonia flux (He et al., 2018), higher K_{ov} (Ding et al., 2006; EL-Bourawi et al., 2007; He et al., 2018; W. T. You et al., 2014) and higher selectivity (Ding et al., 2006; El-Bourawi et al., 2006; He et al., 2018). What will happen with the total flux is unknown.

Effect of cross-flow velocity

Higher cross-flow velocity can lower the effect of polarisation by working in a turbulent scheme (see Section 2.3.4). Operating at a turbulent flow will lead to better mixing of the fluid in the flow cell and

reduce polarisation effects. This increases the total flux and the K_{ov} of the membrane; it is, however, unclear how it affects selectivity.

Research confirms that flux and K_{ov} increase with higher cross-flow velocities (Ding et al., 2006; El-Bourawi et al., 2007; He et al., 2018; W.-T. You et al., 2015; W. T. You et al., 2014). However, opinions are more divided on how this affects selectivity. Some studies report that the selectivity increases (Ding et al., 2006; El-Bourawi et al., 2007), but other articles suggest that it will not change with a change in cross-flow (W. T. You et al., 2014) or even decrease (He et al., 2018).

Effect of salt
The effect of salt in VMS is not described in literature. Some information was however found on the effect of salt on the different mechanism in the VMS, see Section 2.2.

1.3.3 Research objectives

To complete the current knowledge on the mass transport mechanisms of water and ammonia in the VMS, it was necessary to identify the remaining knowledge gaps. Also some research has to be done to be able to move from synthetic wastewater to real waste water. To achieve this objective the following research questions were addressed:

Effect of cross-flow velocity
Most parameters that could optimise the VMS have already been extensively researched. The only uncertain parameter is the cross-flow in the VMS module at the feed side. Section 2.3.4 explains that the cross-flow velocity of the feed can influence the polarisation effects at the feed side, and thus the mass and heat transport from the feed to the permeate. However, it is unclear how much this influences the flux, and if this may influence the selectivity.

Research question
What cross-flow velocity is preferable in terms of flux and selectivity?

Effect of Salt
Some sort of wastewaters such as reject water and urine contain a high amount of salt, it is therefore interesting to know what effect salt has on the VMS process. No information could be found on the effect of salt on the VMS. In Section 2.2.1 different effects of salt addition are discussed. Three main effects are identified: salting-out effect, changes in equilibrium, and polarisation. How they influence the VMS result is unclear, as they may influence each other. It would therefore be interesting to know how the addition of salts affects vapour pressure and the selectivity of ammonia and water in the VMS process.

Research questions
What effect does ionic strength have on the vapour pressure of dissolved ammonia?

How does the salt concentration in the feed water affect the ammonia selectivity?

Condensation of permeate vapour
Condensation of the permeate vapour can be interesting, as theory suggests that it may concentrate the ammonia in the vapour (see Section 2.4); another benefit is that the energy freed from the condensation of the permeate can be used to heat the feed. Therefore, this study looks more closely at how partly compensating the permeate vapour would affect the permeate quality.

Research questions
Will only water condensate from the permeate vapour mixture of VMS, or will ammonia diffuse into the condensate?

To what extent will ammonia in the permeate vapour mixture of VMS be concentrated with the condensation of permeate vapour?

What is the lowest TAN concentration of feed water that reaches the goal of 5m%NH_3 in the permeate to make ammonia fuel for SOFC with the VMS + condensation?

Membrane fouling

One of the biggest changes in going from real to synthetic water is the presence of other components in the water, which can influence the VMS. The effect of salt is already mentioned, but other compounds can also foul the membrane. Different fouling mechanisms are explained in Section 2.5. It would be interesting to research which components can foul the membrane, how they influence the performance of the VMS, and if they negatively affect the VMS when using ammonia-rich industry water from amide production.

Research questions

What compounds found in wastewater can lead to fouling of the membrane, and how can this be avoided?

What is the effect of the fouling components on the water and ammonia flux?

How does fouling affect the selectivity of the membrane for ammonia?

How does the cross-flow velocity influence fouling?

Energy requirements for stripping

The last issue to research before the VMS was be used on actual wastewater was if it is energetically feasible to use the VMS. If the system needs high energy input to run, it would not be able to produce more energy than needed, and more conventional treatments may be a better option. Hence, it was essential to create an energy balance of the system and to optimise it in a way that it uses the least amount of energy per kg of ammonia removed possible.

Research questions

In terms of energy, is it possible to use VMS in combination with an SOFC to produce energy?

When is extracting more ammonia no longer feasible in terms of energy and fuel restrictions of the SOFC (m%NH_3)?

How does cross-flow velocity influence energy consumption?

Considering energy, material cost, selectivity and fouling, is there an optimum cross-flow velocity?

1.3.4 Approach

Experimental approach

To be able to answer the question presented above, a combination of theory, PHREEQC simulations and experiments were used. The experimental part consisted of experiments with the VMS with synthetic and real wastewater and analysis of the real waste water and the membrane. The experiments were performed in the Waterlab of TU Delft.

Outline

The report is divided into multiple parts:

Section 1 Introduction: Describes the problem, introduces the state-of-the-art knowledge, and presents a research plan.

Section 2 Theoretical background: Introduces the different parameters and mechanisms present in the study.

Section 3 Methods and materials: Describes the experimental approach in detail.

Section 4 Results: Presents and analyses the results from the experiments.

Section 5 Discussion: Discusses the strengths and weaknesses of the study.

Section 6 Conclusion: Elaborates upon what can be concluded from the study, and on how the different research questions were answered.

Section 7 Recommendations for further research: Identifies the remaining knowledge gaps that should be investigated further in continuous research.

2 Theoretical background

The next section examines different theories, parameters and mechanisms that need to be understood to implement this study.

2.1 The chemical equilibria in ammonia-rich wastewaters

Different equilibria reactions occur in water; these reactions need to be understood to be able to say something about the composition of the wastewater. This section is largely based on the book Chemistry by Housecrofts & Constable,(2010)

2.1.1 How equilibria work

Most reactions are an equilibrium of a forward and a backward reaction taking place simultaneously when exposed to a mixture of products and reactants. An example of an equilibrium reaction is given in Equation 10.

$$aA + bB \leftrightarrow cC + dD \tag{10}$$

Where A and B are reactants and C and D are products, a, b, c and d are integers indicating the mole ratios. This equilibrium will remain constant until something in the system changes. Then Le Chatelier's principle applies: "When an external change is made to a system in equilibrium, the system will respond so as to oppose the change". This means that if more of one product or one reactant is added to the system, the system will counteract this by moving the equilibrium in the opposite direction. The equilibrium of a reactant can be quantified with the use of an equilibrium constant (K) (see Equation 11)

$$K = \frac{[C]^c[D]^d}{[A]^a[B]^b} \tag{11}$$

Where [i] is the activity of the compound i. Activity is often seen as equal to molality. This holds for dilute solutions, however with stronger solutions the activity has to be determined. The activity is given in equation 12.

$$[i] = \gamma_i \cdot \frac{m_i}{m_i^o} \tag{12}$$

Where γ_i is the activity coefficient, m_i the molality and m_i^0 standard state molality. m_i^0 is often defined as 1 and the equation can be reduced to:

$$[i] = \gamma_i \cdot m_i \tag{13}$$

The activity constant can be calculated with the extended Debye-Huckle law (Atkins & De Paula, 2006), as seen in Equation 14.

$$\log \gamma_i = \frac{-Az_i^2\sqrt{I}}{1 + B\sqrt{I}} - CI \tag{14}$$

Where A, B and C are dimensionless constants, z_i is the charge number of the ion i, I is the dimensionless ionic strength and is given in Equation 15.

$$I = \frac{1}{2}\sum m_i z_i^2 \tag{15}$$

K is also temperature-dependent given the relation shown in Equation 16.

$$\ln K = -\frac{\Delta H^o}{RT} + c \quad (16)$$

Where ΔH^o is the standard enthalpy change of a reaction, R is the gas constant, T is the temperature and c is a constant. This means that in an exothermic reaction the number of products will increase with temperature, while in an endothermic reaction the number of reactants will increase.

2.1.2 The self-ionisation of water

Water itself is ionised to a small extent and H_2O is divided into equal parts of H^+ and OH^- ions (see Equation 17).

$$H_2O \leftrightarrow H^+ + OH^- \quad (17)$$

The equilibrium of water lies far to the left side, and almost no ions are present in pure water. The equilibrium constant of ionising of water (K_w) is shown in Equation 18.

$$K_w = \frac{[H^+][OH^-]}{[H_2O]} \quad (18)$$

This reaction is an exothermic reaction, meaning that with increasing temperature more ions will be formed.

2.1.3 TAN equilibrium

Ammonia and ammonium exist in equilibrium with each other in water as given in Equation 19.

$$NH_4{}^+(aq) + OH^-(aq) \leftrightarrow NH_3(aq) + H_2O(l) \quad (19)$$

This gives an equilibrium constant of the equilibrium as shown in Equation 20.

$$K = \frac{[NH_3][H_2O]}{[NH_4^+][OH^-]} \quad (20)$$

This equilibrium reaction is exothermic, meaning that increasing the temperature will increase the ammonia concentration compared to the ammonium concentration.

Also, due to the reaction including OH^- it is pH-dependent, increasing the pH; hence increasing the amount of OH^- in the water will push the reaction towards the right and increase the ammonia concentration. The effect of pH on the ammonia/TAN ratio was simulated with PHREEQC as seen in Figure 10. It shows that for a pH of 10 the ratio is arund 90% for temperatures above 35°C.

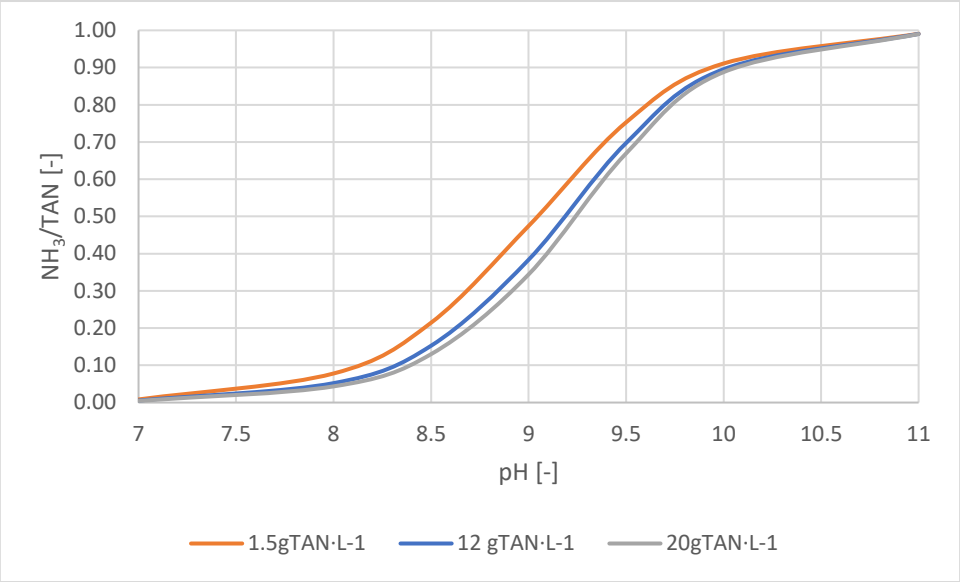

Figure 10 Effect of pH on relation between NH_3 and TAN at 35°C made with PHREEQC

2.1.4 Total inorganic carbon equilibrium

The equilibrium reaction of total inorganic carbon (TIC) is a bit more complicated as it contains four states instead of two (see Equation 21).

$$CO_2(aq) + H_2O(l) \leftrightarrow H_2CO_3(aq) \leftrightarrow H^+(aq) + HCO_3(aq) \leftrightarrow 2H^+(aq) + {CO_3}^{2-}(aq) \qquad (21)$$

The higher the pH the more the equilibrium will shift to the right. Increasing the pH would remove H^+ from the solution, as the solution would want to counteract this due to Le Chatelier's principle, the equilibrium point would move to the right to increase the H^+ concentration. The effect on the TIC equilibrium is shown in Figure 11. It demonstrates that with a pH of 8 or higher, no CO_2 should be found in the solution.

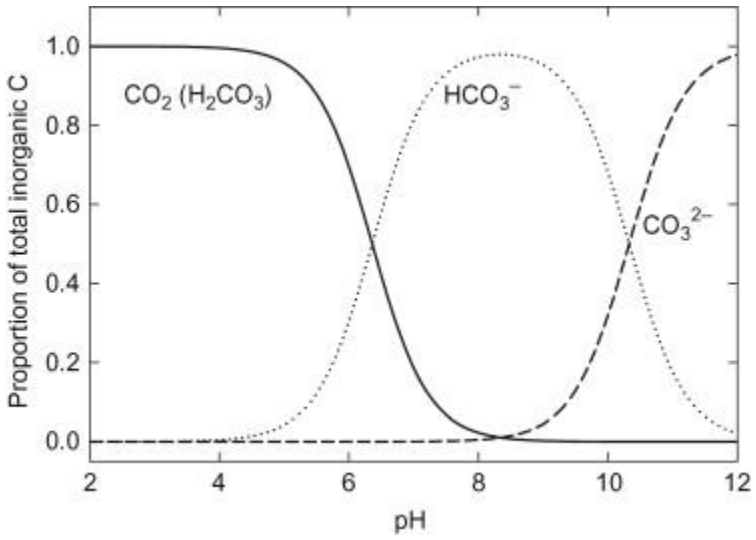

Figure 11 Effect of pH on the TIC equilibrium (Dodds & Whiles, 2010)

2.1.5 Dissociation of fatty acids

When fatty acids are dissolved in water, a fatty acid generates the following equilibrium:

$$HA + H_2O = H_3O^+ + A^- \qquad (22)$$

where HA is the standard fatty acid and A the dissociated fatty acid. This relation is however strongly pH-dependent, and the reaction will shift to the right in alkaline conditions, increasing the amount of dissociated acid in the water (Priyananda & Chen, 2006).

However, dissociated acids are more polar than undissociated acid due to the added charge, making them more hydrophilic. This means that the solubility of fatty acids increases along with the pH (Brinck et al., 2000).

2.2 Vapour pressure in water

Vapour pressure in water is dependent on the composition of the water. This section discusses the effect of concentration of vapour pressure and the effect of salt. This is important, as it will say something about how the driving force and thereby the flux in the VMS will react with different water compositions.

2.2.1 Effect of concentration

The vapour pressure of one component in the liquid is dependent on the mole fraction present in that component. For an ideal solution the behaviour can be explained with Raoult's law, as seen in Equation 23.

$$p_i = x_i \cdot p_i^{\circ} \tag{23}$$

Where p_i is the partial pressure of component i, x_i the mole fraction of component i and p_i° is the vapour pressure of the pure component i.

For an ideal dilute solution, however, the vapour pressure of the solute follows Henry's law, as seen in Equation 24.

$$p_i = x_i \cdot K_i \tag{24}$$

Where K_i is Henry constant for component i.

Most solutes will behave somewhere in-between Henry's law and Raoult's law (see Figure 12). However, it can be concluded that the vapour pressure of the components in a liquid is dependent on the concentration of the solution.

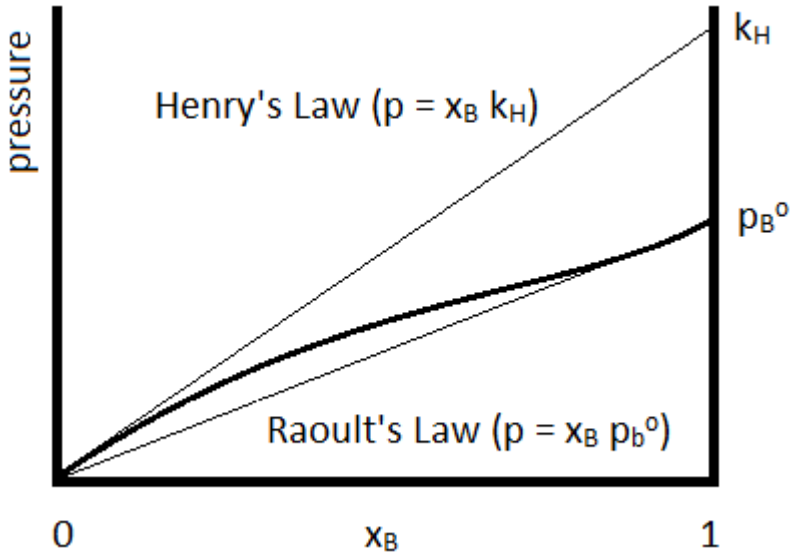

Figure 12 Illustration of relationship between vapour pressure and the mole fraction of the solution. Illustrating Henry's law Raoult's law and non-ideal solution.

2.2.2 Effect of salt concentration

When salt is added to the feed solution, different effects occur. The vapour pressure of water and ammonia in the feed changes, a polarisation layer due to accumulation (see Section 2.3.4) is created at the membrane surface, and the solution feels the salting-out effect. This means that the fluxes of

water and ammonia and the selectivity of ammonia are influenced by the amount of salt in the wastewater.

Effect on the partial pressures of ammonia and water

Adding salt to the feed solution will reduce the vapour pressure of the water, lowering the driving forces. This means that less water passes through the membrane, which lowers the water flux. Also, will increasing the ionic strength of the solution move the ammonia equilibria from ammonia to ammonium. Decreasing the ammonia concentration(Johansson & Wedborg, 1980).

Salting-out effect

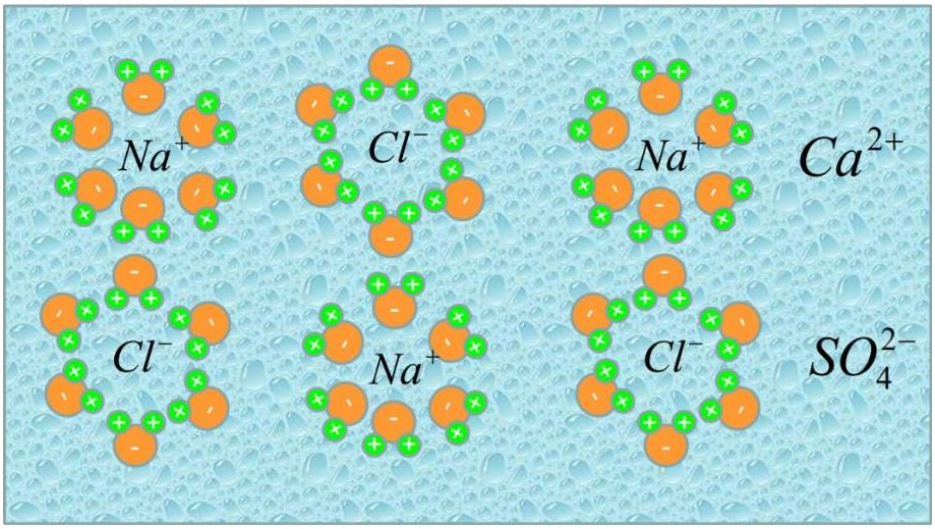

Figure 13 Illustration shielding at high salt concentration (van Breukelen, 2016)

The salting-out theory suggests that by increasing the salt concentration in a water solution, the solubility of nonelectrolytes or weak electrolytes will decrease in the presence of strong electrolytes (Görgényi et al. 2006; Masterton & Lee, 1970). Ammonia, being a weak electrolyte, will therefore have a lower solubility in the presence of a strong electrolyte like NaOH or salt than it will have in pure water. This is because at high ionic strength, the water will start to act as a shield for the ions and less water is free to be available as a solvent, see Figure 13 (van Breukelen, 2016). This may lead to higher ammonia vapour pressure due to it being less soluble (Helmenstine, 2014); when the ionic strength increases beyond a certain point the activity will increase instead of decrease.

Polarisation due to accumulation

Polarisation due to accumulation, as explained in Section 2.3.4, increases the salt concentration at the surface of the membrane. This increases the effect of the salting-out and the partial pressure on water and ammonia at the surface of the membrane. It may also have an effect on other polarisation effects and fouling.

2.2.3 PHREEQC simulations

To be able to say something about the effect of salt and ammonia concentration on the performance of the VMS, the effect of salt and consecration on the vapour pressure were simulated. This was done with simulations in PHREEQC, which includes all effects on the vapour pressure.

Effect of ionic strength on water vapour pressure

Firstly, the effect of ionic strength on the vapour pressure of water was simulated with PHREEQC to show how salts lower the vapour pressure. Figure 14 presents the vapour pressure of water as a function of ionic strength due to NaCl addition. Evidently, more salt increases the ionic strength and therefore reduces the vapour pressure of water.

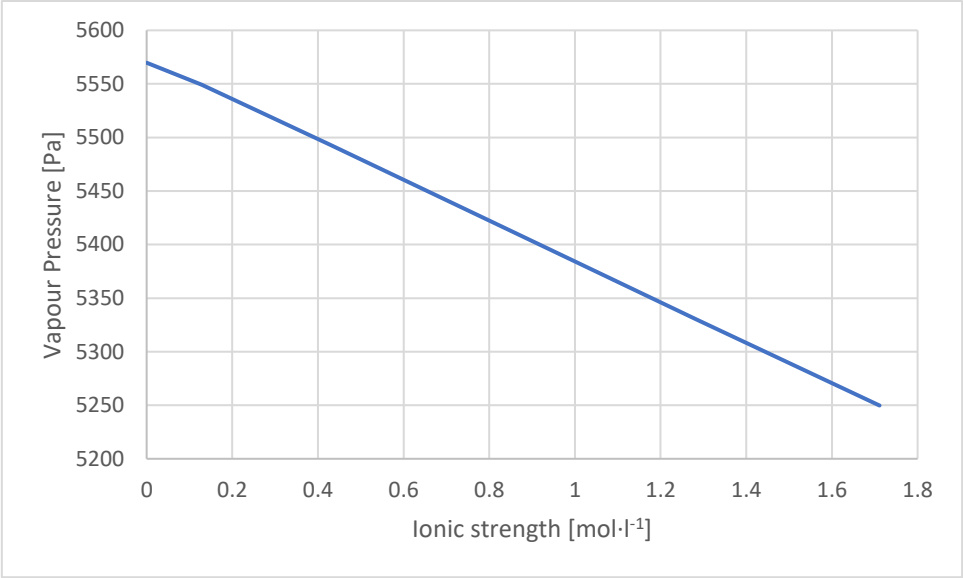

Figure 14 Vapour pressure of water over ionic strength

Vapour pressure of ammonium hydroxide versus ammonium bicarbonate

To investigate the effect of salt on the vapour pressures of ammonia, the difference between the vapour pressures of ammonium hydroxide and ammonium bicarbonate solutions were simulated with PHREEQC. Where ammonium hydroxide has a low ionic strength and ammonium bicarbonate has a high ionic strength. The purpose of the simulation was to know whether the change of vapour pressure in the bulk is the reason for the difference in performance with high ionic strength compared to low ionic strength, or if other effects play a role.

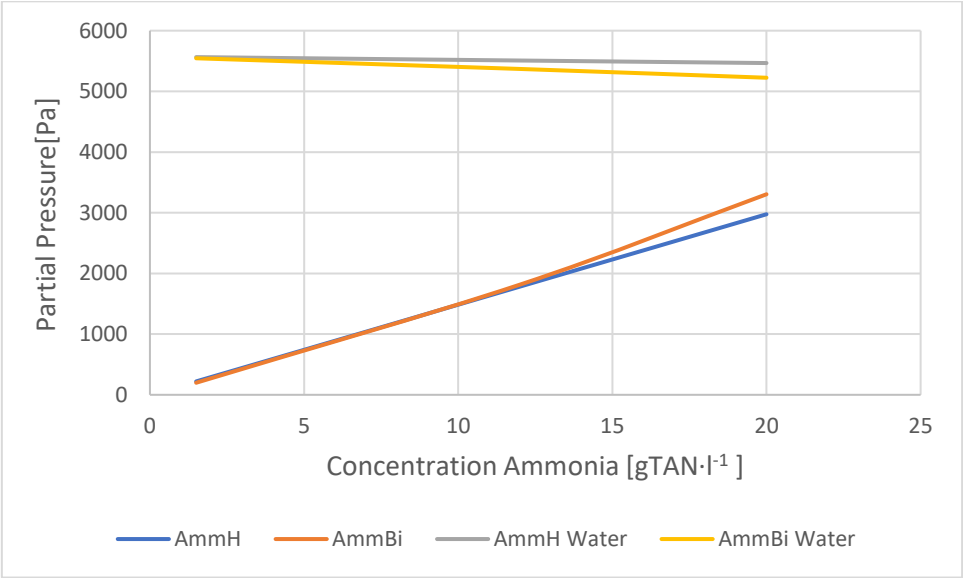

Figure 15 Partial pressure for water and ammonia for ammonium hydroxide and ammonium bicarbonate feed solutions at different concentrations.

The results of the simulation are shown in Figure 15. It reflects a decreasing trend in the vapour pressure of water for both solutions, with the ammonium hydroxide solution decreasing more slowly than the ammonium bicarbonate. This result was expected, as ammonium bicarbonate has a higher ionic strength than ammonium hydroxide at the same TAN concentration, and should therefore have a lower vapour pressure.

As for ammonia vapour pressure, the pressure for ammonium hydroxide was initially higher than for ammonium bicarbonate, but the ammonium bicarbonate later surpassed that for ammonium hydroxide. This finding is explained by the salting-out effect (see Section 2.2.1).

2.3 Vacuum membrane stripping

To facilitate the understanding of the reasons behind the different results and how the underlying mechanism works, the different parts and mechanisms in the VMS are presented below.

2.3.1 Hydrophobic membranes

In the VMS the liquid on the feed side must not penetrate the dry pores of the membrane, therefore a hydrophobic membrane is used. The hydrophobicity of the membrane prevents the liquid feed from entering the pores, as it rejects water. This is possible as water molecules like to form hydro bonds, and due to the hydrophobic surface being non-polar the water molecules will minimise the contact with the surface to make as many hydro bonds as possible. Hereby the surface of the membrane expels the liquid water, separating the liquid feed phase and the gaseous vapour phase. This results in a liquid/vapour interface at the entrances of the membrane pores, which can only be entered by gaseous molecules that migrate to the permeate (Barnes & Gentle, 2005; Khayet & Matsuura, 2011).

2.3.2 Hydraulics of the VMS flow cell

The hydraulics of a channel is determined by its flow regime, which can generally be divided into three flow regions: fully laminar flow, transition flow, and fully turbulent flow. Laminar flow occurs when there is almost no mixing in the channel, and turbulent flow occurs when the channel is almost perfectly mixed; everything in-between is transition flow. Having a turbulent flow may lower the effect of polarisation, which is explained in Section 2.3.4.

The Reynolds number can be used to describe the flow regime of the channel. The Reynolds number is given in Equation 25.

$$Re = \frac{\rho \cdot u \cdot d_h}{\mu} \tag{25}$$

The ρ is the water density of the solution, u is the average cross-flow velocity, d_h is the hydraulic diameter, and μ is the dynamic viscosity of the solution. The water's dynamic viscosity and density is temperature-dependent. Changing the flow in the membrane cell can, in turn, change the average cross-flow velocity, and the hydraulic diameter is dependent on the geometry of the channel. To learn more about the hydraulic diameter of the membrane cell, see Appendix A.

A spacer is commonly used to increase the mixing and ensure turbulent flow in the membrane. This changes the hydraulics of the membrane cell, since the membrane cannot be described using open channel theory. Therefore, the transition of different flow regimes differs from open channel flow, and requires a separate description. Mojab et al. (2014) documented the division of flow regimes as a function of the Reynolds number for spacer flow, and presented various flow regimes for a spacer-filled channel. They found that laminar flow occurs for a Reynolds numbers below 250, transition flow occurs between Re 250 and 500, and turbulent flow occurs where the Reynolds number is greater than 500. Figure 16 demonstrates that with a Reynolds number of 200 no mixing occurs and that the flow is increasingly mixed, approaching a Reynolds number of 500, where the flow is close to fully mixed. Not much changes between the Reynolds numbers 500 and 1,000.

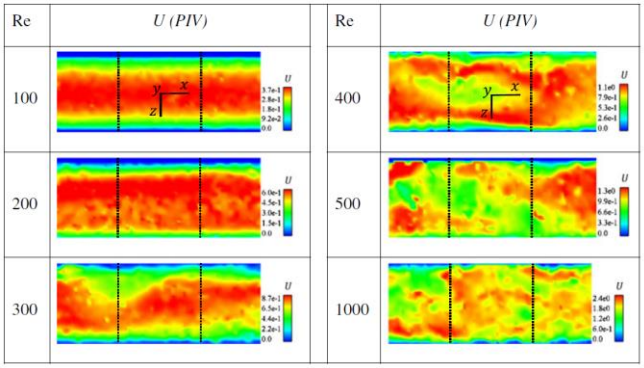

Figure 16 Hydraulic patterns for various Reynolds numbers (Mojab et al., 2014)

2.3.3 Transport mechanism in the VMS module

Different transport mechanisms occur in the membrane module as mass and heat are transferred from the feed to the permeate.

Heat transport

Heat is transported from one side of the membrane to the other by way of a phase change from liquid to gas. This is caused by the water being transported as a vapour, rather than a liquid, through the membrane. The total heat transferred from the feed to the permeate can then be calculated by Equation 26 (Q_T) (El-Bourawi et al., 2006; Khayet & Matsuura, 2011).

$$Q_T = \sum_{i=1}^{n} J_i H_{v,i} \tag{26}$$

Here $H_{v,i}$ is the latent heat coefficient of component i and J_i is the flux of component i. No other effect of other heat mechanisms in the membrane cell or heat loss through the membrane is indicated in the literature (Khayet & Matsuura, 2011).

Mass transport

In VMS, the driving force is maintained by applying a continuous vacuum at the permeate side (below the equilibrium vapour pressure). In the case of mass transport of a single component, i, through the membrane, the flux (J_i) is written as shown in Equation 27 (Bandini et al., 1992; Khayet & Matsuura, 2011).

$$J_i = K_{m,i}\left(P_{mf.i} - P_{mp,i}\right) \tag{27}$$

Here $K_{m,i}$ is the mass transport coefficient of the membrane for component i, $P_{mf,i}$ is the partial pressure of component i at the liquid feed/membrane interface, and $P_{mp,i}$ is the partial pressure of component i at the permeate/membrane interface.

The mass transport mechanisms through porous and hydrophobic membranes in VMS are mostly described by the Knudsen flow model, because the membranes for the VMS process should have small pore sizes in order to avoid wetting when in contact with feed solutions, which are often aqueous solutions of organic liquids with low surface tension (Khayet & Matsuura, 2011). According to the Knudsen flow model, the $K_{m,i}$ is calculated by(El-Bourawi et al., 2006; Izquierdo-Gil & Jonsson, 2003):

$$K_{m,i} = \frac{2}{3RT}\frac{\varepsilon \cdot \bar{r}}{\tau\delta}\left(\frac{8RT}{\pi M_i}\right)^{\frac{1}{2}} \quad (28)$$

Here R is the gas constant, T is the absolute temperature, r is the mean pore radius assumed to be uniformly applied for all pores, ε is the membrane porosity, τ is the pore tortuosity, δ is the membrane thickness, and M_i is the molecular weight of component i.

Apart from the temperature and the molecular weight, all variables are constant for the same membrane. Equation 28 can then be simplified to:

$$K_{m,i} = a\frac{1}{\sqrt{TM}} \quad (29)$$

Returning to the formula for flux through the membrane, since the pressure at the membrane is difficult to determine, a more general formula that uses the bulk pressure in the feed and the permeate was used. The partial pressures in the bulk can be determined by simulations executed in the simulation programme PHREEQC, and the partial pressure in the permeate is calculated with help of the pressure of the vacuum pump. This gives the general formula in Equation 30.

$$J_i = K_{ov,i}\left(P_{f,i} - P_{p,i}\right) \quad (30)$$

Where $K_{ov,l}$ is the overall mass transfer coefficient, $P_{f,i}$ is the partial pressure of component i in the bulk of the feed, and $P_{p,i}$ is the partial pressure of component i in the bulk of the permeate.

Here $K_{ov,i}$ consists not only of $K_{m,i}$ but also of the mass transport coefficient in the feed($K_{f,i}$) and the permeate($K_{p,i}$) as seen in Equation 31.

$$\frac{1}{K_{ov,i}} = \frac{1}{K_{f,i}} + \frac{1}{K_{m,i}} + \frac{1}{K_{p,i}} \quad (31)$$

The mass transport coefficient in the permeate, however, is much larger than the other two and can be assumed to be negligible, which means that the $K_{ov,i}$ consists of the membrane resistance and the feed resistance (Khayet & Matsuura, 2011). Equation 31 is then reduced as follows:

$$\frac{1}{K_{ov,i}} = \frac{1}{K_{f,i}} + \frac{1}{K_{m,i}} \quad (31)$$

$K_{ov,i}$ can then calculated as shown below:

$$K_{ov,i} = \frac{P_{f,i} - P_{p,i}}{J_i} \quad (32)$$

Using this definition, the K_{ov} can be calculated after the fluxes are found experimentally and the vapour pressures are simulated with PHREEQC.

This way of calculating $K_{ov,i}$ differs from methods often used in literature, where $K_{ov,c}$ is found with the help of Equation 33 (El-Bourawi et al., 2006; He et al., 2018).

$$K_{ov,c,i} = \frac{V}{A_m t} ln\left(\frac{C_{0,i}}{C_{t,i}}\right) \quad (33)$$

$K_{ov,c,\,i}$ is the overall mass transfer coefficient of element i, V is the feed volume, A_m is the membrane area, t time, $C_{0,i}$ concentration at start and $C_{t,i}$ concentration at time t. This $K_{ov,c}$ has a different unit of $m \cdot s^{-1}$ and gives the flux in $mol \cdot m^{-2} \cdot s^{-1}$ when multiplied with the change in concentration in the feed water. The relation between K_{ov} and $K_{ov,c}$ is given in Equation 34.

$$K_{ov} = \frac{K_{ov,c} \cdot M}{RT} \tag{34}$$

Where R is the gas constant, T is temperature and M is the molar mass.

The problem with calculating $K_{ov,c}$ with Equation 33 is that a constant volume has to be maintained to make the calculation of $K_{ov,c}$ accurate, and as mass is lost through the membrane this assumption is hard to fulfil with small-volume experiments. Next to that, it is impossible to calculate the $K_{ov,c,i}$ for water with this method, due to the impossibility of finding the concentration of a solute. Therefore, the definition given in Equation 33 of $K_{ov,i}$ is chosen instead for this study.

Another important parameter is the selectivity (β), which says something about how much the $m\%NH_3$ has been increased from the feed to the permeate. The selectivity is calculated as shown in Equation 35.

$$\beta = \frac{m\%NH_{3,permeate}}{m\%NH_{3,feed}} \tag{35}$$

2.3.4 Polarisation effects

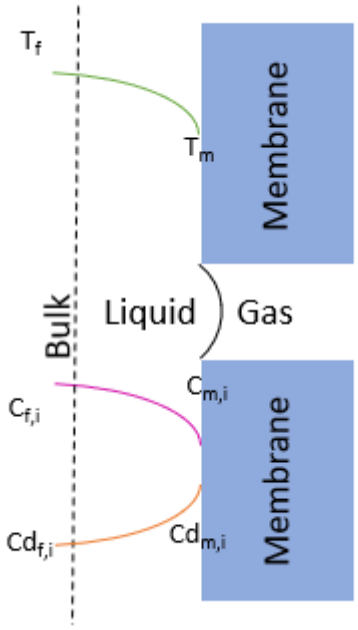

Figure 17 Illustration of the polarisation effects at the feed side of the VMS

Because the feed is not perfectly mixed, there is a difference in concentration and temperature between the feed bulk and the membrane interface. This difference is known as polarisation and can be seen in Figure 17. This indicates that the actual driving force over the membrane, the pressure between liquid/vapour interface and the permeate, is smaller than the pressure difference between the feed and the permeate. Reducing the polarisation effect increases the driving force over the membrane and thus also the flux (Khayet & Matsuura, 2011).

Polarisation effect can be divided into three categories: temperature polarisation, concentration polarisation due to depletion, and concentration polarisation due to accumulation. The three polarisation types are described below.

Temperature polarisation

The temperature polarisation results in the flux being lower than expected because the temperature at the membrane is lower than the bulk temperature used for calculations. This is due to the heat transport explained in Section 2.3.3. Due to this heat transport, the temperature at the membrane drops, which is demonstrated in the Equation 36(Brilman et al., 2015; Khayet & Matsuura, 2011).

$$\mathrm{Q_T} = \alpha\left(T_f - T_m\right) \tag{36}$$

Q_T is the total heat transferred through the membrane, T_f is the temperature in the bulk, T_m is the temperature at the membrane and α is a heat transport coefficient that can be found with the help of the Nusselt number (Nu), see Equation 37.

$$Nu = \frac{\alpha \cdot d}{\lambda} \tag{37}$$

where d is the characteristic length and λ is the thermal conductivity.

The Nusselt number is a function of the Reynolds number and the Prandtl number (Pr) as seen in Equation 38.

$$Nu = f_1(Re, \mathrm{Pr}) \tag{38}$$

The function for the Nusselt number is known for certain flow regimes and geometrical configurations (Brilman et al., 2015).

This lowering of the temperature at the membrane due to heat loss through the membrane will lower the flux due to two reasons.

Firstly, the $K_{m,i}$ will change, as this Equation 29 provided in Section 2.3.3 demonstrates. There it is shown that $K_{m,i}$ is dependent on temperature and an increase in T increases the $K_{m,i}$ value, which in turn increases the flux.

Next, the driving force at the membrane changes, and lowering the temperature lowers the partial pressures at the membrane exponentially, thereby lowering the K_f and thus the overall flux. The water and ammonium pressure are dependent on temperature, as seen in Figure 18.

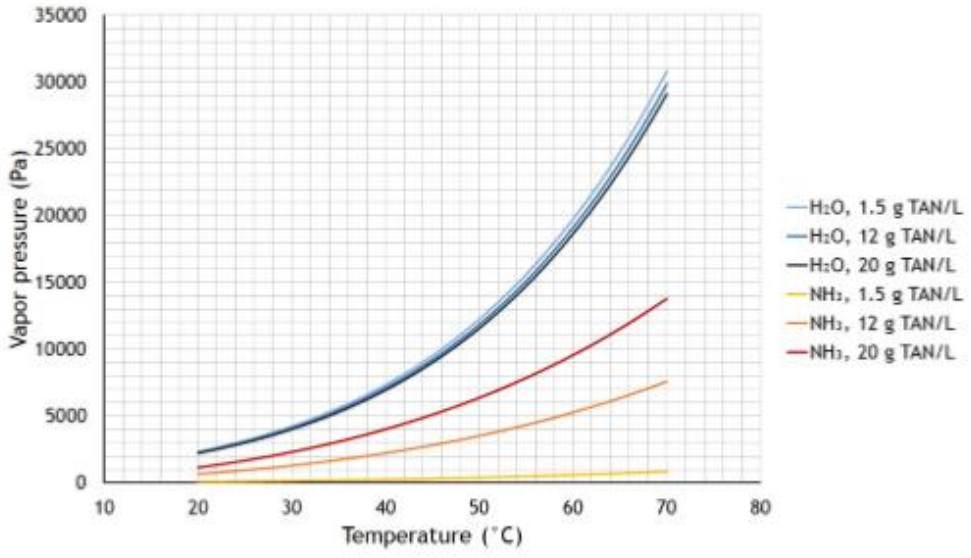

Figure 18 Partial pressure of ammonia and water at different temperatures (Martens, 2017)

Concentration polarisation due to depletion

The concentration polarisation lowers the concentration of ammonia at the membrane. This happens only when the selectivity of ammonia is greater than the selectivity of water, which is due to ammonia being removed from the surface of the membrane in higher amounts than the rest of the components, which lowers the amount of available ammonia at the membrane. This lowers the partial pressure of the ammonia. Due to the water being dominant, it is assumed that the same effect does not significantly affect the water pressure (Brilman et al., 2015; Khayet & Matsuura, 2011).

The concentration change can be calculated with help of Equation 39.

$$J_i = k_i\left(C_{f,i} - C_{m,i}\right) \tag{39}$$

Where k is the mass transport coefficient, which can be calculated using the Sherwood number (Sh)(see Equation 40).

$$Sh = \frac{k * L}{D} \tag{40}$$

D is the diffusion coefficient and L is the characteristic length. The Sherwood number is also a function of the Reynolds number and the Schmidt number (Sc) as seen in equation 41.

$$Sh = f_2(Re, Sc) \tag{41}$$

With a combination of Equation 40 and 41 the mass transport coefficient due to polarisation due to depletion can be calculated in theory, in practise this is often not possible.

Concentration polarisation due to accumulation

The last type of polarisation is due to a cumulation of other components in the water at the surface of the membrane. This happens when the selectivity of the components is lower 1 or even 0, which occurs when water is removed from the surface, but the component is left at the surface. This can lead to an accumulation of contaminants at the surface of the membrane, leading to a higher concentration at the membrane ($Cd_{m,i}$) than in the bulk ($Cd_{f,i}$). Reducing the activity of the water to be lower at the membrane than in the bulk lowers the flux of the water through the membrane and also increases the salting-out effect and chances of fouling (see Sections 2.2.1 and 2.5). Also, increased salt concentration can change the effect of polarisation by depletion, by changing the viscosity of the water; this again can affect temperature polarisation. Due to all three polarisation effects being highly linked, it can be difficult to determine their individual properties if two or more are present.

2.4 Condensation of the permeate vapour

One of the options to improve the permeate quality is to condense the water after VMS. Condensation of the permeate vapour changes the ammonia concentration in the permeate, if the water condenses faster or slower than the ammonia can diffuse into the condensed water, see reactions shown in Equation 42 and 43.

$$H_20(g) \rightarrow H_2O(l) \tag{42}$$

$$NH_3(g) \rightarrow NH_3(aq) \tag{43}$$

The hypothesis is that ammonia diffuses into water less efficiently than water condenses, increasing the concentration of ammonia in the permeate vapour.

Some research literature demonstrates this effect. Research by Philpott and Dean reveals that the concentration of ammonia in the vapour increases over time in a tube condenser, which indicates that concentrating the vapour with condensation is possible (see Figure 19). This figure demonstrates a trend of increasing ammonia vapour concentration throughout a tubular condenser and indicates that when more water is removed via condensation, the vapour concentration increases. The significance of this effect, and how much of the ammonia diffuses back into the water, is not clear (Philpott & Deans, 2004).

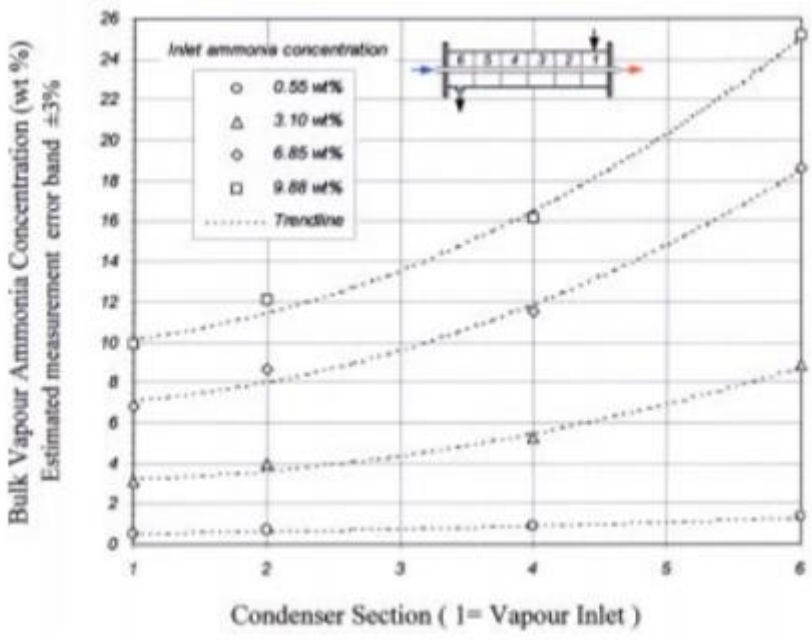

Figure 19 Ammonia concentration in vapour over the length of a tube condenser (Philpott & Deans, 2004)

Van Zalen in his master thesis (2012) demonstrates the same effects. Van Zalen checked the effect of single stage separation with a flash tank at different temperatures and with the help of distillation. These results also demonstrate that compensating an ammonia/water vapour solution could cause an increase in the concentration of ammonia in the vapour state (Van Zalen, 2012).

2.4.2 The possibility of energy recovery from condensation

Another advantage of condensing the permeate could be the possibility to recover some of the energy lost in the membrane (see Section 2.3.3). The energy is freed when the water is condensed (Q_C) (see Equation 44)

$$Q_{c=} \sum_{i=1}^{n} \frac{mass_{cond,i}}{\Delta t} H_{v,i} \tag{44}$$

Where $H_{v,i}$ is the latent heat coefficient of component i, $mass_{cond,I}$ is the mass condensed for element i and Δt is the time of the run. This extra heat recovered can make the whole process more energy beneficial.

2.5 Membrane fouling

One of the most significant problems with membranes is that they tend to foul. Fouling is when deposits gather on the membrane, increasing the membrane's resistance. Membrane fouling can be classified into two categories, reversible and irreversible fouling.

Reversible fouling occurs due to the cake layer or concentration polarisation of materials at the membrane rejection surface. Backwashing or chemical cleaning can remove this kind of fouling.

In the case of irreversible fouling, removal is not possible. This means that the membranes must go through extensive chemical cleaning or be replaced.

Membrane fouling can be caused by physical and chemical interactions between contaminants in the feed solution and the membrane surface. Mass transport mechanisms can lead to adsorption, accumulation, or attachment of contaminants on the membrane surfaces and/or within the membrane pores. Previous studies have demonstrated that membrane fouling and the characteristics of fouling are determined by feed water composition, the concentration of the major contaminants, water chemistry, temperature, membrane properties, operation, and hydrodynamic properties (Guo et al., 2012).

In general, the types of contaminants can be classified into the following four categories:

Particulates: Inorganic or organic particles or colloids that physically bind to the membrane surface and block the pores or develop a cake layer and hinder transport.

Organic: Dissolved components and colloids that attach to the membrane with the help of adsorption.

Inorganic: Dissolved components that tend to precipitate onto the membrane surface due to pH change or oxidation. Coagulant/flocculant residuals may also be present as inorganic contaminants.

Microbiological organisms: The microbiological category covers algae and microorganisms such as bacteria, which can adhere to the membranes and cause biofilm formation.

Due to working at high pH, no fouling by microbial organisms is expected. Also, particulates can easily be removed with some filtration before VMS and are therefore also not expected to be a problem. This leaves inorganic and organic fouling as the main concerns when it comes to VMS of ammonia (Guo et al., 2012).

2.5.1 Inorganic fouling

Research has shown that membrane scaling due to inorganics is the biggest fouling mechanism in membrane distillation applications in desalination and other fields. The deposit formed on the hydrophobic surface of the membrane causes the pores close to the deposit to be filled with liquid, which results in a wetting of parts of the membrane and a leakage of feed to the permeate side (see Figure 20). Membrane scaling, therefore, results in a loss of quality and quantity of the water produced. In the membrane distillation process, the effect of polarisation increases with feed concentration, making the potential for membrane scaling more serious. Membrane scaling is closely related to the composition of the feed and should only be a problem with salt-rich wastewaters (Wang et al., 2014).

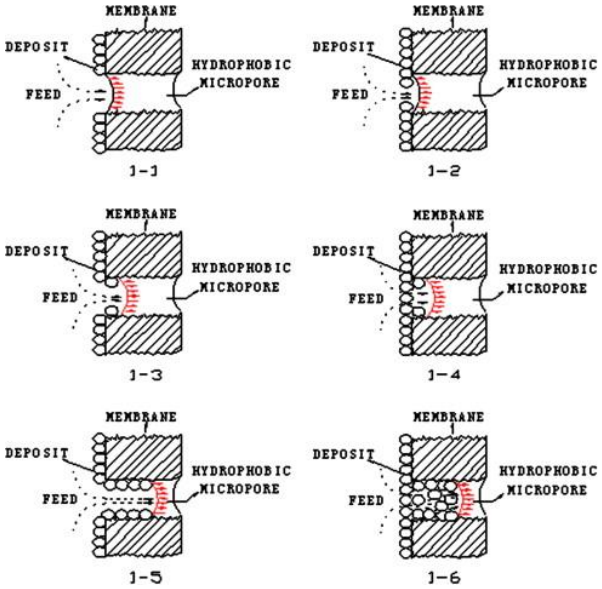

Figure 20 Fouling mechanism scaling (Wang et al., 2014)

2.5.2 Organic fouling

Organic fouling is when organic compounds are absorbed into the membrane. There is some research on fatty acids and fouling. Studies by Amin et al (2010; 2010) show that long chain fatty acid in a glyceride solution does foul the membranes in an ultrafiltration setup, as seen in Figure 21. This figure also shows that the flux decreases over time due to fouling, especially for stearic and oleic acid, which are the expected organic compounds in industrial ammonia-rich wastewater.

The upper picture is from an experiment with a PES membrane; the lower picture shows a PVDF membrane. The PES membrane is more hydrophobic than the PVDF membrane. The hydrophobic membrane also showed more flux decrease. Both membranes also showed a decrease in rejection of contaminants.

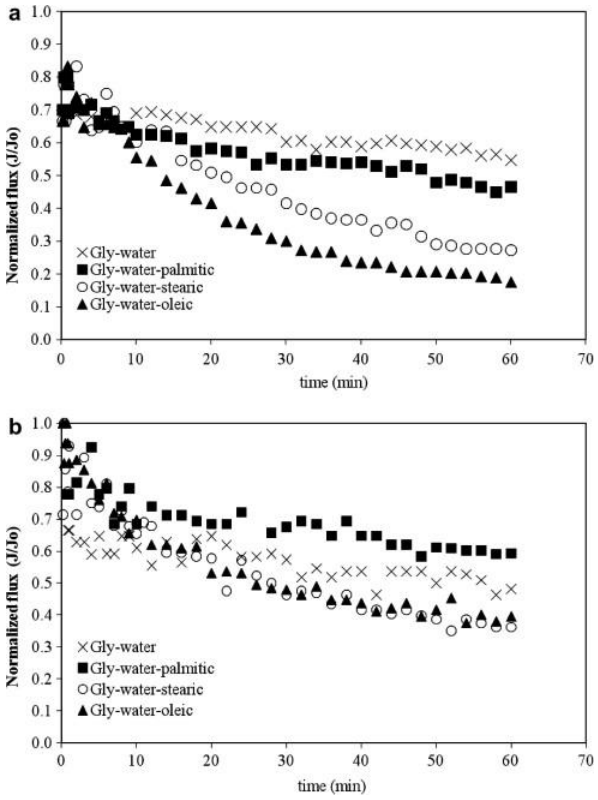

Figure 21 Effect of organic fouling on ultrafiltration membranes

Brinck et al. (2000) also demonstrate that fouling depends on how hydrophobic the organics are. Firstly, the less hydrophobic the solution, the more soluble it is and the lower the chance of fouling. Also, the membrane is hydrophobic and therefore absorbs hydrophobic better than hydrophilic compounds.

Another important factor is the effect of pH on the fouling of membranes, due to fatty acids going from acids to fatty acids to fatty acid salt (see Section 2.1.5). Fatty acid salt is an anionic surfactant, and surfactants are known to change the properties of hydrophobic surfaces. When dissolved in aqueous solutions at low concentration it is energetically favourable for the surfactant to migrate to any available hydrophobic interface and orient itself with its hydrophobic portion towards the interface and the surfactant hydrophilic portion in the aqueous phase (Amin et al. 2010; Barnes & Gentle, 2005; Hoeft & Zollars, 1996). This adsorption of surfactants will lower the surface tension of the hydrophobic surface, making it more hydrophilic. The biggest concern with the possibility of the organics adsorbing the membrane surface lowering the surface tension and making it more hydrophilic is that this could lead to wetting of the surface pores. This will obstruct the liquid-gas interphase that a hydrophobic membrane ensures (see Section 2.3.1).

Fatty acids and amides in industrial ammonia-rich wastewater

Organics are expected in the actual waste water that is going to be tested, i.e. the ammonia-rich industrial waste water from amide production. And organic fouling is identified as the most likely source of fouling. The water is left over from amide production, and the organics found are expected to be the same as those used in the production. It is known that water comes from animal fat. Therefore, the vegetable-based amides and fats can be disregarded from the industrial ammonia-rich wastewaters. The website of Croda states that they make oleamide and stearamide from animal fat. Therefore, it is expected to mostly find stearic acid, oleic acid, oleamide and stearamide in the water.

Fatty acid and amides both have a hydrophilic functional group and a hydrophobic carbon chain (Amin et al, 2010). The properties of the amides and the fatty acids are dependent on chain length. At smaller chains the polarity of the acid group will make the molecule hydrophilic and let it dissolve in water, however, the longer the chain, the harder it is to dissolve it in water. This is due to the c-chain being hydrophobic (Neuss, 2007). As the expected organics in the water are long chain molecules, it is expected that they display both hydrophobic and hydrophilic behaviour.

3 Methods and materials

3.1 Selection of conditions for VMS experiments

Now that the research objectives are set, and the necessary theory is presented, the conditions to examine can be determined. In the next section, different conditions will be chosen.

3.1.1 pH and temperature

The effect of temperature on ammonia flux and selectivity is discussed in Section 1.3.2, which demonstrates that higher temperatures increase ammonia flux but lower ammonia selectivity. An ideal balance between the two occurs around 35°C, so the experiments were done at 35°C.

The effect of pH is discussed in Section 1.3.2 which demonstrates that a higher pH is beneficial for ammonia stripping due to the TAN equilibrium and the total inorganic carbon equilibrium. A pH of 10 both minimises the amount of carbon and maximises the amount of ammonia, so a pH of at least 10 was used in the experiment involving ammonia.

3.1.2 Cross-flow Velocity

As described in Section 2.3.2, different cross-flow velocities lead to different Reynolds numbers. Because Reynolds numbers are a more universal way to examine the hydraulics of the flow cell between different solutions, different Reynolds numbers were chosen instead of specific velocities.

As indicated in Section 2.3.2 a Reynolds number below 250 is laminar, 250-500 is transition flow, and above 500 is turbulent. To test those claims, tests were performed with demi-water and salt solutions with cross-flows at different Reynolds numbers (see Section 4.1.1). Based on these tests, it was concluded that a Reynolds number of 200 is definitely laminar and a Reynolds number 500 is certainly turbulent. Therefore, from now the laminar flow is at 200 Reynolds and the turbulent flow is at Reynolds number 500.

Moreover, it was proven that a cross-flow with turbulent flow gives a better selectivity than laminar flow (see Section 4.1.2). Therefore, a turbulent cross-flow was used when only one flow regime was tested.

3.1.3 Solutions and concentrations

Salt concentration

For the salt experiments, concentrations of 7.5, 50, and 100 $gNaCl \cdot L^{-1}$ were chosen with the help of PHREEQC simulations. These concentrations were chosen because their ionic strength be similar due to the ionic strength of 1.5, 12, and 20 $gTAN \cdot L^{-1}$ of ammonium bicarbonate respectively. This is due to that the conductivities are similar to the conductivity measured at 1.5, 12, and 20 $gTAN \cdot L^{-1}$ of ammonium bicarbonate in Martens' (2017) experiments.

Ammonia concentrations

The experiment with ammonia used the same concentrations as in Martens' (2017) research: 1.5, 12, and 20 g $gTAN \cdot L^{-1}$. The reasoning behind these three values is that 1.5 $gTAN \cdot L^{-1}$ is the concentration of reject water without a pre-concentration step. Taking bipolar ED as a concentration step, the concentration factors found with bipolar ED is 4 and urine having a concentration of 5-6 $gTAN \cdot L^{-1}$ gives a feed concentration of about 20 $gTAN \cdot L^{-1}$ for a single stage of ED. To see whether a trend could be observed, the third concentration of 12 $gTAN \cdot L^{-1}$ was included as well. In addition to these three concentrations, it was also necessary to know how the system would react with a specific industrial ammonia-rich wastewater with a concentration of 100 $gTAN \cdot L^{-1}$.

Ammonium hydroxide and ammonia carbonate
Both solutions made with ammonium hydroxide and solutions made with ammonium bicarbonate were used, because ammonium hydroxide does not add salt to the water and therefore creates low conductivity comparable to the industrial ammonia-rich wastewater from amide production, while ammonia carbonate contains salt in the solution, both from the salt itself and from the addition of NaOH to increase the pH, which is, therefore, more comparable to the composition of urine and reject water. Also, using both should reveal how salt affects the performance of the VMS.

Real wastewater
As for real wastewater, it was decided to focus on industrial ammonia-rich wastewater from amide production. This is due to this wastewater having the highest ammonia concentration and therefore showing the most promise to use directly in the SOFC after VMS without pre-treatment, while the other options mentioned most likely need pre-treatment beforehand.

The industrial ammonia-rich wastewater contains some particulates. This can lead to fouling, and as it is easy to remove, both unfiltered and filtered water where the particulates are removed from the wastewater were tested.

3.1.4 Condensation of permeate vapour
Next, to the experiments with the general setup, experiments were conducted with a condensation element added to the setup, to test the effect of condensation on permeate vapour quality. This was done with a condensation tube with cooling water with different temperatures in the range from 0-30°C. Due to limited equipment availability, the work was carried out at 5-10°C, 15-20°C and 25-30°C. These are the temperatures achieved by cooling water with ice, cooling water in an ice bath, and cool water from the tap.

3.1.5 Overview of the different experiments with the VMS
Based on the considerations listed above, a set of experiments was chosen that would cover most of the alternatives. This is presented in Table 2.

Table 2 Table showing the different conditions for the different VMS experiments

Experiment	Reynolds	Solution	Concentration	Setup
1	200, 300, 400, 500, 600, and 800	Demi-water		General
2	200, 300, 400, 500, 600, and 800	Salt water	7.5 $gNaCl \cdot L^{-1}$	General
3	500	Salt water	7.5, 50, and 100 $gNaCl \cdot L^{-1}$	General
4	200 and 500	Ammonium hydroxide	1.5 $gTAN \cdot L^{-1}$	General
5	500	Ammonium hydroxide	1.5, 12, 20, and 100 $gTAN \cdot L^{-1}$	General
6	200 and 500	Ammonium bicarbonate	1.5 $gTAN \cdot L^{-1}$	General
7	500	Ammonium bicarbonate	1.5, 12, and 20 $gTAN \cdot L^{-1}$	General
8	500	Ammonium hydroxide	1.5 $gTAN \cdot L^{-1}$	Condensation
9	500	Industrial ammonia-rich wastewater unfiltered and filtered		General

3.2 Test with the VMS flow cell

3.2.1 Experimental setup

Two different setups were used for the experiments with VMS. One general setup used for the for all experiments besides the one with condensation of permeate vapour and one with an added condensation tube, used for the condensation experiments.

General setup

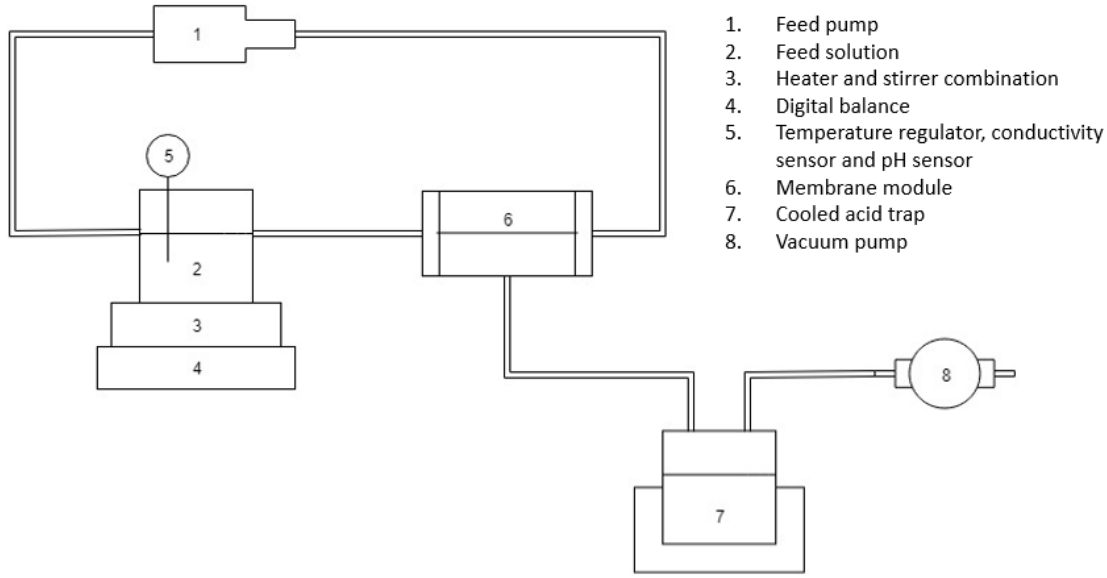

Figure 22 Scheme of the general set up

The setup consists of a membrane flow cell (Sterlitech CF042 acrylic crossflow cell) including a membrane (Sterlitech flat-sheet PTFE membranes with PP backing) with 36 mm^2 of active membrane area with a pore size of 0.1 µm and two spacers (Sterlitech CF042 PP). On the feed side, the membrane flow cell is connected with tubes to the feed bottle and feed pump (Watson-Marlow Sci-Q 300 Series peristaltic pump). The feed bottle is placed on a heating plate and magnetic stirrer combination (IKA RH digital) with a heat regulator (IKA ETS-DS) and a digital balance (Kern PCB 6000-1). A pH sensor (WTW TetraCON 925 EC) and a conductivity sensor (WTW IDS SenTix 940 pH) are also placed in the feed bottle and connected to a mustimeter (WTW digital precision meter Multi 3630 ID) (see Section 3.2.3). On the permeate side, the membrane flow cell is connected to a cooled acid trap that is connected to a vacuum pump (KNF N816.3KT.45.18).

Condensation setup

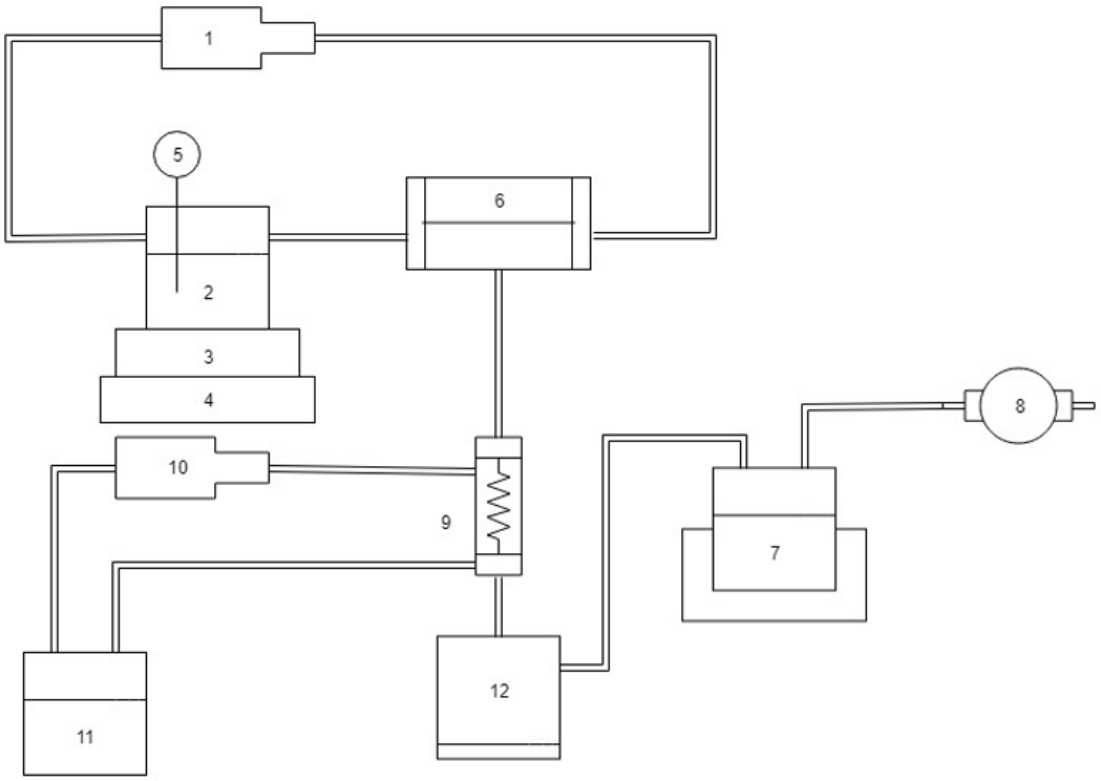

1. Feed pump
2. Feed solution
3. Heater and stirrer combination
4. Digital balance
5. Temperature regulator, conductivity sensor and pH sensor
6. Membrane module
7. Cooled acid trap
8. Vacuum pump
9. Condensation tube
10. Cooling recirculation pump
11. Cooling water
12. Condensation collection flask

Figure 23 Scheme of the condensation set-up

For the condensation experiments, the general setup was used as a base, but with an extension on the permeate side between the acid trap and the membrane. There a condensation tube (Allihn condenser 0.5m) was added, together with a condensation collection flask. Next to this, a cooling circuit was added containing a liquid pump (Watson-Marlow Sci-Q 300 Series peristaltic pump) and a cooling water feed bottle.

3.2.2 Solution preparation

Salt solution

The salt solution was made by adding pure NaCl to the water to make the desired solution. The solution was mixed with 3.75 g NaCl in 500 mL of demi water to make the 7.5 $gNaCl \cdot L^{-1}$solution, 25 g NaCl in 500 mL of demi water to make the 50 $gNaCl \cdot L^{-1}$solution, and 50 g NaCl in 500 mL of demi water to make the 100 $gNaCl \cdot L^{-1}$solution. The solution was then put on the heater stirrer combination to be mixed and heated to 35°C in a closed flask.

Ammonium hydroxide solution

The ammonium hydroxide solution was made by pre-heating 500 mL of demi-water to the desired temperature of 35°C. Then the concentrated ammonia solution (Sigma-Aldrich NH_4OH 25%) with 250 $gTAN \cdot L^{-1}$ was added to the water to make the desired solution. According to the calculations, this

should be 3 mL for the 1.5 gTAN·L^{-1} ammonia solution, 24 mL for the 12 gTAN·L^{-1} solution, and 40 mL for the 20 gTAN·L^{-1} solution. In practice, it turned out that a bit of extra solution was needed to achieve the desired concentration; therefore, the experiments were implemented with 3.5 mL for the 1.5 gTAN·L^{-1} solution, 30 mL for the 12 gTAN·L^{-1} solution, and 45 mL for the 20 gTAN·L^{-1} solution. The solution was then put on the heater stirrer combination to be mixed and heated to 35°C in a closed flask.

Ammonia carbonate solution

The ammonia carbonate solution was made by pre-heating 500 mL of demi-water to the desired temperature of 35°C. Ammonia carbonate salt(Sigma-Aldrich NH_4HCO) was then added, 6.6 g for the 1.5 gTAN·L^{-1} solution, 52.6 g for the 12 gTAN·L^{-1} solution, and 87.7 g for the 20 gTAN·L^{-1} solution, based on calculations with molar masses of 18.0 g·mol^{-1} for ammonium and 79.1 g·mol^{-1} for ammonia carbonate. Then a NaOH solution (Broom NaOH 32% technical grade) was added to the water to increase the pH of the solution to approximately 10. The solution was then put on the heater stirrer combination to be mixed and heated to 35°C in a closed flask.

Cooling water

Cooling water between 5-10°C

The cooling water was prepared by filling a litre flask with tap water and adding ice cubes to the water. The ice cubes then cooled the water until the desired temperature.

Cooling water between 15-20°C

The cooling water was prepared by filling a litre flask with tap water and putting it in a cooling bath. The bath consisted of water and cooling elements. The cooling bath then cooled the water until the desired temperature.

Cooling water between 25-30°C

The cooling water was prepared by filling a litre flask with tap water directly.

Industrial ammonia-rich wastewater from amide production

Unfiltered industrial ammonia-rich wastewater

The industrial ammonia-rich wastewater was in this case put on the magnetic stirrer and pre-heated to 35°C before the experiments.

Filtered industrial ammonia-rich wastewater

The industrial ammonia-rich wastewater was filtered with a 0.45 µm syringe filter, then put on the heating plate and magnetic stirrer combination and pre-heated to 35°C before the experiments.

3.2.3 Measurements

General measurements

Mass feed bottle

The mass of the bottle filled with feed solution was weighed on a balance, and the weight was recorded in the software Balance Connection on a laptop for data transmission every 30 seconds.

pH, conductivity, and temperature

The pH, conductivity, and temperature were recorded using a pH sensor (WTW TetraCON 925 EC) and a conductivity sensor (WTW IDS SenTix 940 pH) connected to a mustimeter (WTW digital precision meter Multi 3630 ID). Using a USB cable, the measurements were directly transferred to the computer and recorded in Microsoft Excel every 30 seconds.

TAN concentration

The ammonia sample was taken from the feed cycle with a 1 mL syringe every 15 minutes. The test was then diluted to a concentration of between 300 and 2,000 mgTAN·L^{-1} to be tested with test kits (MACHEREY-NAGEL NANOCOLOR Ammonium 2000). The tube tests were then tested in a spectrophotometer (NANOCOLOR VIS II).

Density solution

A set volume sample was taken from each solution and weighed to be able to calculate the density of the solution.

Condensation measurements

Some extra measurements were needed in addition to the general measurements for the condensation experiments.

Mass condensed water

The condensed water in the collection flask was collected and weighed with a digital balance at the end of the condensation experiments to measure the weight of the condensed water.

Concentration condensed water

A sample of the condenced water was then taken, and the ammonia concentration was tested as described under TAN concentration.

Fouling measurements

COD

For the experiments with real water, the organics were also measured, next to the mass balance of water and ammonia. This was done by taking a sample of the feed water before and after the experiment. The samples were prepared with test kits (HACH LANGE LKC014) and incubated in an oven (DRB 200 Reactors) for two hours before being tested with a spectrophotometer (DR 6000™ UV-VIS)

3.2.4 Experimental procedure and conditions

All feed solutions were prepared as described in Section 3.2.2, and all experiments were completed under the conditions described in Table 2. After the solutions were made, the measurement equipment was started. For the condensation experiment, the circulation pump of the cooling water was turned on. Then the feed pump was turned on and the solution was pumped through the system until the tubes were filled and no air bubbles were left in the tubes or the flow cell. The vacuum pump was then turned on. The system was given some time to stabilise, then the experimental runtime began. The first sample was taken for the ammonia solutions experiments. The demi-water and salt water experiments ran for 20 minutes each, and the ammonia experiments ran for about one hour. After the experiments, the system was rinsed with demi-water.

3.3 Other experiments

3.3.1 Testing the industrial ammonia-rich wastewater from amide production

To be able to say something about the type of fouling occurring on the membrane when using the real wastewater, it is essential to know what it consists of. Therefore, the water was analysed in various ways.

Simple Analysis

Section 3.2.3 describes how pH, conductivity, TAN and COD concentration were tested during the experiments. The beginning values from those measurements were also used to analyse the compensation of the water.

3.3.2 Analysis of membrane

Membrane surface

To find out more about the fouling of the membrane, the membrane was examined visually after the test with the real wastewater. This was to see whether the fouling led to changes visible to the naked eye.

Contact angle

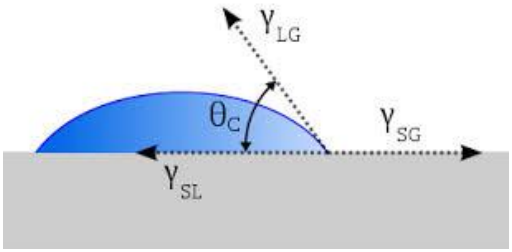

Figure 24 Illustration of the contact angle

A simple test to check the hydrophobicity of a surface is to measure the contact angle of a demi-water droplet on the surface (see Figure 24). The larger the contact angle the more hydrophobic the surface (Barnes & Gentle, 2005). The contact angles of the membrane before and after the VMS experiments with industrial ammonia-rich wastewater were measured. This was done by taking a picture of the membrane from the side and determining the contact angle between the membrane and a demi-water droplet.

3.3.3 Energy balance

Also, an energy balance for the system was made to determine whether the energy needed by the VMS is close to the energy produced by the SOFC. This was determined by using a combination of research literature and the results from the completed experiments.

3.4 Data Processing

3.4.1 Calculation VMS experiments

Calculating the total flux

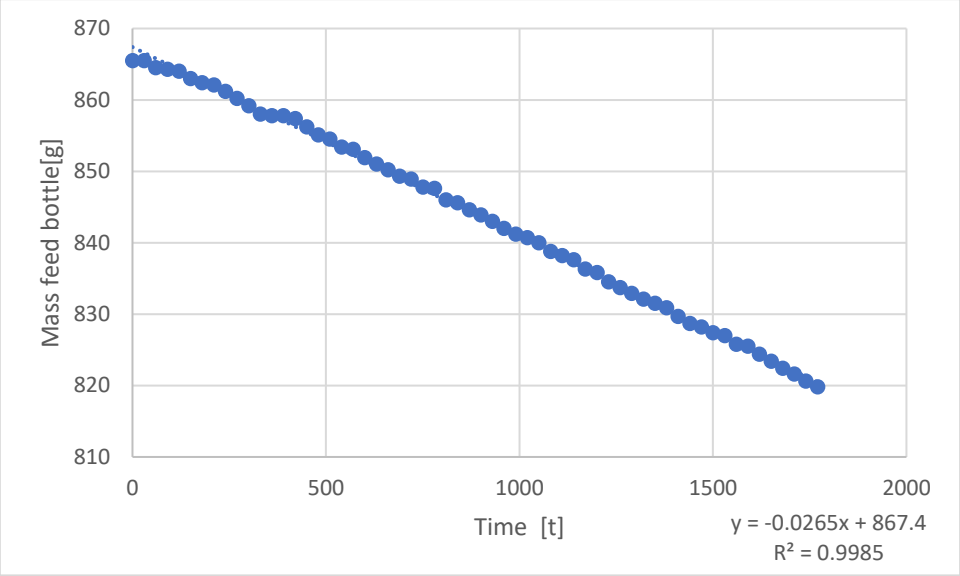

Figure 25 Mass measurements of the mass of the feed bottle for a demi water experiment over time

The mass in the feed flask was measured every 30 seconds (see Section 3.2.3), taking the slope of the decrease of the mass over time (s_{mass}) (see Figure 25). The mass removed per second can be calculated with Equation 45.

$$s_{mass} = \frac{\Delta mass}{\Delta t} \tag{45}$$

To obtain the total flux, s_{mass} is divided by the membrane surface (A_m):

$$J_{T=} \frac{s_{mass}}{A_m} \tag{46}$$

Calculating the ammonia flux

To calculate the flux of ammonia, ammonia mass ($mass_{amm,t}$) is needed; this is done by taking the concentration of ammonia ($C_{amm,t}$) and the volume of feed solution ($V_{feed,t}$) at a certain time (see Equation 47)

$$mass_{amm,t} = C_{amm,t} \cdot V_{feed\ ,t} \tag{47}$$

The volume of the feed solution is calculated with the help of the initial volume of the feed ($V_{feed,s}$) the mass change in the feed bottle and the density of the feed (ρ_{feed}):

$$V_{feed,t} = V_{feed,i} - \frac{mass_{feedbottle,i} - mass_{feedbottle,t}}{\rho_{feed}} \tag{48}$$

When the mass of ammonia is known the change in mass over time can be calculated with help of Equation 47, and with help of the membrane area the ammonia flux (J_{amm}) can be calculated with Equation 49.

$$J_{amm} = \frac{\Delta mass_{amm}}{\Delta t \cdot A_m} \tag{49}$$

Calculating the water flux

As it is assumed that only water and ammonia are passing through the membrane, due to the pH being too high for CO_2 to be present. Then, the water flux (J_w) can be calculated with the total flux and the ammonia flux (see Equation 50)

$$J_{w=}J_T - J_{amm} \tag{50}$$

Calculating the selectivity

To be able to say something about how good the membrane is in concentrating the ammonia, the selectivity is calculated with Equation 35 given in Section 2.3.3:

$$\beta = \frac{m\%NH_{3_{permeate}}}{m\%NH_{3_{feed}}} \tag{35}$$

The selectivity compares the mass percentage of ammonia in the feed ($m\%NH_{3\,feed}$) with the mass percentage in the permeate ($m\%NH_{3\ permeate}$).

The mass percentage of ammonia in the feed is calculated with help of the starting feed ammonia concentration ($C_{amm,i}$) and the density of the feed as Given in Equation 51:

$$m\%NH_{3_{feed}} = \frac{C_{amm,i}}{\rho_{feed}} \cdot 100 \tag{51}$$

The mass percentage in the permeate is calculated with the help of the ammonia flux and the total flux (see Equation 52).

$$m\%NH_{3_{permeate}} = \frac{J_{amm}}{J_T} \cdot 100 \tag{52}$$

Calculating the vapour pressure

Feed

By using PHREEQC, the saturation index (SI) of each component in a solution can be simulated. The partial pressure of each component ($P_{i,f}$) can then be calculated with the simulated saturation index and the atmospheric pressure (P_{atm}) (See Equation 53).

$$P_{i,f} = P_{atm} \cdot 10^{SI} \tag{53}$$

Permeate

It is known that the pressure in the vacuum is 1500 Pascal ($P_{t,p}$). With this, the partial pressure of the gases in the permeate side can be calculated with Dalton's law stating that all partial pressures (P_i) in a gas sum op to the total pressure (Atkins & De Paula, 2006) (see Equation 54).

$$P_{t,p} = \sum_{i=1}^{n} P_{i,p} \tag{54}$$

And that each partial pressure is the total pressure times the mole fraction of the gas(x_i) (see Equation 55).

$$P_{i,p} = x_i \cdot P_{t,p} \tag{55}$$

Mole fraction can be calculated with equation 56.

$$x_i = \frac{\frac{J_i}{M_i}}{\sum_{i=1}^{n} \frac{J_i}{M_i}} \tag{56}$$

Calculating the mass transfer coefficient

The mass transfer coefficient is defined in Section 2.3.3. It can be calculated for each component with help of the flux, partial pressure feed and partial pressure permeate for each component, as seen in Equation 57.

$$K_{ov,i} = \frac{J_i}{P_{i,f} - P_{i,p}} \tag{57}$$

3.4.2 Calculation condensation

Percentage Condensed

The percentage condensed (%cond) can be calculated by taking the mass condensed ($mass_{cond}$) and dividing it by the change in mass at the feed ($\Delta mass_{feed}$), which equals the total mass in the permeate before condensation (see Equation 58)

$$\%\text{cond} = \frac{mass_{cond}}{\Delta mass_{feed}} \tag{58}$$

Concentration factor

The concentration factor is the mass percentage of ammonia in the permeate after condensation ($m\%NH_{3\ aftercond}$) divided by the mass percentage of ammonia before condensation ($m\%NH_{3\ permeate}$):

$$CF = \frac{m\%NH_{3_{aftercond}}}{m\%NH_{3_{permeate}}} \tag{59}$$

The mass percentage of ammonia before condensation is given in Section 3.2.3 in Equation 52.

The mass percentage of ammonia after condensation is found by taking the mass of ammonia in the permeate ($\Delta mass_{amm}$) minus the mass of condensed ammonia ($mass_{amm,cond}$) divided by the change of total mass in the permeate, as seen in Equation 60.

$$m\%NH_{3_{aftercond}} = \frac{\Delta mass_{amm} - mass_{amm_{cond}}}{\Delta mass_{feed} - mass_{cond}} \tag{60}$$

The mass of the condensed ammonia can be calculated with Equation 61 by taking the total mass condensed, the density of the solution ($\rho_{solution}$) and the concentration of ammonia condensed ($C_{amm\ cond}$).

$$mass_{cond,amm} = \frac{mass_{cond}}{\rho_{solution}} \cdot C_{amm_{cond}} \tag{61}$$

3.4.3 Energy balance calculations

Here the calculation for the energy is given; a detailed example of how to calculate the energy balance can be found in Appendix D.

Thermal energy balance

The thermal energy balance of the system consists of the thermal energy lost in the stripping process (Q_T) (see Section 2.3.3), energy recovered with condensation (Q_C) (see Section 2.4.1) and the energy produced by the SOFC ($SOFC_{Th}$) (see Section 1.2.3), as seen in Equation 62.

$$EB_T = SOFC_{Th} - \mathrm{Q_T} + \mathrm{Q_C} \tag{62}$$

The energy lost in the stripping process is due to the evaporated vapour leaving the bulk and is given by Equation 26 in section 2.3.3:

$$\mathrm{Q_T} = \sum_{i=1}^{n} J_i H_{v,i} \tag{26}$$

The energy from condensation is given in Equation 44 in Section 2.4.1:

$$\mathrm{Q_C} = \sum_{i=1}^{n} \frac{mass_{cond,i}}{\Delta t} H_{v,i} \tag{44}$$

Mass condensed is only measured for ammonium hydroxide solution with a concentration of 1.5 gTAN·L^{-1}. To be able to estimate the mass condensed for the other solutions some assumptions were made based on Section 4.3. Firstly it was assumed that the total amount of water evaporated was 40% ($\%_E$). Giving Equation 63.

$$mass_{cond} = \Delta mass * \left(1 - m\%NH_{3_{permeate}}\right) \cdot \%_{\mathrm{E}} \tag{63}$$

To find the mass of the condensed ammonia the following assumptions where made: 1) the ammonia concentration of the condensed water is neglectable, giving Equation 64 and 65.

$$mass_{cond,amm} = 0 \tag{64}$$

$$mass_{cond,w} = mass_{cond} \tag{65}$$

2) the thermal energy produced by the SOFC is 4.2 MJ·kg-N^{-1}.

Electrical Energy balance

The electrical energy balance consists of the energy needed to run the circulation pump (E_r), the vacuum pump (E_{va}) and the electrical energy produced in the solid oxide fuel cell ($SOFC_E$) (see Equation 66)

$$EB_E = SOFC_E - \mathrm{E}_r - \mathrm{E}_{va} \tag{66}$$

The energy needed for the vacuum pump is calculated in Appendix D with help from information based on vacuum stripping of methane in a drinking water plant of Vitens (Spannenburg) and is 0.28MJ·kg-gas^{-1}.

The energy of the circulation pumps can be calculated with the help of the density of the feed, flow feed (Q_{feed}), gravitational constant (g) and the heat loss over the membrane ($\Delta H_{membrane}$) (see Equation 67)

$$E_r = \rho_{feed} * Q_{feed} * g * \Delta H_{membrane} \tag{67}$$

The electrical energy produced by the SOFC is 8.4 MJ·kg-N^{-1}.

4 Results

In this section the result from the experiment explained in Methods and materials (see Section 3) are presented.

4.1 The effect of different flow regimes

This section examines the effect of flow regime on the performance of the VMS. In Section 2.3.4 it is described what the difference between turbulent and laminar flow is due to the polarisation effect. For an alternate solution, different polarisation effects play a role. For demi-water, the effect is only caused by temperature polarisation, while salt has both temperature polarisation and polarisation due to accumulation, ammonium hydroxide has temperature polarisation and polarisation resulting from depletion, and ammonium bicarbonate has temperature polarisation and polarisation due to both depletion and accumulation.

4.1.1 The effect of different flow regimes demi-water and salt solution

In Section 2.3.2 it was claimed that laminar flow occurs below a Reynolds number of 250, transitional flow for 250 to 500 and turbulent flow develops above 500. In order to examine this statement and to observe how the system reacts to different cross-flow velocities, water and salt solutions of 7.5 $gNaCl \cdot L^{-1}$ were tested at different Reynolds numbers. The experiments were performed at 35°C.

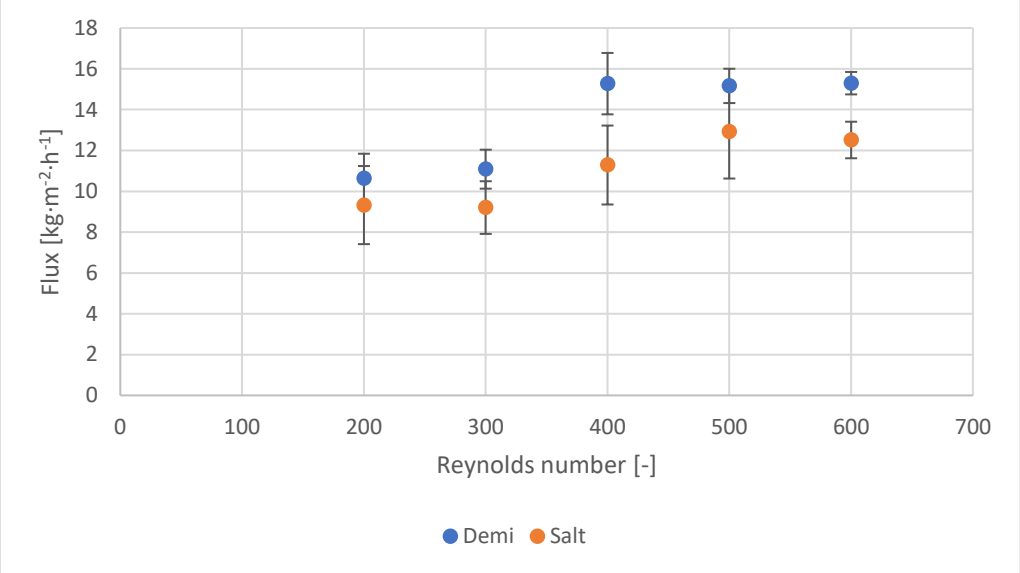

Figure 26 The water flux of demi water and salt water solution for different Reynolds numbers

As Figure 26 indicates, the demi-water exhibited a clear distinction between laminar and turbulent flow between the Reynolds numbers of 300 and 400. At laminar flow, the flux was only 70% of the turbulent flow. However, there was no further improvement in flux when the turbulent flow was reached. This finding is comparable to the theory, as 300 is close enough to 250 to suggest a nearly laminar state. The only deviation between what was expected from literature and the results found (see Section 2.3.2), is for a Reynolds of 400, where the result appeared to be more turbulent than transitional. Nevertheless, the standard deviation for this measurement point is major, which could account for this discrepancy between the theory and the experimental result.

According to Figure 26, the Reynolds numbers for the experiment with the 7.5 $gNaCl \cdot L^{-1}$ salt solution are comparable to literature-based predictions (see Section 2.3.2). The Reynolds numbers of 200 and

300, which should be approaching laminar, had a lower flow than the expected turbulent flows of 500 and 600 Reynolds, where the laminar flow was 72% of the turbulent flow. The flow of 400 Reynolds number was between the laminar flows and the turbulent flows as expected, as it should be a transition flow.

Interestingly, the salt fluxes were consistently lower than the fluxes of demi-water. This finding cannot be explained by the difference in vapour pressure due to the salt solution which is a 5% lower vapour pressure than that of demi water (see Section 2.2.3). The difference in flux was 12-18% (excluding the 400 Reynolds measurement), which is much higher than the 5% difference in vapour pressure. This implies the presence of one or more additional effects, beyond temperature polarisation. This result could be explained by polarisation that resulted from the accumulation of salt at the membrane surface, which would lower the water pressure at the membrane and thereby reduce the flux. Because this effect was not avoided by shifting from laminar to turbulent flow, it is likely that a polarisation effect was present even at turbulent flow.

4.1.2 The effect of different flow regimes ammonia solutions

In Section 4.1.1 it was shown that turbulent flow would give higher water flux than laminar flow for a demi-water and salt solution. To see if this is also the case for a solution including ammonia, and how flow regime does affect the ammonia flux experiment with both an ammonium hydroxide solution with 1.5 gTAN·L^{-1} and an ammonium bicarbonate solution with 1.5 gTAN·L^{-1} were conducted.

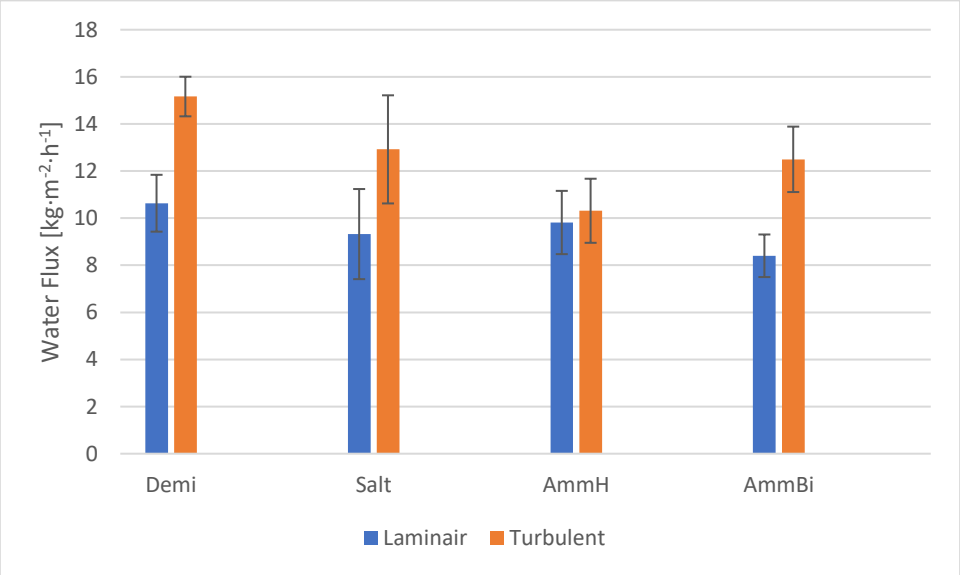

Figure 27 Water flux for demi water, salt water, ammonium hydroxide and ammonium bicarbonate solution at laminar and turbulent flow. (In this study, laminar flow and turbulent flow corresponded with 200 Reynolds and 500 Reynolds, respectively.)

To see the effect of flow regimes of water flows the different fluxes for the different solutions at laminar and turbulent flow were plotted in Figure 27. It can be seen that turbulent cross-flow clearly increases the water flux compared to laminar flow, this is the case for all solutions apart from the ammonium hydroxide 1.5 gTAN· L^{-1} solution. With the laminar flux being 70%, 72%, 95% and 67% of the turbulent flow for the demi water, salt solution, ammonium hydroxide solution and the ammonium bicarbonate solution, respectively.

One explanation for the limited difference of the water flux between laminar and turbulent flow for ammonium hydroxide is that the polarisation due to depletion of ammonia positively influences the flux. This would mean that with laminar flow the concentration of ammonia is lower at the membrane surface than with turbulent flow, and this would positively influence the water flux at

laminar flow. Leading to a vapour pressure of water at the membrane that exceeds the vapour pressure of water in the bulk, as less ammonia was present than expected and consequently the water pressure in the bulk is higher (see Section 2.2.1). If this phenomenon affects the flux equally as the temperature reduction at the membrane due to temperature polarisation, it could account for the small difference in laminar and turbulent water flux for the ammonium hydroxide solution.

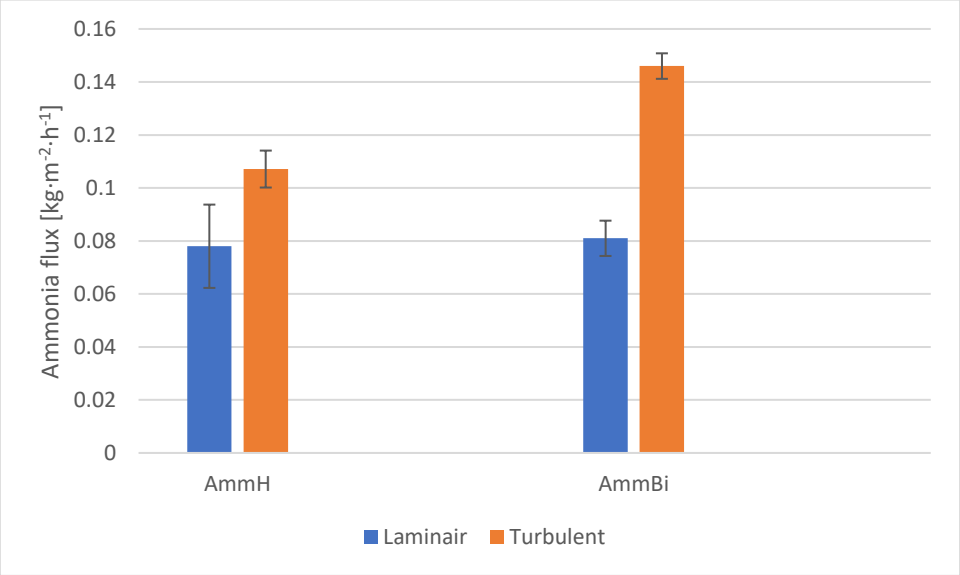

Figure 28 Ammonia flux for ammonium hydroxide and ammonium bicarbonate feed solutions at laminar and turbulent flow

As the VMS is used to strip ammonia, the effect of flow regimes on ammonia flux is also interesting. In Figure 28 the ammonia flux of the ammonium hydroxide 1.5 gTAN·L^{-1} solution and the ammonium bicarbonate 1.5 gTAN·L^{-1} solution is plotted. There it is conveyed that turbulent cross-flow increased the ammonia flux compared to laminar cross-flow. In Section 1.3.2 the result of cross flow in literature is discussed, there it is stated that an increase in crossflow would increase both the water and ammonia flux. The result gotten showed an increase in water flux for ammonium bicarbonate and an increase in ammonia flux for ammonium hydroxide and ammonium bicarbonate which is in line with what is found in literature only the result of the water flux of ammonia hydroxide did differ.

Notably, the difference between laminar and turbulent flows was much more pronounced for ammonium bicarbonate than for ammonium hydroxide, with the laminar flow being 75% and 55% of the turbulent flow, respectively. The extra polarisation effect of accumulation for ammonium bicarbonate, which was not present for ammonium hydroxide, could account for this finding.

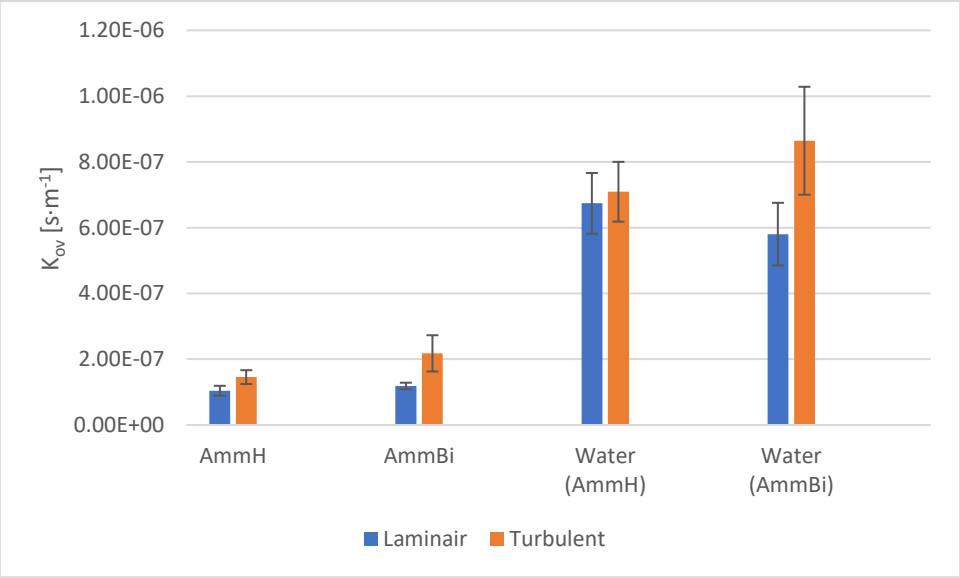

Figure 29 Overall mass transfer coefficient (K_{ov}) for water and ammonia at laminar and turbulent flow.

In Figure 29 the K_{ov} for water and ammonia is depicted. The K_{ov} shows whether the increase in flux was due to higher vapour pressures or due to the transport mechanisms in the liquid side of the membrane. The K_{ov} for water was much higher than for ammonia, which means that the higher water flux was not only due to the higher vapour pressure for water but also due to that water was more easily passed through the membrane module and experiences less polarisation effects. For ammonia, the study of He et al (2018) found a K_{ov} of $1.74 \cdot 10^{-9}$ $s \cdot m^{-1}$ for a temperature of 45°C, and in the study of Ding et al. (2006) at a temperature of 43°C a K_{ov} of $7.51 \cdot 10^{-8}$ $s \cdot m^{-1}$ was found. Both studies found a K_{ov} that is lower than the K_{ov} found in this research for both laminar and turbulent flow at 35°C.

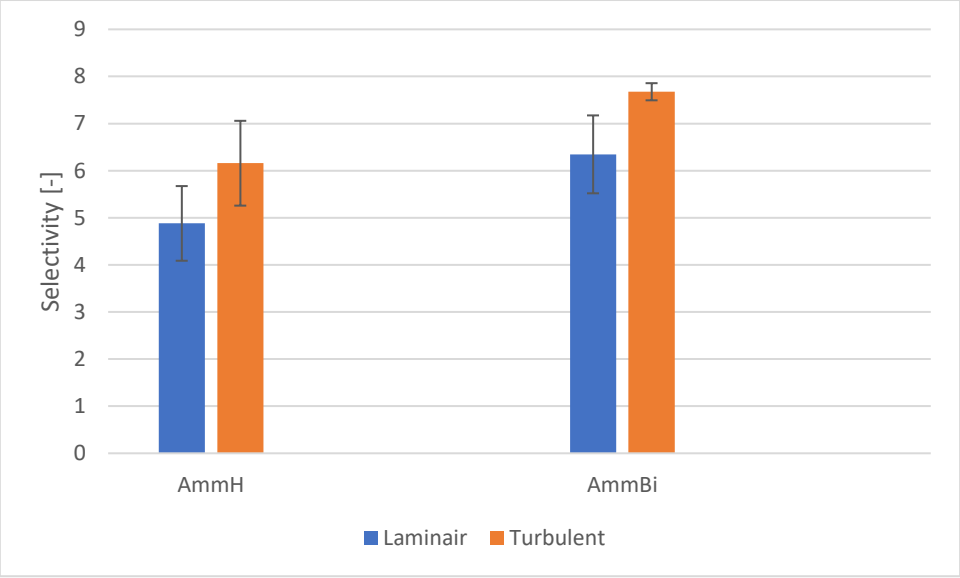

Figure 30 Ammonia selectivity for ammonium hydroxide and ammonium bicarbonate feed solutions at laminar and turbulent flow

After investigating the effect of flow regime for the water flux and the ammonia flux, the relationship of the two was investigated. This is interesting due to this research aimed at an as high as possible ammonia concentration the permeate to fuel the SOFC. This relationship is shown with help of the selectivity (see Section 2.3.3). In Figure 30 the selectivity of ammonia is plotted, which reveals that the selectivity for the turbulent flow was higher than for the laminar flow for both ammonium

hydroxide and ammonium bicarbonate, with the selectivity of the laminar flow being 79% and 83% of the turbulent flow, respectively. Thus, the effect of polarisation was less significant for the water flux than for the ammonia flux and if a high ammonia concentration is desired, then turbulent flow is preferable.

In Section 1.3.2, the effect of selectivity of ammonia in VMS in literature is discussed. However, literature stated contradicting results about the effect on selectivity. If the selectivity found in this study is compared with that of the study carried out by Ding et al (2006), which is one of the more comparable studies as ammonia hydroxide was used as an ammonia source as well, the same trend was found. In this study selectivity between 5 and 11.5 was found, the results of this study is inside this range.

4.2 The effect of salt on the performance of the VMS

To explore the effect of salt, e.g. the ionic strength, on the performance of the VMC, multiple experiments were conducted with ammonium hydroxide (low ionic strength) and ammonium bicarbonate (high ionic strength) solution. In addition, some simulations were completed with Phreeqc. Section 2.2.3 elaborates on those simulations.

To test the effect of salt different experiments with different ammonium hydroxide and ammonium bicarbonate solutions were performed under turbulent conditions.

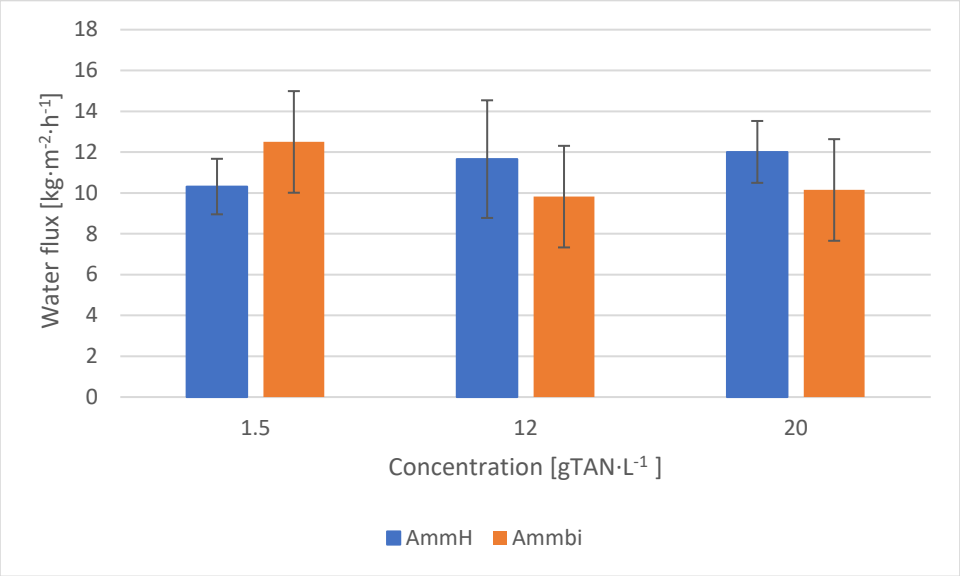

Figure 31 Water flux for ammonium hydroxide and ammonium bicarbonate feed solution at different TAN concentrations.

Firstly, the effect of salt on the water transport through the membrane was investigated. The results are shown in Figure 31, which provides the water fluxes for ammonium hydroxide and ammonium bicarbonate at various concentrations. The standard deviations were sizeable, and the values did not differ substantially, which makes it hard to make any conclusion on the trends of the water fluxes. Nonetheless, the ammonium hydroxide water flux seemingly underwent a slight increase from a flux of 10.3 $kg \cdot m^{-2} \cdot h^{-1}$ for a concentration of 1.5 $gTAN \cdot L^{-1}$ to 12.0 $kg \cdot m^{-2} \cdot h^{-1}$ for a concentration of 20 $gTAN \cdot L^{-1}$, while the flux for ammonium bicarbonate slightly decreased from a flux of 12.5 $kg \cdot m^{-2} \cdot h^{-1}$ for a concentration of 1.5 $gTAN \cdot L^{-1}$ to 10.2 $kg \cdot m^{-2} \cdot h^{-1}$ for a concentration of 20 $gTAN \cdot L^{-1}$.

Interestingly, the ammonium bicarbonate started with a higher water flux than ammonium hydroxide before it became lower. The simulation in Section 2.2.3 showed a decrease in vapour pressure of water with higher ammonia concentrations and that the vapour pressure of water for the ammonium bicarbonate should decrease more. This would mean that without any other effect playing a role, one would expect a decline in ammonia flux for both solutions. The result does not show this decrease for ammonia hydroxide. However, it is hard to make a significant conclusion due to the high error margin in the experiments.

Next to the water fluxes the ammonia fluxes were found. The fluxes differed substantially during a run due to lowering ammonia concentration, therefore, the results are given for 15 min interval over the exact starting concentration of that interval in Figure 32. The figure shows linear trend lines for the ammonia fluxes versus TAN concentration for the ammonium hydroxide and ammonium bicarbonate solutions.

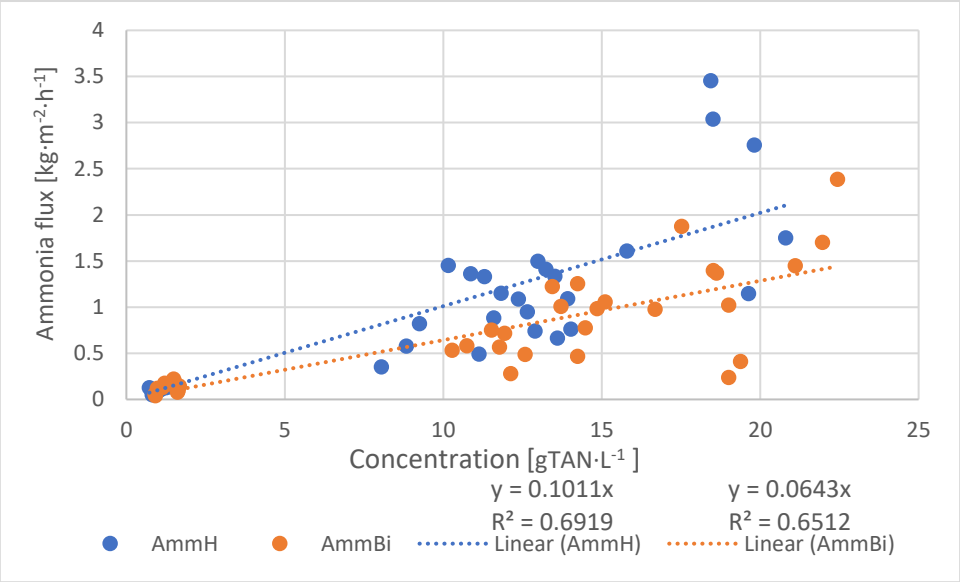

Figure 32 Ammonium flux for ammonium hydroxide and ammonium bicarbonate feed solution over TAN concentration.

These results contradict the expectations in Section 2.2.3, as the ammonia flux of ammonium bicarbonate starts higher than the ammonia flux of ammonium hydroxide, but the ammonia flux of ammonium hydroxide then exceeded the ammonia flux of ammonium bicarbonate. The simulated vapour pressure showed an opposite trend, indicating that other factors play a bigger role than only the change in vapour pressure and that addition of salt lowers the ammonia flux at higher salt concentrations.

Different polarisation effects might have contributed to this result. The ammonium bicarbonate solution may have had a higher ionic strength at the membrane than was expected, which would increase the vapour pressure of ammonium bicarbonate; however, when it becomes too high, it can hinder the diffusion of ammonia from the bulk to the membrane, which negatively affects the flux of ammonia.

No literature on the effect of salt on the performance of VMS has been found. However, in section 1.3.2 the effect of feed concentration was discussed. Contradictory results were found in literature on the effect on the total flux. However, previous results in the 'From pollutant to power' project showed that the total flux stays the same for different TAN concentrations from ammonium bicarbonate solutions. The result from this research did not show a clear trend for ammonium bicarbonate and an increase for ammonium hydroxide in total flux (as both ammonia and water flux increased). It was also found that the ammonia flux should increase with TAN concentration, which was also the case. It was not possible to do a quantitative analysis comparing the found fluxes with literature due to total flux differing in literature for different setups and different pressures at the vacuum side. These varying experiment conditions make the flux values not comparable to the fluxes obtained in this research (El-Bourawi et al., 2006; He et al., 2018).

To be able to say more about how the fluxes differ from what is expected from the calculated driving force the mass transport coefficients of water and ammonia were calculated (see Section 3.4.1).

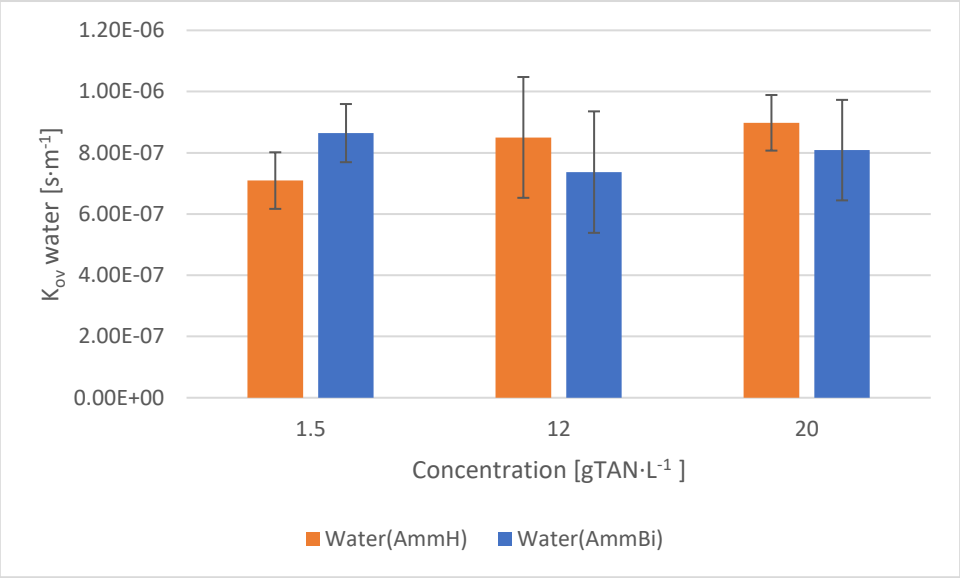

Figure 33 Mass transport coefficient of water for ammonium hydroxide and ammonium bicarbonate feed solution at different TAN concentrations.

Figure 33 presents the mass transport coefficients of water for the ammonium hydroxide and ammonium bicarbonate solutions. For the water mass transport coefficient, high standard deviations render the trends unclear, but there seemed to be an increase in the water flux for the ammonium hydroxide and no clear trend for the ammonium bicarbonate. The rise for ammonium hydroxide could be a consequence of water vapour pressure that was higher than expected because of polarisation due to the depletion of ammonia, which would produce less ammonia at the membrane than anticipated and thereby increase the water pressure.

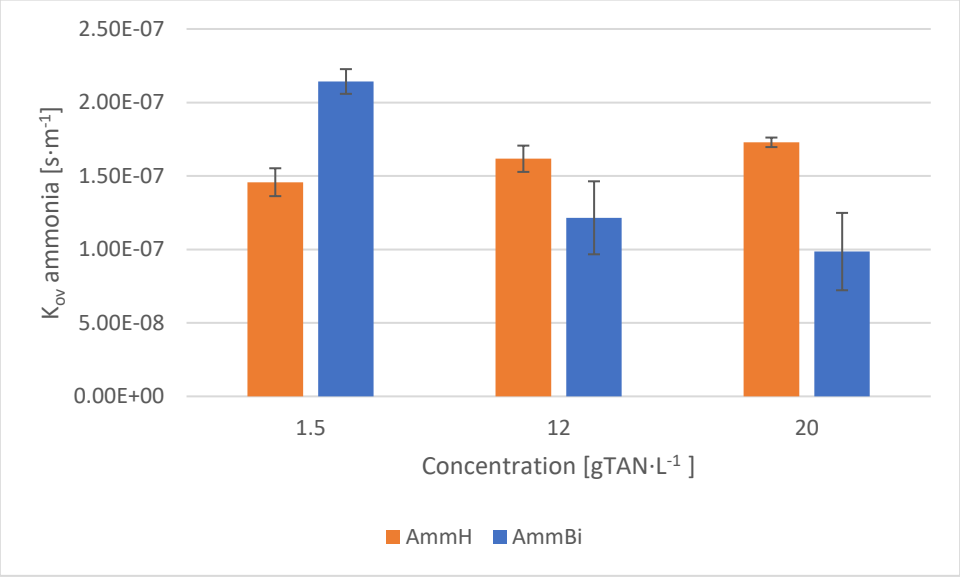

Figure 34 Mass transport coefficient of ammonia for ammonium hydroxide and ammonium bicarbonate feed solution at different TAN concentrations.

Figure 34 displays the mass transport coefficients of ammonia for the ammonium hydroxide and ammonium bicarbonate solutions. As seen in Section 4.1.2 the K_{ov} for ammonia is much lower than for water. The mass coefficient for ammonium hydroxide slightly increased with the concentration, which may indicate that the effect of polarisation of depletion is less significant at high ammonia concentrations than at low ones. However, the K_{ov} for ammonium bicarbonate decreased with the

concentration, possibly because of elevated salt concentrations limits mass transport of ammonia in the liquid phase.

Another aspect is how the water flux changes with different TAN concentrations compared to ammonia flux; this is done by using the selectivity (see Section 3.4.1) and is shown in Figure 35.

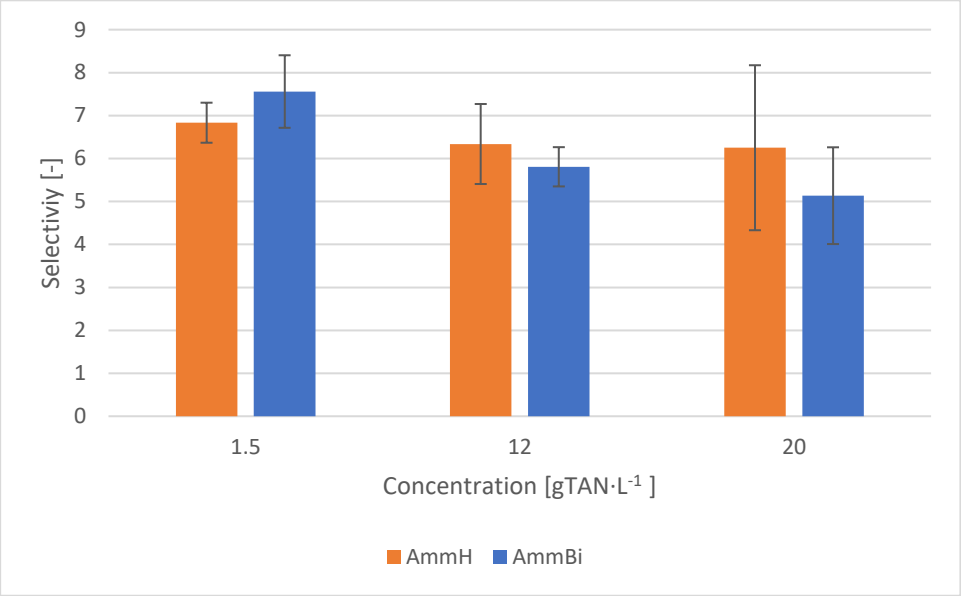

Figure 35 Ammonia selectivity for ammonium hydroxide and ammonium bicarbonate feed solution at different TAN concentrations.

The selectivity of ammonia of the VMS with both the ammonia carbonate and ammonium bicarbonate solutions decreased as the TAN concentration increased. The selectivity of both solutions decreased with concentration TAN in the feed. The selectivity of ammonium bicarbonate is initially higher than that of ammonium hydroxide, but the selectivity of ammonium hydroxide becomes higher at higher concentrations. A decrease in selectivity with higher TAN concentrations was expected, due to the ratio between the relation between the vapour pressures, of ammonia and water, and the mass percentage of the feed decreased with higher contractions (see Appendix B). The decrease in selectivity was predicted to be higher for ammonium hydroxide than for ammonium bicarbonate, which was not the case, suggesting an impact of polarisation effects.

In literature, the selectivity was reported to stay the same or decrease over feed concentration (see Section 1.3.2). The previous result from this project also showed a decrease in selectivity over feed concentration of TAN. The selectivity in Figure 35 also showed a decrease for both solutions and is therefore in line with literature and previous results.

The final goal of the research was to be able to produce permeate vapour with more than a 5m%NH_3. Therefore, the percentage was plotted over the TAN concentration, in Figure 36.

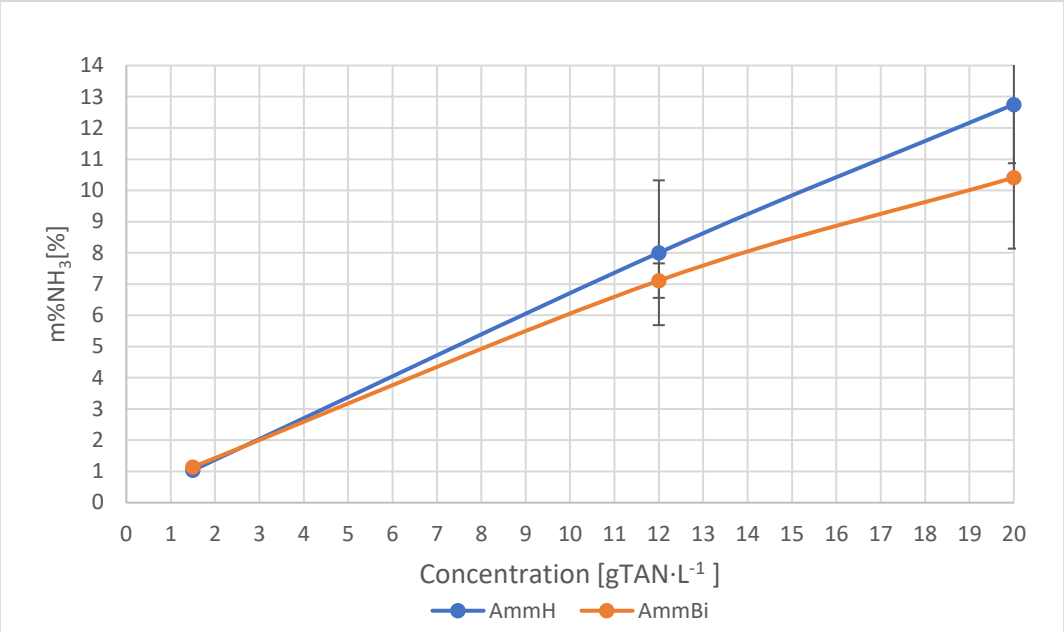

Figure 36 Mass percentage ammonia in the permeate for ammonium hydroxide and ammonium bicarbonate feed solution at different TAN concentrations.

The mass percentage of ammonium hydroxide exceeded that of ammonium bicarbonate at all concentrations besides the 1.5 gTAN·L^{-1} solution. The 5%mNH_3 limits for the SOFC were reached for both ammonium hydroxide and ammonia carbonate between 1.5 and 12 gTAN·L^{-1} in the feed solution. From Figure 36, it can be assumed that the 5m%NH_3 should be reached at a feed TAN concentration of approximately 7.5 gTAN·L^{-1} for ammonium hydroxide and around 8 gTAN·L^{-1} for ammonium bicarbonate.

4.3 Condensation of permeate vapour

To examine the effect of condensing of the permeate vapour on the ammonia concentration, the permeate experiment was performed with a condensing tube (see Section 3.2.1). The experiments utilised a concentration of 1.5 gTAN·L^{-1} of ammonium hydroxide solution.

4.3.1 Condensation of water

The first thing to look at is how much water the condensation tube was able to condensate.

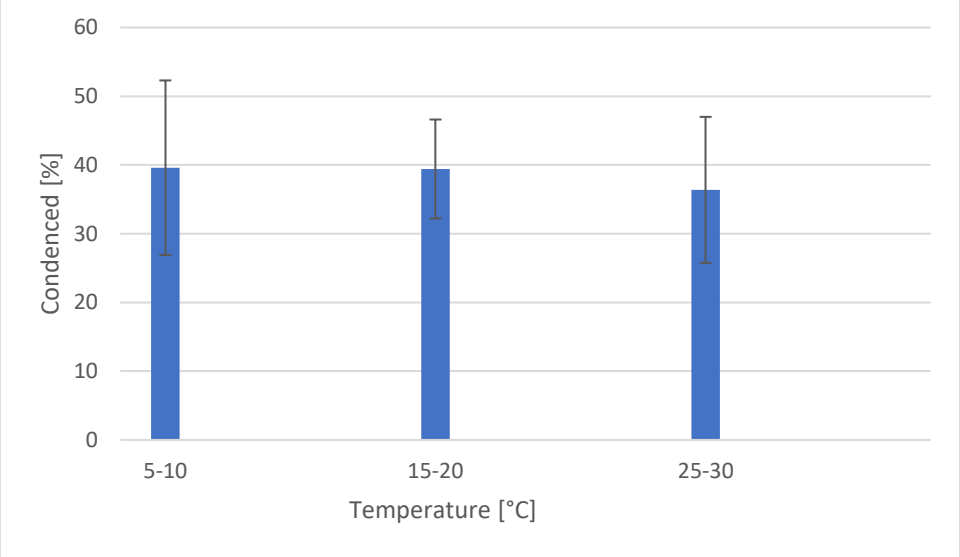

Figure 37 Percentage of permeate solution condensed in condensation tube.

Figure 37 reports the percentage of the solution that was condensed with the condensation tube. Since the error is considerable, it is difficult to describe the trends for the three temperature ranges. The condensation for all temperatures was slightly below 40% on average.

4.3.2 Concentration factor for ammonia

The most important parameter is how much the condensation managed to concentrate the ammonia in the permeate vapour. The concentration factor of the condensation was found and reported in Figure 38, for the different cooling water temperatures.

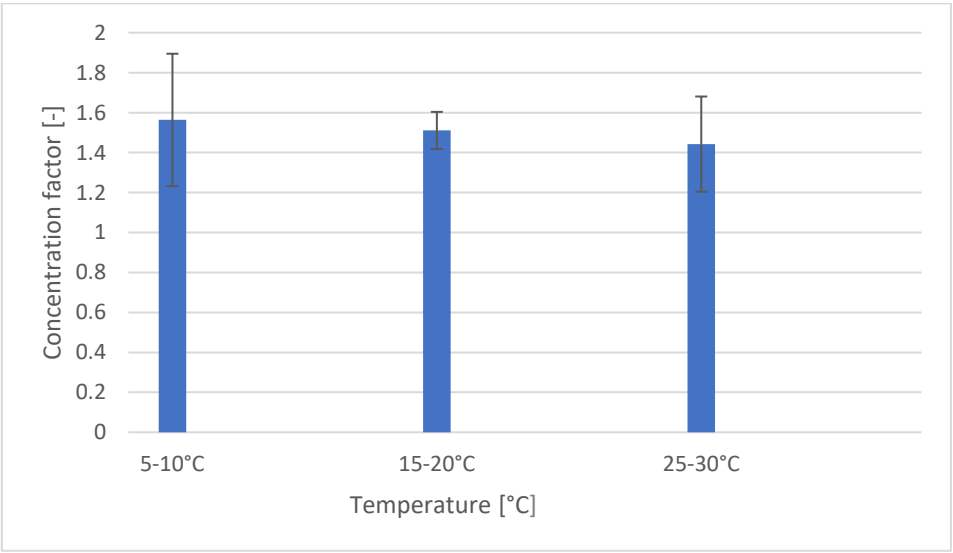

Figure 38 Concentration factor ammonia in permeate after concentration step with condensation

At all cooling water temperatures, an increase in the ammonia concentration from before the condensation was observed with a concentration factor above one. The concentration factor did also increase with the decreasing cooling water temperatures. This shows that condensation of the permeate vapour can concentrate the ammonia in the vapour phase.

The effect of condensation of the permeate vapour was reviewed in literature in Section 2.4. There it was found that condensing the permeate water was expected to concentrate the ammonia in the water. This is also what was found in the experiments done, confirming the expectation that condensation after VMS can increase the mass percentage of ammonia in the vapour. In the study of Philpott et al (2004) the m%NH_3 went from 10 to 24 in the vapour in the condensation tube, resulting in a concentration factor of 2.4, which is significantly higher than what was found in this study. This may suggest that the system still has the potential to be improved even further to increase the concentration factor.

4.3.3 Total concentration factor of the VMS with condensation

To assess whether the concentration factor influences the needed feed concertation some simple calculations were done.

Table 3 Total effect condensation on end quality vapour. Assuming same concentration factor for all concentrations

Concentration [gTAN·L^{-1}]	**%mNH4 feed [%]**	**Concentration factor VMS [-]**	**Concentration factor Condensation [-]**	**%mNH3 permeate vapor before condensing [%]**	**%mNH3 permeate vapor after condensation [%]**
1.5	0.15	6.83	1.56	1.03	1.54
12	1.21	6.34	1.56	7.65	11.48
20	2.02	6.25	1.56	12.63	18.94

Table 3 indicates the effect of condensation of the permeate vapour on the total concentration factor of the system for ammonium hydroxide. While it was insufficient to raise the 1.5 gTAN·L^{-1} above the set requirement of 5m%NH_3 that is needed for the SOFC, it did significantly raise the mass percentages for the 12 gTAN·L^{-1} and 20 gTAN·L^{-1} solution above the set requirement of 5m%NH_3.

If a selectivity of 6.83 is assumed, same as for 12 gTAN·L^{-1} between 1.5 gTAN·L^{-1} and 12 gTAN·L^{-1} and a condensation factor of 1.56, the 5m%NH_3 would be reached at around 5 gTAN·L^{-1} in the feed solution.

4.4 VMS with ammonia rich-industry water from amide production

In order to test fouling of the membrane, an extended analysis of the ammonia-rich industrial water was conducted first to identify contaminants that could lead to fouling the membrane. Secondly, tests were performed with synthetic wastewater that consisted of a solution of ammonium hydroxide with a concentration of 100 $gTAN \cdot L^{-1}$. The findings were then compared with the result of running the VMS with ammonia-rich industrial wastewater. In addition, the post-fouling membrane hydrophobic properties were tested by examining the contact angle of water on the surface.

4.4.1 Analysis ammonia rich-industry water

Some simple tests with the ammonia-rich industrial water were done and compared to synthetic wastewater, see Table 4. The ammonia concentrations of the unfiltered water and the synthetic water were comparable, whereas the filtered water had a slightly lower ammonia concentration. All concentrations were between 80 and 100 $gTAN \cdot L^{-1}$. The pH of the synthetic water was slightly higher than that of the actual wastewater but was above the pH limit of minimally 10 for all water solutions. Interestingly, the conductivity was the same for all three solutions. This suggests that no salts were present in the ammonia-rich industrial water, as one would otherwise expect a higher conductivity compared to the synthetic water. The synthetic water lacked any chemical oxygen demand (COD); however, the ammonia-rich industrial water contained a substantial amount of COD, which is supported by the information in Section 1.1.1.

Table 4 Comparison between results from simple analysis of synthetic wastewater and industrial ammonia-rich wastewater from amide production both filtered and unfiltered.

	Synthetic wastewater	**Industrial wastewater unfiltered**	**Industrial wastewater filtered**
Ammonia concentration [$gTAN \cdot L^{-1}$]	100±6	97±11	84±4
pH	12.16±0.16	11.58±0.21	11.52±0.06
Conductivity [$\mu S \cdot cm^{-1}$]	1124±7	1131±5	1128±9.2
COD [$gO_2 \cdot L^{-1}$]	Below detection limit	31.9	27.5

The findings in Table 10 predict organic fouling as a significant amount of COD indicates a high amount of organics in the waste water that can lead to organic fouling. However, no salt is present, which can lead to inorganic fouling.

4.4.2 VMS with actual wastewater

Synthetic wastewater vs Actual wastewater

To say something about the expected water and ammonia fluxes and the ammonia selectivity expected, firstly, a test with synthetic wastewater was performed, followed by the test with the actual wastewater. The result of the actual wastewater was compared with the result from the synthetic wastewater.

During one run with this high concentration of ammonia, the vapour pressure of ammonia was quite high in the feed and a high flux was observed this leads to a drastic drop in concentration of ammonia during one run, this is seen in Figure 39.

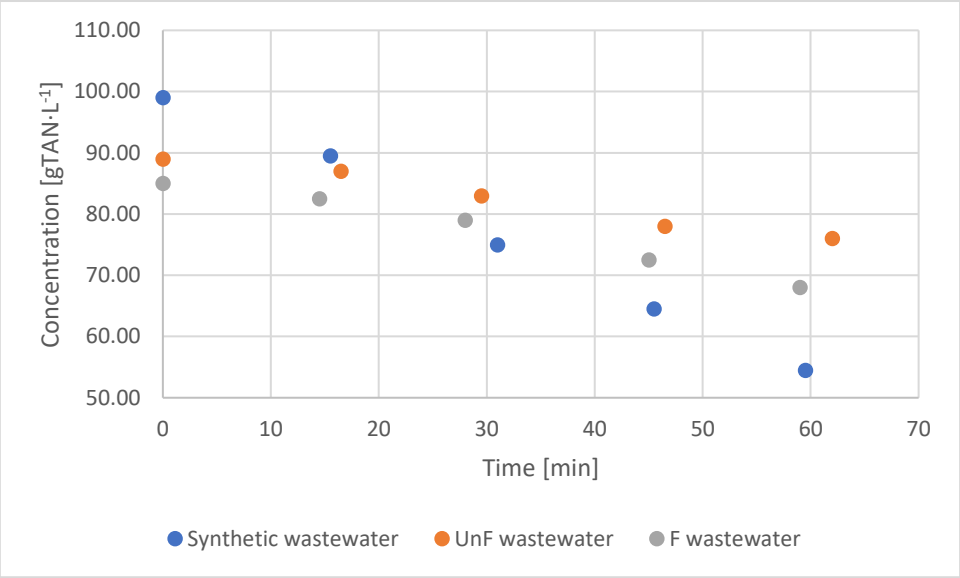

Figure 39 Ammonia concentration over time during VMS experiments with actual wastewater

In Figure 39 it is also clearly shown that the decrease in concentration is much larger for synthetic water than the filtered and the unfiltered ammonia-rich industrial wastewater. To assess this effect the average water flux and ammonia flux and the selectivity for the ammonium hydroxide solution of 100 gTAN·L^{-1} (synthetic water), the un-filtered ammonia-rich industrial wastewater (UnF wastewater) and filtered ammonia-rich wastewater (F wastewater) were compared in Figure 40.

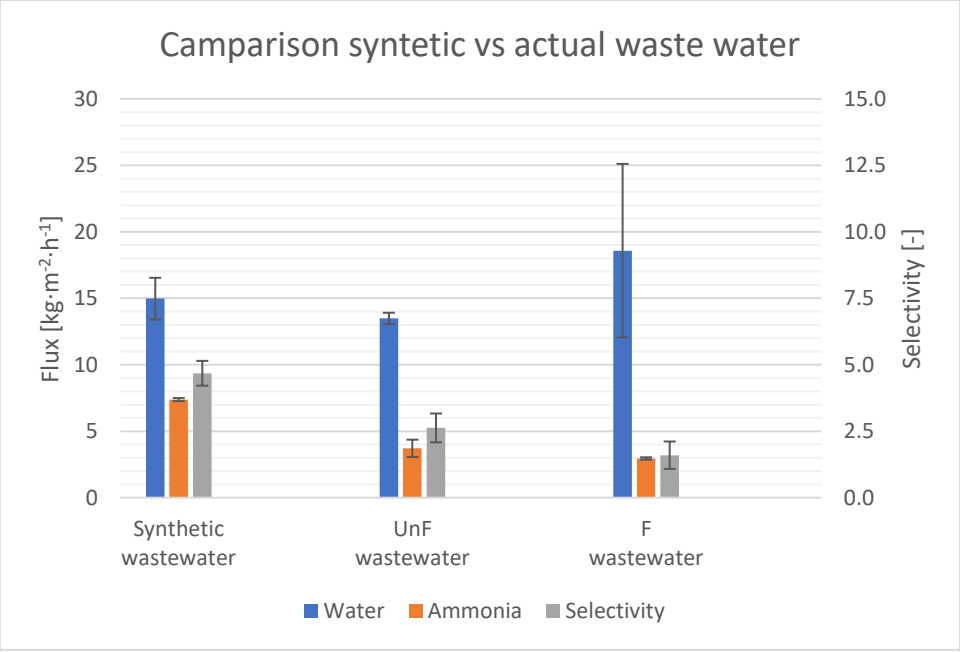

Figure 40 Comparison between results experiments with synthetic wastewater and industrial ammonia-rich wastewater from amide production both filtered and unfiltered.

The result of the synthetic water represents the expected outcome if no fouling occurs. The water flux of the UnF wastewater was comparable to that of the synthetic water; however, its ammonia flux and selectivity were much lower compared to the synthetic water. For the F wastewater, the water flux was substantially higher than that of the synthetic water. However, it has a high standard

deviation, while the ammonia flux was lower and comparable to the unfiltered water; therefore, the selectivity was even lower than of the unfiltered water.

The ammonia fluxes for the actual wastewaters were less than half of the expected figures, and the selectivity was nearly one for the filtered wastewater. This result implies that the water was partly sucked up in liquid form and no longer evaporated.

In Section 2.5.2 it is shown that with organic fouling the total flux of ultrafiltration is lowered. However, this was not necessarily the case for our membrane; the unfiltered water showed indeed a lower flux, whereas the filtered water even showed a slight increase in flux. However, ultrafiltration functions quite differently than VMS, which may explain this difference. As the pores are bigger and not necessarily blocked when fouled and the effect on the hydrophobicity of the membrane is more important (than? Or is hydrophobicity more important for VMS) for the performance of the VMS membranes.

Fouling observed

During the runs, it was seen that liquid in the form of foam was extracted from the membrane indicating that the liquid-gas interface was broken. It was clearly observed how foam was sucked into the acid trap. This also indicated that the organics were pushed through the membrane. This was confirmed with COD test done on the feed solution and of the acid traps at the end of a run. The COD concentration in the feed water after a run with the unfiltered and the filtered wastwater stayed aproximately the same with 27.5 $gO_2 \cdot L^{-1}$ and 31.9 $gO_2 \cdot L^{-1}$, respectively, before the VMS run and 26.9 $gO_2 \cdot L^{-1}$ and 32.0 $gO_2 \cdot L^{-1}$, resperctively, after the VMS run. In the acid trap, a COD of 2679 $mgO_2 \cdot L^{-1}$ was observed after the run with unfiltered water and 2422 $mgO_2 \cdot L^{-1}$ was observed after the filtered run.

4.4.3 Analysis of the membrane

The fouling on the membrane was analysed. Firstly, a visual analysis was done of the membrane right after the VMS run and later when the membrane had dried the permanent change was checked by measuring the contact angle of water on the membrane.

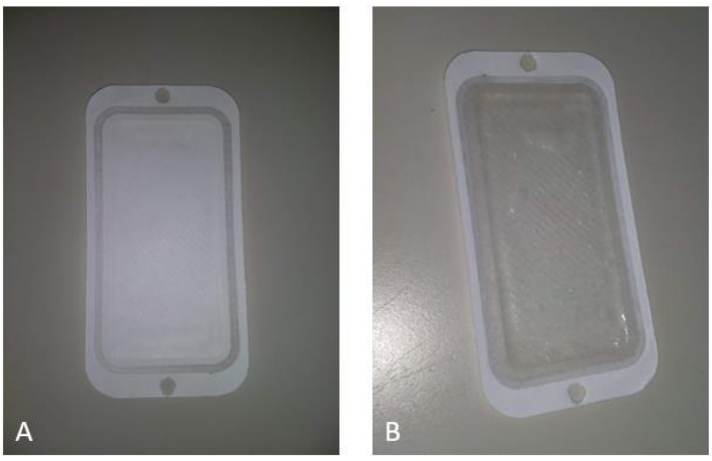

Figure 41 Picture of a membrane after a run with synthetic water(A) and after a run with the ammonia-rich industrial water from amide production (B).

The membranes showed signs of wetting after being run with the ammonia rich-industry water, as shown in Figure 41, where a clear difference can be seen between the clean membrane after a run

and the fouled membrane after a run. The clean membrane is not affected by the VMS run, while the left membrane has become transparent and has foam on it.

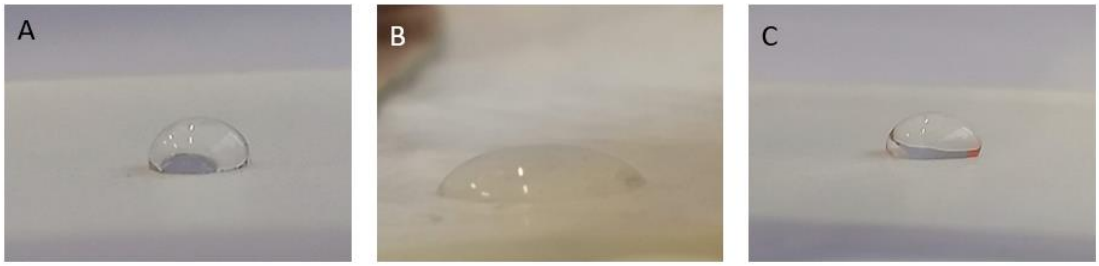

Figure 42 Water droplets on a clean membrane (A), membrane after run with UnF waste water(B) and after run with F waste water(C)

To see if the organics permanently changed the properties of the membrane or only during the VMS run a test of the contact angle of the membrane was done. In Figure 42 The different contact angles for a clean membrane, membrane after a run with UnF waste water run and membrane after a run with F waste water are shown. For the clean membrane (Picture A), the droplet clearly lays on top of the membrane and the angle was measured to be 115°, this indicates strong hydrophobic properties. For the run for the unfiltered water the surface is clearly hydrophilic with the contact angle being quite big with an angle of 52°. The last image shows the the droplet after the filtered run here closer to the clean membrane than the picture B, but still does have some wat bigger angle with an angle of 107°, this is still classified as a hydrophobic surface.

In Section 2.5.2 it was also predicted that organic fouling could change the hydrophobic properties of the membrane and make it more hydrophilic. This is in line with what is seen in the result presented above.

4.5 Energy balance

To determine whether the technology would be feasible in practice it is necessary to assess the energy needed for it to run the filtration and to evaluate the energy balance.

4.5.1 Thermal energy balance

Thermal energy is dependent only on the mass percentage of ammonia. The calculation used for energy calculation is described in Section 3.4.3. Thus, it is possible to compose a graph over a mass percentage without considering the feed solution to determine the permeate quality that is needed to be energetically beneficial.

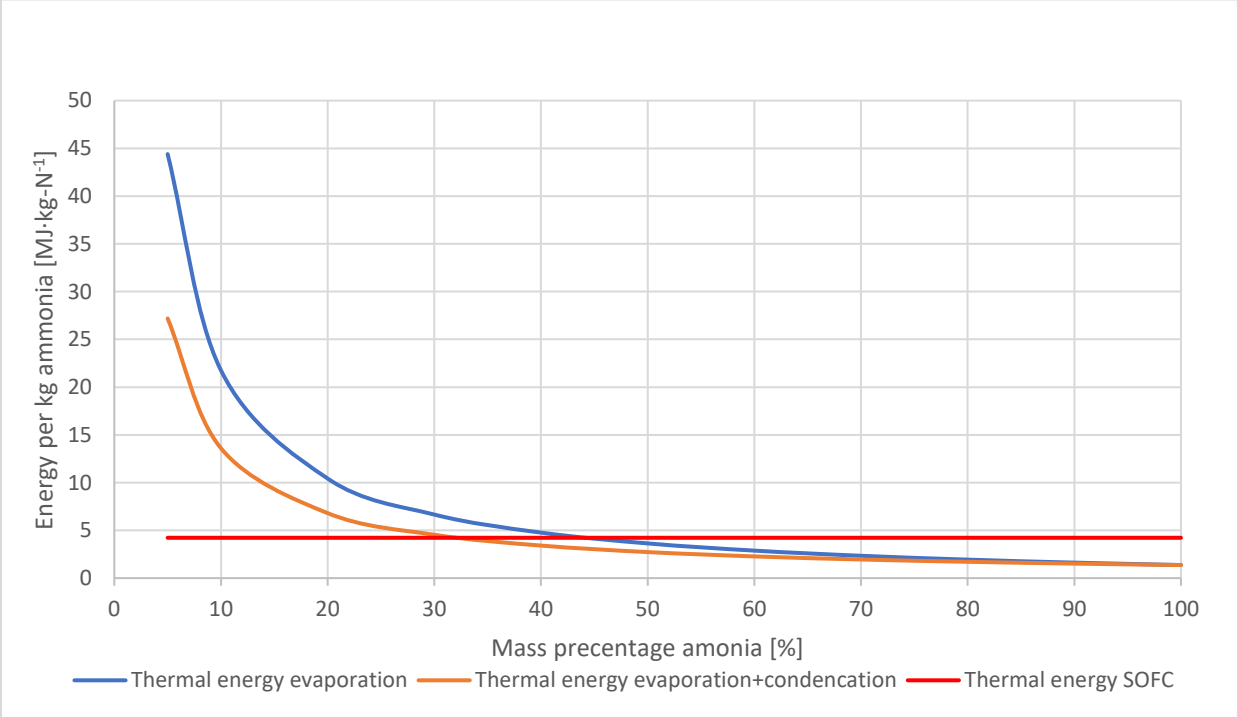

Figure 43 Graph showing the energy needed for evaporation, the energy needed for evaporation minus the heat recovered with condensation and the thermal energy produced in the SOFC over the m%NH_3 in the permeate.

Figure 43 establishes the amount of energy that is theoretically needed for evaporation of ammonia and water, the required amount of energy needed if the energy freed by condensation could be recovered and the theoretical thermal energy that is available from the SOFC for various mass percentages. The energy rapidly declines before levelling off. The thermal energy from the SOFC would meet the theoretically needed energy for evaporation at around 42m%NH_3 and for evaporation with the recovery of condensation heat at 32 m%NH_3. These m%NH_3 are for the permeate waters before condensation. These are the mass percentages of the permeate needed to make the system energy neutral in terms of thermal energy.

4.5.2 Total energy balance

The total energy balance consists of the necessary thermal energy and needed electrical energy. Section 3.4.3 describes the calculation of electrical energy and of thermal energy. The total energy is the energy that is needed plus the energy that has been obtained from the SOFC, which are 8.4 MJ·kg-N^{-1} electrical energy and 4.2 MJ·kg-N^{-1} thermal energy.

Table 5 specifies the electrical and thermal energies that are needed as well as the total electrical and thermal energies that are needed for the different synthetic feed solutions, without considering the energy that is recovered from condensation. Appendix D contains an example of the full calculation for the ammonium hydroxide solution of 1.5 gTAN·L^{-1} with turbulent flow and with laminar flow.

Table 5 Results of energy balance for different feed solutions with ammonium hydroxide and ammonium bicarbonate.

Solution	**Electrical energy [MJ·kg-N^{-1}]**	**Thermal energy [MJ·kg-N^{-1}]**	**Total Electrical Energy [MJ·kg-N^{-1}]**	**Total Thermal Energy [MJ·kg-N^{-1}]**
AmmH 1.5 gTAN·L^{1}	32.0	219.4	-23.5	-215.2
AmmH 1.5 gTAN·L^{1} Laminar	36.4	286.4	-28.0	-282.1
AmmH 12 gTAN·L^{1}	4.2	28.7	4.3	-24.5
AmmH 20 gTAN·L^{1}	2.5	17.0	5.9	-12.8
AmmH 100 gTAN·L^{1}	0.6	3.7	7.8	0.5
AmmBi 1.5 gTAN·L^{1}	28.2	198.2	-19.8	-194.0
AmmBi 1.5 gTAN·L^{1} Laminar	30.3	236.3	-21.9	-232.1
AmmBi 12 gTAN·L^{1}	4.8	31.4	3.7	-27.2
AmmBi 20 gTAN·L^{1}	3.4	20.9	5.1	-16.7

The only solution that was energetically positive was the 100 gTAN·L^{-1} ammonia solution with a surplus of 0.5 MJ·kg-N^{-1} thermal energy and 7.8 MJ·kg-N^{-1} electrical energy. All other solutions used more thermal energy than the SOFC could produce. The 12 gTAN·L^{-1} and 20 gTAN·L^{-1} solution for both ammonium hydroxide an ammonium bicarbonate have a surplus of electrical energy when run, this does however not cover the missing thermal energy.

In addition, the laminar flow runs for ammonium hydroxide and ammonium bicarbonate both used more thermal energy and electrical energy per kilogram of ammonia than the equivalent turbulent run. This implies that turbulent flow is more energy beneficial per kilogram ammonia than laminar flow.

These results do not consider the effect of condensation on the energy used because it is hard to say anything about the condensation as this is not investigated fully. However, if an estimate is made assuming only water is condensed for the 1.5 gTAN·L^{-1}, 12 gTAN·L^{-1} and the 20 gTAN·L^{-1} 91%, 93% and 88% of the water in the permeate needs to be condensed, respectively, to get the thermal heat below 4.2 MJ·kg-N^{-1}.

5 Discussion

5.1 Effect of cross-flow velocity

To determine the transition from laminar to turbulent flow, only the demi-water and the salt solution were tested experimentally. There may be some deviation for the ammonium hydroxide and the ammonia bicarbonate solutions. To be sure this would not influence the results, the experiments were conducted further inside the turbulent and laminar region and not at the edge. Due to the differences being insignificant for the flux inside the laminar and the turbulent flow region, this would be enough to determine a preferable cross-flow.

To decide whether it is preferable to work in a laminar or a turbulent condition for the selectivity of ammonia, only 1.5 $gTAN \cdot L^{-1}$ ammonium hydroxide and ammonium bicarbonate solutions were used. However, according to Section 4.2.1, the concentration of the solution may significantly change the selectivity. Therefore, it is possible that the deviation between turbulent and laminar flows may change at different concentrations, but this is not to be expected.

5.2 Effect of Salt

To determine the vapour pressures of dissolved ammonia in the ammonium hydroxide and ammonium bicarbonate solutions, PHREEQC simulation was used. The values varied slightly, depending upon which PHREEQC database was used to simulate the vapour pressure, since the different databases give slightly different input values. Therefore, this is more an estimation than a set answer.

Additionally, the simulated value may not reflect the real-life value if a slightly different composition of water was used compared to the value in PHREEQC. A simulation is often a simplification of the real world. Moreover, the real water may be slightly different to that used as input for PHREEQC.

The biggest problem is that it is difficult to determine which mechanisms are behind the result in Section 4.2.1, as only the simulated vapour pressures at the bulk and the global K_{ov} were found. It is not possible to establish certain conclusions about what is happening between the feed bulk and the permeate, as there is a lack of information about polarisation effects and mass transport coefficients in the feed and in the membrane.

5.3 Condensation of permeate vapour

The experiment involved a simple setup that was not optimised in any way. Thus, there is probably ample room to improve the result, and it is expected that optimised systems can achieve higher condensation percentages and concentration factors.

When assessing the amount of ammonia that was caught in the condensation tube and that the rest remained in the vapour and was not found elsewhere in the system the ammonia vapour was captured in the acid trap. The acid trap which was then weighed, and the concentration was measured to create a full mass balance (see Appendix C). From the ammonia mass balance, it was found that besides one run with a loss of 38% and one with 16% of ammonia not accounted for, the rest had no more deviation than ±10% from a complete mass balance. The unaccounted-for ammonia can also be due to measuring errors. The mass balance also proves that there were most likely no significant leaks of ammonia in the setup for the other VMS experiments either.

All experiments utilised a 1.5 $gTAN \cdot L^{-1}$ ammonium hydroxide solution. To be able to do calculations with other solutions it was assumed that the concentration factor, condensed amount of water and condensed ammonia would be the same for other solutions as well. This was not necessarily the

case, as a higher ammonia concentration may influence the amount of water and condensed ammonia. Therefore, these results are only a rough estimate.

5.4 Membrane fouling

The result is unpromising when directly using the ammonia-rich industrial wastewater in the VMS. The flux of ammonia and the selectivity were substantially lower than expected. Also, the interaction with organics in the wastewater caused the membrane to lose its hydrophobic properties. In view of this, VMS may not be a suitable method to strip ammonia from this type of wastewater.

Because the removal of organics would be a difficult task, an alternative method without the membrane is advised. However, such a method would require a larger footprint. A simple setup of vacuum stripping without the membrane was tested (see Appendix E). In this test, it was confirmed that vacuum stripping could be an option if anti-foamant was added.

The discouraging result for this wastewater with a high concentration of organics does not mean that VMS may not be an alternative for other types of wastewater. On the contrary, the membrane seems to work with a high salt concentration (see Section 4.2.1); the results were somewhat lower compared to a sample without salt. Nevertheless, there is a clear selectivity for ammonia, and little or no fouling of the membrane was observed in the tests without organics.

As the membrane was severely fouled after a short run in the test with real wastewater, it was not possible to test the effect of cross-flow velocity for this type of fouling. Thus, no conclusions could be made about the effect of cross-flow on fouling.

5.5 Energy

The calculation of the thermal heat that is needed is only theoretical. Only the evaporation is included, so heat loss to the surroundings is not considered, and it is assumed that the system is perfectly isolated. However, this is never the case, as some heat is always lost to the surroundings. Thus, the amount of heat needed is underestimated, and some additional thermal heat is likely to be necessary.

The estimate of heat derived from condensation was made under the assumption that all heat can be recovered. That is incorrect, as heat is also lost, and no heat exchanger is 100% efficient. However, this can still be used as an estimate.

Moreover, it is assumed that 40% of water is condensed with no ammonia. This is not the case, as some ammonia will always diffuse into the condensed water. Also, the 40% is slightly higher than the results from Section 4.3.1. However, our system is not optimised, therefore, more water may be condensed with a better setup.

Another improvement is that the condensed water was left in the system during the run. Removing the condensed water continually would lower the extent of ammonia diffused into the water. Thus, while the assumption may not be fully correct, it indicates how much energy can be recovered with condensation. This is why the recovered energy from condensation is not included in Table 5.

The calculation of the potential energy for the SOFC uses the theoretical energy in ammonia and the efficiency of SOFC found in the literature (see Section 1.2.3). However, this energy is significantly higher than the energy produces with a test with the SOFC done in our project for vapour with 5%mNH_3. This means that the practical energy released by the SOFC can be lower than what is used in the calculations.

For the feed pump, theoretical energy is used. This means that this is most likely an underestimation, and most pumps would need more energy to handle the same heat and flow, due to friction in the pump and energy lost to the surroundings. The result for the vacuum pump comes from data obtained from industry. Here it is not known whether the energy may change if the vacuum pump used is of a different scale. This means that those values had to be seen as estimates and not set values.

Only the 100 $gTAN \cdot L^{-1}$ ammonium hydroxide solution was energy positive. Accordingly, all other solutions required more energy than they produced. Nevertheless, the technology could still be feasible. Current methods to remove ammonia also use extensive energy. Therefore, if only a small amount of energy is needed it would still be better than current methods.

Furthermore, much of the energy that is needed is thermal heat. Residual heat is often available, especially in industrial areas. The system only needs to be heated to 35°C, and even low-grade waste heat can be harnessed to heat the water. This energy would most likely otherwise be lost.

The energy balance does not consider the energy that may be needed to pre-concentrate the wastewaters before using the VMS to extract ammonia. As almost all energy produced with SOFC may be needed for ED (see Section 1.2.1), there will most likely be no net energy production. This means that for wastewater below 12 $gTAN \cdot L^{-1}$ where another concentration step before the VMS is needed, the electrical energy that may be produced could be lost in the energy needed for the pre-concentration.

5.6 General

Most experiments were duplicated or triplicated to minimise possible random errors from the measurements. However, remarkable errors still emerged in some results, such as in Figure 26 and 36, which made it challenging to draw conclusions. This limitation could be avoided by performing more replications. In addition, adding further data points may lower the standard deviation found and help to clarify trends.

Many of the graphs present an average result over a one-hour run. However, conditions can change in one hour as the ammonia is removed from the water. Therefore, during a run, the ammonia concentration decreased together with the pH, and the conductivity increased. This could account for some of the large errors in the results, especially for the water fluxes.

It was assumed that CO_2 vapour pressures could be neglected as the experiments applied a pH value of 10. This assumption may be inaccurate, as some CO_2 may still be present in the solution and influence the result. This is because the pH may start at 10, but was slightly lower at the end of the experiments. Also, the pH at the membrane could be different to what was measured at the bulk. However, a pH of 10 is far above a pH of 8 where no CO_2 is suspected in the water, and therefore this should not be a problem in terms of CO_2.

The last assumption was that most of the TAN was ammonia and not ammonium at 10 pH. However, in reality, a small amount is still ammonium. The pH at the membrane is not known and might influence the real vapour pressure of ammonia at the membrane.

6 Conclusion

Section 1.3.3 identified five research topics and proposed research questions for each topic. This report attempts to answer these questions. The following conclusions can be drawn on the basis of the present work:

6.1 Effect of cross-flow velocity

What cross-flow velocity is preferable in terms of flux and selectivity?

The increase in the ammonia flux is more significant than the increase in the water flux when increasing the cross-flow from laminar to turbulent. After a turbulent flow was reached, no more improvement was seen. Thus, it was found that VMS that runs on a turbulent flow has improved selectivity. In view of this, turbulent cross-flow should be chosen to optimise the ammonia concentration in the vapour, but to limit energy consumption the cross-flow should not be increased further once a turbulent flow is reached.

6.2 Effect of Salt

What effect does ionic strength have on the vapour pressure of dissolved ammonia?

To determine the effect of salt on vapour pressure, PHREEQC simulations were performed (see Section 2.2.3). As Figure 15 reveals, an increase in salt concentration would increase the vapour pressure of ammonia in a water solution.

How does the salt concentration in the feed water affect the ammonia selectivity?

Experiments were carried out with ammonium hydroxide, which has low ionic strength, and ammonium bicarbonate, which has higher ionic strength. The experimental result showed a lower ammonia flux for ammonium bicarbonate that includes salts than for ammonium hydroxide that does not include salts. The water flux is also lowered for ammonium bicarbonate whereas it is increased for ammonium hydroxide, with increasing TAN concentration. The selectivity for both ammonium hydroxide and ammonium bicarbonate decreased with increasing concentration of TAN in the feed solution, but the decrease in ammonium bicarbonate was more rapid and went from being higher than ammonium hydroxide to being lower. It may be concluded that salt does lower the selectivity at high concentration. At moderate concentration it may, however, increase the selectivity.

6.3 Condensation of permeate vapour

Will only water condensate from the permeate vapour mixture of VMS, or will ammonia diffuse into the condensate?

The concentration of ammonia found in the condensate water was lower than the concentration in the permeate. Therefore, it can be concluded that some ammonia will diffuse into the condensate water, but that this process is slower than the condensation of water.

To what extent will ammonia in the permeate vapour mixture of VMS be concentrated with the condensation of permeate vapour?

As the diffusion of ammonia into the water was lower than the condensation of water, an increase in ammonia concentration in the permeate vapour was observed. With the use of the relatively simple system, a concentration factor of 1.5 was reached. This result is quite promising as it can likely be improved further by optimising the system.

What is the lowest TAN concentration of feed water that reaches the goal of 5m%NH_3 in the permeate to make ammonia fuel for SOFC with the VMS + condensation?

Condensation of the vapour increases the ammonia concentration. However, the system still cannot directly utilise reject water. It was shown that the SOFC can use water with a concentration above 5 $gTAN \cdot L^{-1}$ without pre-treatment and still reach the requirement of 5 m%NH_3 in the SOFC fuel.

6.4 Membrane fouling

The membrane was fouled to such a degree that VMS for this wastewater can be disregarded as a feasible stripping method. The fouling led to wetting of membrane, which changed its properties from hydrophobic to hydrophilic and no longer reinforced a strict liquid-vapour interface. Consequently, the vacuum sucked up liquid.

What compounds found in the wastewater can lead to fouling of the membrane, and how can this be avoided?

A high COD concentration of 31.9 $gO_2 \cdot L^{-1}$ was found in the wastewater, and this was thought to be the main risk factor for fouling. Fouling was observed when the VMS was run with the real wastewater, which led to the membrane's properties changing.

What is the effect of the fouling components on the water and ammonia flux?

Due to the fouling changes the properties of the membrane from hydrophilic to hydrophobic, the liquid-vapour interface is no longer present. This resulted in that the ammonia flux was 50% and 40% of what was reached with VMS with synthetic water for VMS with unfiltered industrial wastewater and filtered industry wastewater. The water fluxes remained approximately the same.

How does fouling affect the selectivity of the membrane for ammonia?

It lowers it drastically, from a selectivity of 4.7 for the VMS with synthetic water to a selectivity of 2.6 and 1.6 for VMS with unfiltered and filtered industrial wastewater respectively. This is most likely due to the fatty acids acting as surfactants and changing the membrane from hydrophobic to hydrophilic, not introducing any clear liquid-vapour interface at the membrane.

How does the cross-flow velocity influence fouling?

This aspect was not tested, because the fouling was extensive enough to deem the use of VMS unsuitable to strip ammonia from ammonia-rich industrial wastewater.

6.5 Energy requirements for stripping

In terms of energy, is it possible to use VMS in combination with an SOFC to produce energy? When is extracting more ammonia no longer feasible in terms of energy and fuel restrictions of the SOFC (m%NH_3)?

On its own, the ammonia concentration in the feed must be above around 100 $gTAN \cdot L^{-1}$ for a system to be energetically positive. However, in combination with the use of waste heat, it could still be a suitable option to use feed solution of 12 $gTAN \cdot L^{-1}$. At this point, the concentration restriction to use the SOFC to produce energy is reached (5m%NH_3) and the system is still beneficial in terms of electrical energy.

How does cross-flow velocity influence energy consumption?

As Table 5 indicates, the total energy was higher for laminar flow than for turbulent flow. This result is due to the fact that lower selectivity with laminar flow reduces the amount of ammonia produced

compared to the amount of permeate vapour, which increases the energy needed to produce a kilogram of ammonia. This effect is much more significant than the energy saved by lowering the energy needed to achieve the desired cross-flow.

Considering energy, material cost, selectivity and fouling, is there an optimum velocity?

A state of turbulent flow is preferable for both the energy balance and the selectivity. The material cost would also be the same. The fouling was not analysed. However, progressing from turbulent to more turbulent seemed to hardly have an effect on the water flux (see Section 4.1.1). Therefore, further increasing the cross-flow after reaching a turbulent flow would lead only to higher energy costs for pumping.

6.6 General

The main goal of this thesis was to get a better understanding of the mass transport mechanisms in the VMS and to go from synthetically made wastewater to real wastewater when experimenting with VMS. Some understanding of the mass transport mechanisms where achieved. However, due to extensive fouling, the extraction of ammonia was not successful. However, this does not mean that VMS technology cannot be used to extract ammonia from another type of wastewater than the industrial ammonia-rich wastewater from amide production tested in this thesis. However, this would be needed to be tested further.

7 Recommendations for further research

Some major advances were made towards the use of real wastewater in the VMS module to produce ammonia gas. However, some hurdles still need to be overcome.

The understanding of the effect of different flow regimes is progressing quite well; the effect of salt in synthetic water was also thoroughly researched. However, some issues may still need further investigation, such as higher concentrations of ammonia and salt with laminar flow. In addition, more theoretical work may be needed to fully understand the polarisation effect.

The effect of ion strength was described quite extensively. However, the mechanisms behind that effect could be subjected to additional study. The overall mass transport coefficient was found, but it was not possible to divide it between the mass transport coefficient for the feed and the membrane.

It was proven that condensing the permeate vapour would increase the ammonia concentration in the vapour. However, this was done with quite simple experiments, and only simple attempts were made to optimise the process. Therefore, it would be advisable to further optimise the setup to increase the concentration factor.

The result of the VMS test with industrial ammonia-rich wastewater from amide production was not promising. A simple test with vacuum stripping was performed (see Appendix E). As with condensation, this was more a proof of principle instead of a full test. Thus, more research is needed before concluding on the potential effectiveness of this method.

Moreover, other potential wastewaters still need to be tested. The method may not work with wastewaters with high organic concentration. However, this does not mean that all types of wastewaters are off-limit. It would be advisable to test more types of wastewater in the VMS, maybe in combination with ED and condensation of the permeate vapour, to achieve the desired concentration of the vapour required for the SOFC.

Another point for research is to add the pre-concentration steps into the energy balance. Only the VMS and SOFC were included in this thesis, but most types of wastewater would need a pre-concentration step prior to being used in the SOFC. This would cost energy; therefore, the total balance should be made including ED.

8 Bibliography

Amin, I. N. H. M., Mohammad, A. W., Markom, M., & Peng, L. C. (2010). Effects of palm oil-based fatty acids on fouling of ultrafiltration membranes during the clarification of glycerin-rich solution. *Journal of Food Engineering*, *101*(3), 264–272. https://doi.org/10.1016/j.jfoodeng.2010.07.006

Amin, I. N. H. M., Mohammad, A. W., Markom, M., Peng, L. C., & Hilal, N. (2010). Flux decline study during ultrafiltration of glycerin-rich fatty acid solutions. *Journal of Membrane Science*, *351*(1–2), 75–86. https://doi.org/10.1016/j.memsci.2010.01.033

Atkins, P., & De Paula, J. (2006). *Atkins' Physical chemistry* (8th ed.). Oxford University Press.

Bandini, S., Gostoli, C., & Sarti, G. C. (1992). Separation efficiency in vacuum membrane distillation. *Journal of Membrane Science*, *73*(2–3), 217–229. https://doi.org/10.1016/0376-7388(92)80131-3

Barnes, G. T., & Gentle, I. R. (2005). *interfacial science: an introduction* (2nd ed.). Oxford University Press.

Brilman, D. W. F., van der Hoef, M. A., & Weinhart, T. (2015). *Transport Phenomena*. Enschede: Universiteit Twente.

Brinck, J., Jönsson, A. S., Jönsson, B., & Lindau, J. (2000). Influence of pH on the adsorptive fouling of ultrafiltration membranes by fatty acid. *Journal of Membrane Science*, *164*(1–2), 187–194. https://doi.org/10.1016/S0376-7388(99)00212-4

Da Costa, A. R., Fane, A. G., & Wiley, D. E. (1994). Spacer characterization and pressure drop modeling in spacer-filled channels.pdf. *Journal of Membrane Science*, *87*, 79–98.

Dekker, N., & Rietveld, B. (2005). Highly Efficient Conversion of Ammonia in Electricity By Solid Oxide Fuel Cells. *Journal of Fuel Cell Science and Technology*, *3*(5), 499.

Ding, Z., Liu, L., Li, Z., Ma, R., & Yang, Z. (2006). Experimental study of ammonia removal from water by membrane distillation (MD): The comparison of three configurations. *Journal of Membrane Science*, *286*(1–2), 93–103. https://doi.org/10.1016/j.memsci.2006.09.015

Dodds, W. K., & Whiles, M. R. (2010). *Freschwater ecology* (2nd ed.). Academic Press. https://doi.org/10.1016/B978-0-12-374724-2.00013-1

El-Bourawi, M. S., Ding, Z., Ma, R., & Khayet, M. (2006). A framework for better understanding membrane distillation separation process. *Journal of Membrane Science*, *285*(1–2), 4–29. https://doi.org/10.1016/j.memsci.2006.08.002

EL-Bourawi, M. S., Khayet, M., Ma, R., Ding, Z., Li, Z., & Zhang, X. (2007). Application of vacuum membrane distillation for ammonia removal. *Journal of Membrane Science*, *301*(1–2), 200–209. https://doi.org/10.1016/j.memsci.2007.06.021

Fernandez-Gonzalez, C., Dominguez-Ramos, A., Ibañez, R., Chen, Y., & Irabien, A. (2017). Valorization of desalination brines by electrodialysis with bipolar membranes using nanocomposite anion exchange membranes. *Desalination*, *406*, 16–24. https://doi.org/10.1016/J.DESAL.2016.07.033

Görgényi, M., Dewulf, J., Van Langenhove, H., & Héberger, K. (2006). Aqueous salting-out effect of inorganic cations and anions on non-electrolytes. *Chemosphere*, *65*(5), 802–810. https://doi.org/10.1016/j.chemosphere.2006.03.029

Gu, Y., Li, Y., Li, X., Luo, P., Wang, H., Robinson, Z. P., … Li, F. (2017). The feasibility and challenges of energy self-sufficient wastewater treatment plants. *Applied Energy*, *204*, 1463–1475.

https://doi.org/10.1016/j.apenergy.2017.02.069

Guo, W., Ngo, H. H., & Li, J. (2012). A mini-review on membrane fouling. *Bioresource Technology*, *122*, 27–34. https://doi.org/10.1016/j.biortech.2012.04.089

He, Q., Tu, T., Yan, S., Yang, X., Duke, M., Zhang, Y., & Zhao, S. (2018). Relating water vapor transfer to ammonia recovery from biogas slurry by vacuum membrane distillation. *Separation and Purification Technology*, *191*(August 2017), 182–191. https://doi.org/10.1016/j.seppur.2017.09.030

Helmenstine, A. (2014). What Are Electrolytes? - Strong, Weak, and Non Electrolytes. Retrieved June 17, 2018, from https://sciencenotes.org/electrolytes-strong-weak-and-non-electrolytes/

Hoeft, C. E., & Zollars, R. L. (1996). Adsorption of single anionic surfactants on hydrophobic surfaces. *Journal of Colloid and Interface Science*, *177*(1), 171–178. https://doi.org/10.1006/jcis.1996.0018

Housecrofts, C. E., & Constable, E. C. (2010). *Chemistry* (4th ed.). essex: Pearson Education Limited.

Izquierdo-Gil, M. A., & Jonsson, G. (2003). Factors affecting flux and ethanol separation performance in vacuum membrane distillation (VMD). *Journal of Membrane Science*, *214*(1), 113–130. https://doi.org/10.1016/S0376-7388(02)00540-9

Johansson, O., & Wedborg, M. (1980). *The Ammonia-Ammonium Equilibrium in Seawater at Temperatures Between 5 and 25~*. *Journal of Solution Chemistry* (Vol. 9).

Jönsson, H., Stenström, T.-A., Svensson, J., & Sundin, A. (1997). Source separated urine-nutrient and heavy metal content, water saving and faecal contamination. *Water Science and Technology*, *35*(9).

Karwowska, B., Sperczyńska, E., & Wiśniowska, E. (2016). Characteristics of reject waters and condensates generated during drying of sewage sludge from selected wastewater treatment plants. *Desalination and Water Treatment*, *57*(3), 1176–1183. https://doi.org/10.1080/19443994.2014.989633

Khayet, M., & Matsuura, T. (2011). *Vacuum Membrane Distillation*. *Membrane Distillation*. https://doi.org/10.1016/B978-0-444-53126-1.10012-0

Krakat, N., Demirel, B., Anjum, R., & Dietz, D. (2017). Methods of ammonia removal in anaerobic digestion: a review. *Water Science and Technology*, *76*(8), 1925–1938. https://doi.org/10.2166/wst.2017.406

Lambot, S., Slob, E. C., Van Bosch, I. Den, Stockbroeckx, B., & Vanclooster, M. (2004). Modeling of ground-penetrating radar for accurate characterization of subsurface electric properties. *IEEE Transactions on Geoscience and Remote Sensing*, *42*(11), 2555–2568. https://doi.org/10.1109/TGRS.2004.834800

Martens, E. L. J. (2017). *Vacuum membrane distillation for the production of ammonia fuel gas for solid oxide fuel cells*. (Unpublisched master thesis) TU delft.

Masterton, W. L., & Lee, T. P. (1970). Salting coefficients from scaled particle theory. *Journal of Physical Chemistry*, *74*(8), 1776–1782. https://doi.org/10.1021/j100703a020

Mei, Y., & Tang, C. Y. (2018). Recent developments and future perspectives of reverse electrodialysis technology: A review. *Desalination*, *425*, 156–174. https://doi.org/10.1016/J.DESAL.2017.10.021

Mojab, S. M., Pollard, A., Pharoah, J. G., Beale, S. B., & Hanff, E. S. (2014). Unsteady Laminar to

Turbulent Flow in a Spacer-Filled Channel. *Flow, Turbulence and Combustion*, *92*(1–2), 563–577. https://doi.org/10.1007/s10494-013-9514-4

Neuss, G. (2007). *IB study guide Chemistry* (2nd ed.). New York: Oxford University Press.

Okanishi, T., Okura, K., Srifa, A., Muroyama, H., Matsui, T., Kishimoto, M., … Eguchi, K. (2017). Comparative Study of Ammonia-fueled Solid Oxide Fuel Cell Systems. *Fuel Cells*, *17*(3), 383–390. https://doi.org/10.1002/fuce.201600165

Philpott, C., & Deans, J. (2004). The Condensation of Ammonia-Water Mixtures in a Horizontal Shell and Tube Condenser. *Journal of Heat Transfer*, *126*(4), 527. https://doi.org/10.1115/1.1778188

Priyananda, P., & Chen, V. (2006). Flux decline during ultrafiltration of protein-fatty acid mixtures. *Journal of Membrane Science*, *273*(1–2), 58–67. https://doi.org/10.1016/j.memsci.2005.11.021

Schock, G., & Miquel, A. (1987). Mass transfer and pressure loss in spiral wound modules. *Desalination*, *64*(C), 339–352. https://doi.org/10.1016/0011-9164(87)90107-X

Stambouli, A. B., & Traversa, E. (2002). Solid oxide fuel cells (SOFCs): A review of an environmentally clean and efficient source of energy. *Renewable and Sustainable Energy Reviews*, *6*(5), 433–455. https://doi.org/10.1016/S1364-0321(02)00014-X

van Breukelen, B. (2016). Module 5 Chemical Reactions. Retrieved from Blackboard

van Linden, N. (2017). N2kWh – from Pollutant to Power. *(Poster) TU Delft*.

Van Zalen, J. W. (2012). *Optimization of a fuel cell system running on ammonia from a wastewater treatment*. (Unpublisched master thesis) TU delft.

Wang, L., Li, B., Gao, X., Wang, Q., Lu, J., Wang, Y., & Wang, S. (2014). Study of membrane fouling in cross-flow vacuum membrane distillation. *Separation and Purification Technology*, *122*, 133–143. https://doi.org/10.1016/j.seppur.2013.10.031

Wilsenach, J., & van Loosdrecht, M. (2003). Impact of separate urine collection on wastewater treatment systems. *Water Science and Technology*, *48*(1), 103–110. https://doi.org/10.2166/wst.2003.0027

You, W.-T., Xu, Z.-L., Dong, Z.-Q., & Zhang, M. (2015). Vacuum membrane distillation–crystallization process of high ammonium salt solutions. *Desalination and Water Treatment*, *55*(2), 368–380. https://doi.org/10.1080/19443994.2014.922499

You, W. T., Xu, Z. L., Dong, Z. Q., & Zhao, Y. J. (2014). Separated performances of ammonium sulphate and ammonium chloride solutions treated by vacuum membrane distillation. *Canadian Journal of Chemical Engineering*, *92*(7), 1306–1313. https://doi.org/10.1002/cjce.21968

Appendix A Hydraulic diameter

This section is based on work done by Niels van Linden.

The hydraulic diameter is crucial for the determination of the hydraulic conditions in flow channels. However, determination hydraulic diameter in spacer-filled channels ($d_{h,sfc}$) is not as straightforward as the hydraulic diameter of an open channel.

To be able to do this Schock et al. (1987) proposed an analogy for spacer-filled channels with packed columns based on volume flow channel (V_c) and total surface area wetted ($A_{t,w}$). The analogy can be found in Equation 68.

$$d_{h,sfc} = \frac{4 * V_c}{A_{t,w}} \tag{68}$$

This equation is correlated to a single mesh, considering that each spacer filament is part of two meshes. Figure 44 shows the dimensions of one mesh.

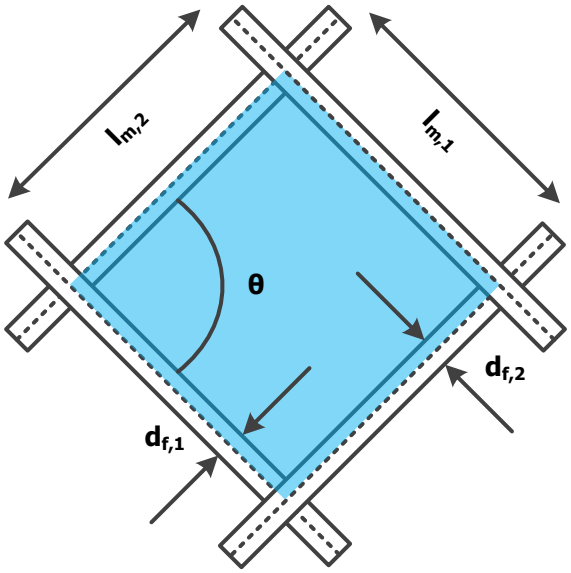

Figure 44 An overview of the dimension in a single spacer mesh. The blue area represents the wetted area.

The flow channel volume refers to the available volume where the water can flow through. The flow channel volume(V_c) is expressed as in Equation 69.

$$V_c = V_t - V_s \tag{69}$$

where the volume of the channel is found with the help of the total volume of the flow cell (V_t) and the volume of the spacer (V_s). This equation is based on the work by Schock et al. (1987).

The total volume considers both the void and the spacer volume and is a function of the considered area and the channel height. It is important to mention that spacer filaments are partially integrated at the crossings, resulting in the assumption that the height of a spacer-filled channel is not the sum of the filaments' thicknesses. Instead, this parameter should be measured, as well as the other dimensions of the spacer.

The considered area can be determined by the distances between the filaments ($l_{m,i}$) and the angle between them and the height of the channel (h_c). The expression for the total volume is shown in Equation 70 (Da Costa et al., 1994).

$$V_t = l_{m,1} \cdot l_{m,2} \cdot sin\theta \cdot h_c \quad (70)$$

e spacer volume is derived from the physical dimensions of the spacer: the diameters of the filaments(d_f) and the distance between the filaments($l_{m,i}$) . Because each filament is part of two meshes, half of the volume and half of the wetted surface area are taken into account for the derivation. Each mesh consists of four filament sides. Da Costa et al. (Da Costa et al., 1994) developed this formula for spacer volume:

$$V_s = 2 \cdot \frac{1}{2} \cdot \left(\frac{1}{2} \cdot \pi \cdot d_{f,1}^2 \cdot l_{m,1}\right) + 2 \cdot \frac{1}{2} \cdot \left(\frac{1}{2} \cdot \pi \cdot d_{f,2}^2 \cdot l_{m,2}\right) = \frac{1}{4}\left(d_{f,1}^2 \cdot l_{m,1} + d_{f,2}^2 \cdot l_{m,2}\right) \quad (71)$$

The total wetted surface($A_{w,t}$) is the surface that will be wetted by both the flat flow channel ($A_{w,fc}$) and the spacer ($A_{w,s}$) (Schock & Miquel, 1987) (see Equation 72).

$$A_{w,t} = A_{w,fc} + A_{w,s} \quad (72)$$

The wetted surface area of the channel is expressed by Da Costa et al. (1994) and considers the area taken by a single mesh at the top and at the bottom of the spacer (see Equation 73). This area is indicated in blue in Figure 44.

$$A_{w,t} = 2 \cdot l_{m,1} \cdot l_{m,2} \cdot sin\theta \quad (73)$$

Thee wetted spacer surface area depends again on the dimensions of the filaments: half the perimeter and the length of each filament. This equation was also presented by Da Costa et al. (1994):

$$A_{w,s} = 2 \cdot \frac{1}{2} \cdot \left(\pi \cdot d_{f,1} \cdot l_{m,1}\right) + 2 \cdot \frac{1}{2} \cdot \left(\pi \cdot d_{f,2} \cdot l_{m,2}\right) = \pi\left(d_{f,1} \cdot l_{m,1} + d_{f,2} \cdot l_{m,2}\right) \quad (74)$$

Based on Figure 45, the dimensions of the spacers used in the membrane distillation setup can be determined, resulting in the dimensions in Table 6.

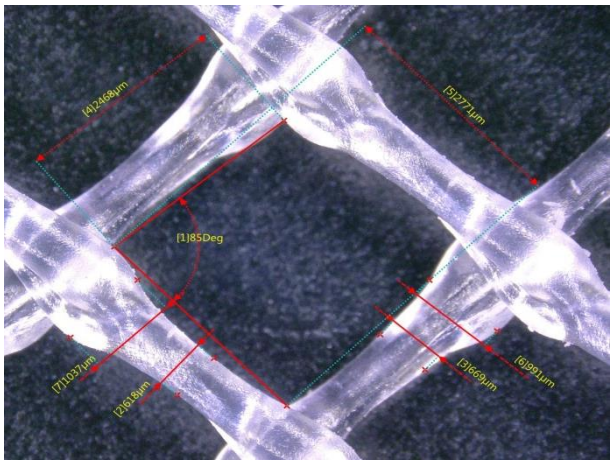

Figure 45 Measurements spacer dimensions done with optical microscope.

Table 6 Spacer dimension measured

Filament diameter ($d_{f,1}$) [m]	8.28E-04
Filament diameter ($d_{f,2}$) [m]	8.30E-04
Distance between filaments ($l_{m,1}$) [m]	2.77E-03
Distance between filaments ($l_{m,2}$) [m]	2.47E-03
The angle between filaments (θ) [°]	1.48
Spacer thickness (h_{sp}) [m]	1.60E-03
Channel height (h_c) [m]	2.30E-03
Channel width (w_c) [m]	3.92E-02

Based on these dimensions and the equations described above, the hydraulic diameter was calculated to be $1.9 \cdot 10^{-3}$ m.

Appendix B Difference vapour pressure ammonia and water compared to the concentration

To be able to say something about whether the change in flux is due to the K_{ov} or the change in vapour pressure, the relative change in vapour pressure compared to concentration was calculated, with Equation 75.

$$b = \frac{\frac{p_{amm}}{p_w}}{m\%NH_{3_{feed}}} \tag{75}$$

As seen in Table 7, the relative vapour pressure of ammonia increases relatively slower than water, leading to water being more dominant at high ammonia concentrations than expected. This will lead to a lower selectivity of ammonia at lower concentrations than at high concentrations. This decrease is, however, lower for ammonia bicarbonate than for ammonium hydroxide.

Table 7 Table with the result from the calculation on the difference vapour pressure ammonia and water compared to concentration

Solution	Mass percentage Ammonia Feed[%]	Percentage vapour pressure ammonia [%]	Relation between the two (b) [-]
AmmH 1.5	0.15	3.81	25
AmmH 12	1.20	24.45	20
AmmH 20	2.00	35.24	18
AmmBi 1.5	0.15	3.56	24
AmmBi 12	1.20	25.14	21
AmmBi 20	2.00	39.94	20

Appendix C Mass balance acid trap

To test of the method of calculating whether the amount of ammonia in the feed and the condensed water is correct, and then to test if the acid trap was able to catch all the ammonia, a mass balance was made over some runs. The mass balance consisted of the ammonia in the feed, the ammonia in the condensed water and the ammonia in the acid trap, see Equation 76.

$$Mass_{amm,t} = Mass_{amm,cond,t} + Mass_{amm,acid,t} \quad (76)$$

For how to calculate mass ammonia feed see Section 3.4.1, and for how to calculate mass ammonia condensed, see Section 3.4.2. The mass of ammonia in the acid is calculated with the change in concentration of the acid trap and the change in volume (see Equation 77).

$$Mass_{amm,acid,t} = C_{amm,i}V_{acid,i} - C_{amm,t}V_{acid,t} \quad (77)$$

The end volume was found by taking the initial volume plus the change in mass in the acid trap divided by the density of the acid solution (ρ_{acid}), giving Equation 78.

$$V_{acid,t} = V_{acid,i} + \frac{\Delta mass_{acid,T}}{\rho_{acid}} \quad (78)$$

The deviation in the mass balance could then be calculated:

$$\%\Delta MB = \frac{Mass_{amm,t} - Mass_{amm,acid,t} - Mass_{amm,cond,t}}{Mass_{amm,t}} * 100 \quad (79)$$

The result from those calculations can be found in Table 8:

Table 8 Result mass balance of condensation experiments

Run	%ΔMB [%]
1	0.748272
2	16.05169
3	-4.59146
4	38.18166
5	-3.40575
6	0.094719
7	8.160041

Appendix D Energy balance calculations for Ammonium hydroxide 1.5 gTAN·L^{-1}.

To illustrate the different calculations for the energy balance, a sample calculation for an ammonium hydroxide 1.5 gTAN·L^{-1} solution was made.

D.1 Given data

First, the different data needed from the different experiments were collected, see Table 9.

Table 9 Data needed for the energy calculations gathered during the other experiments

	Laminar	Turbulent
Total flux [kg·m^{-2}·h]	9.89	10.42
Ammonia flux [kg·m^{-2}·h]	0.08	0.10
M%ammonia [%]	0.79	1.07
Flow [l·h^{-1}]	10	25
Head loss membrane [m]	0.76	1.58

D.2 Thermal energy

The thermal energy consists of three components. The energy needed for evaporation, the energy recovered with condensation, and the energy produced with the SOFC.

D.2.1 SOFC thermal energy produced

First, the thermal energy produced in the SOFC needs to be calculated. In Section 1.2.3 the theoretical energy per mole of ammonia is calculated (MJ·kg-N^{-1}):

$$\Delta H_{f\ T}^{\theta} = \frac{(2*46.11-2*285.78)}{2} = 239.72 \tag{80}$$

This means that given that the molar weight of ammonia (M_{amm}) is 17 g·mol^{-1} the total energy per kilogram ammonia is (MJ·kg-N^{-1}):

$$SOFC_T = \frac{\Delta H_{f\ T}^{\theta}}{M_{amm}} = 14 \tag{81}$$

In Section 1.2.3 it is also stated that 30% can be converted into thermal energy. This gives:

$$SOFC_{Th} = SOFC_T \cdot 30\% = 4.2 \tag{82}$$

This is independent of the feed concentration of the solution put into the SOFC, and is therefore assumed to be for all solutions the same.

D.2.2 Heat loss membrane

The main loss of thermal energy in the system is in the evaporation of gases at the membrane surface, as explained in Section 2.3.3. There also the formula to calculate this loss is given in Equation 29.

$$\mathrm{Q_E} = \sum_{i=1}^{n} J_i H_{v,i} \tag{29}$$

For the ammonia solution given that $H_{v,amm}$ is 1369 kJ·g^{-1} and $H_{v,w}$ is 2255 kJ·g^{-1} the thermal energy lost is (MJ·kg-N^{-1})

$$Q_{E,t} = \frac{J_{amm}H_{v,amm} + J_w H_{v,w}}{m\%NH_{3_{permeate}}} = 219 \quad (83)$$

$$Q_{E,l} = \frac{J_{amm}H_{v,amm} + J_w H_{v,w}}{m\%NH_{3_{permeate}}} = 283 \quad (84)$$

The thermal energy needed for evaporation per kilogram ammonia is clearly higher for a laminar flow than for a turbulent flow. This is due to a higher mass percentage of ammonia in the permeate.

D.2.3 Heat recovery condensation

Some of the energy lost by evaporation can be recovered if some of the energy is condensed. The energy recovered with condensation is given by (see Section 2.4.1) as Equation 44:

$$Q_C = \sum_{i=1}^{n} \frac{mass_{cond,i}}{\Delta t} H_{v,i} \quad (44)$$

This gives:

$$Q_C = \frac{mass_{cond,amm}}{\Delta t} H_{v,amm} + \frac{mass_{cond,w}}{\Delta t} H_{v,w} \quad (85)$$

On how to calculate $mass_{cond,amm}$ and $mass_{cond,w}$ see Section 3.4.2. The total energy gain with condensation is then 8.8 MJ·kg-N^{-1} for turbulent flow and 11.5 MJ·kg-N^{-1} for laminar flow.

D.2.4 Total thermal energy

Using the calculations above and the formula is given in Section 3.4.3:

$$EB_T = SOFC_{Th} - Q_E + Q_C \quad (62)$$

The total energy difference between produced thermal energy and used thermal energy is -206.3 MJ·kg-N^{-1} and -270.6 MJ·kg-N^{-1} for turbulent t and laminar flow respectively. This shows that turbulent flow uses less energy than laminar flow, but that both turbulent and laminar flow with a solution of ammonium hydroxide 1.5 gTAN·L^{-1} is not energy beneficial in terms of thermal energy.

D.3 Electrical energy

D.3.1 SOFC Electrical energy

The electrical energy consists of three components, the energy needed for the feed pump, the energy needed for the vacuum pump, and the energy produced with the SOFC.

In Section 1.2.3 the total energy from the SOFC is given, and it is stated that 60% can be converted into electrical energy. This gives as shown in Equation 86 an electrical energy produced of 8.4 MJ·kg-N^{-1} as seen in Equation 86.

$$SOFC_E = SOFC_T \cdot 30\% = 8.4 \quad (86)$$

This is independent of the quality of the feed solution used in the SOFC and is therefore, for all solutions assumed to be the same.

D.3.2 Feed pump

The formula to calculate the theoretical energy of the feed pump is given in Section 3.4.3 in Equation 67:

$$E_r = \rho_{feed} \cdot Q_{feed} \cdot g \cdot \Delta H_{membrane} \quad (67)$$

The change in head ($\Delta H_{membrane}$) was measured with the help of a digital pressure sensor, and the maximum head difference measured was used. This gave the energy needed as 5 MJ·kg-N^{-1} for the ammonium hydroxide with turbulent flow and 1.35MJ·kg-N^{-1} for laminar flow.

D.3.3 Vacuum pump

This section is based on information from Niels van Linden.

In full-scale vacuum stripping of CH_4 in a drinking water plant of Vitens (Spannenburg) full-scale vacuum pumps are used that are pumping (Q) 63.7 $m^3 \cdot h^{-1}$ of gas at a pressure difference of 1.07 bar. The current of the pump is 15.5 A and the voltage 338 V, giving the pump a power of (W):

$$P = I \cdot V = 5239 \quad (87)$$

Given a gas density of 1 kg·m^{-3} the energy per ammonia is:

$$E_p = \frac{P}{Q \cdot m\%NH_3} \quad (88)$$

Given an energy use of 26.91 MJ·kg-N^{-1} and 35.10 MJ·kg-N^{-1} for the turbulent and laminar flow for ammonium hydroxide with 1.5 gTAN·L^{-1}.

D.3.4 Total electrical energy

Using the calculations above and the formula is given in Section 3.4.3:

$$EB_E = SOFC_E - \mathrm{E}_r - \mathrm{E}_{va} \quad (66)$$

The total energy difference between produced and consumed electrical energy is -23.6 MJ·kg-N^{-1} and -28.0 MJ·kg-N^{-1} for a turbulent and laminar flow respectively. This shows that turbulent flow uses less energy than laminar flow, but that both turbulent and laminar flow with a solution of ammonium hydroxide 1.5 gTAN·L^{-1} is not energy beneficial in terms of electrical energy.

Appendix E Vacuum stripping of industrial ammonia-rich wastewater

The membrane vacuum stripping showed discouraging results with the industrial ammonia-rich wastewater from amide production, therefore, vacuum stripping without a membrane was tested as well. Below the methods of the experiment are presented together with the results, discussion, and the conclusion about the test with vacuum stripping.

E.1 Methods

A very simple experiment was conducted to test the vacuum stripping.

E.1.1 Set up

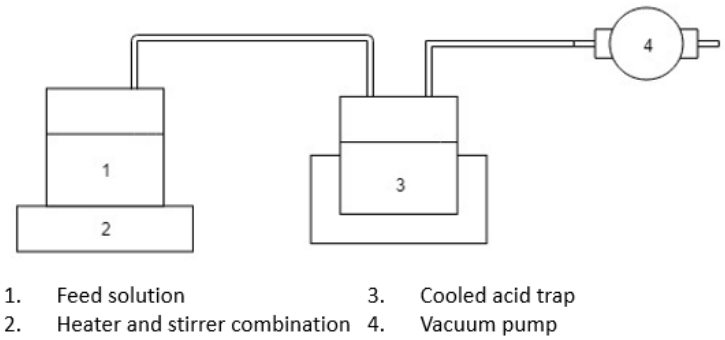

Figure 46 Overview set-up vacuum stripping

The setup consisted of a big feed flask and a heater-stirrer combination. The feed flask was made a vacuum tight with a cork and connected to the cooled acid trap to collect the gas and then again to the vacuum pump.

E.1.2 Experimental procedure and conditions

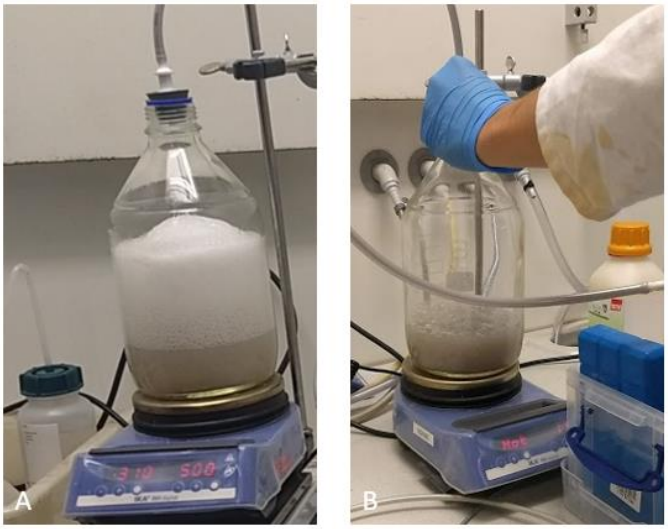

Figure 47 Before(A) and after(B) addition of anti-foaming agent. The foam in picture A would rise even higher and end up in the acid trap if the system was not shut down in time.

First, the feed solution of ammonium hydroxide 1.5 gTAN·L^{-1} was prepared as explained in Section 3.2.2, under unfiltered the industrial ammonia-rich wastewater, next to this one mL of anti-foming agent was added to prevent problems with foaming (see Figure 47). Then the initial samples were

taken before the vacuum pump was turned on for 1.5-3 minutes. Then the vacuum pump was turned off and another measurement was taken, this was repeated five times. This was repeated twice with fresh solution.

E.1.3 Measurements

Before each run, the total weight of the feed flask was measured with a balance and the concentration of ammonia in the bottle (see Section 3.2.3). This was also repeated after each run.

E.1.4 Data processing

Flux total

The total flux is the change of the mass in the flask ($\Delta mass_{flask}$) over the time between each measurement (Δt) times the surface area of the liquid-gas interphase in the feed flask (A_{flask}):

$$J_T = \frac{\Delta mass_{flask}}{\Delta t} \cdot A_{flask} \tag{88}$$

Flux ammonia

The flux of ammonia is the change of ammonia mass over time, times the surface area of the liquid-gas interphase in the feed flask:

$$J_{amm} = \frac{\Delta mass_{amm}}{\Delta t} \cdot A_{flask} \tag{89}$$

To calculate the flux of ammonia it is needed to know the ammonia mass ($mass_{amm,t}$). This is done by taking the concentration of ammonia ($C_{amm,t}$) and the volume of the feed solution ($V_{feed,t}$) at a certain time:

$$mass_{amm,t} = C_{amm,t} \cdot V_{feed\ ,t} \tag{90}$$

The volume of the feed solution is calculated with the help of the initial volume of the feed ($V_{feed,s}$), the mass change in the feed bottle and the density of the feed (ρ_{feed}):

$$V_{feed,t} = V_{feed,i} - \frac{\Delta mass_{flask}}{\rho_{feed}} \tag{91}$$

E.2 Results

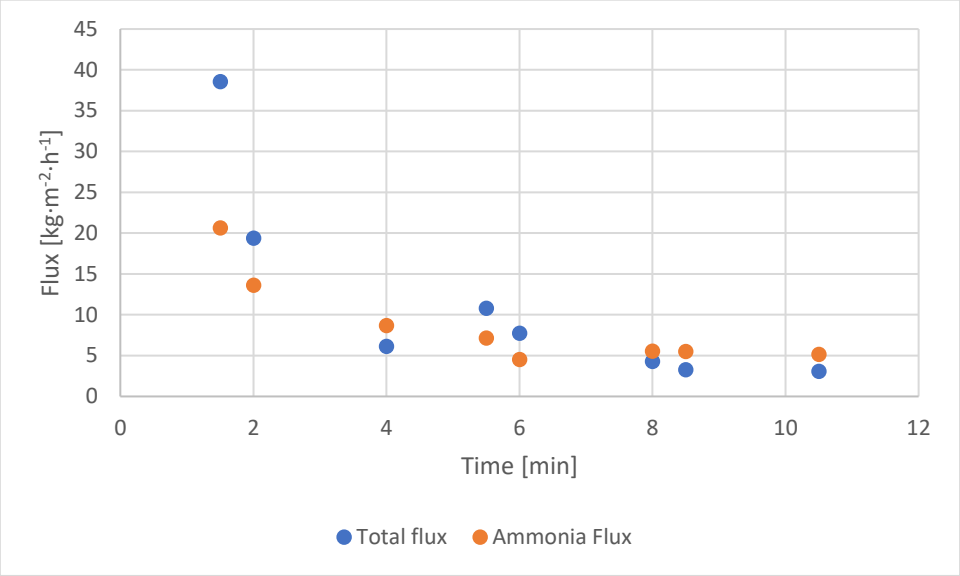

Figure 48 Total flux and ammonia flux over time during the vacuum membrane stripping experiments

As seen in Figure 48, the total flux and the ammonia flux are comparable. However, at some point, the ammonia flux is higher than the total flux. This is not physically possible and indicates a measurement error of some kind.

E.3 Discussion

As mentioned in Appendix section E.2 there is a discrepancy between ammonia flux and total flux, with the ammonia flux being bigger than the total flux, which is physically impossible. This can be due to different reasons.

Firstly, a random error in the measurements can contribute to the discrepancy in the results. Especially the concentration kit showed some differences when the test was repeated. Moreover, if the values of total flux and ammonia flux are close, the ammonia flux may seem higher due to errors in the measured concentration.

Also, the measurement was done in the top layer of the feed. If the stirring was not good enough this concentration could be lower than the average concentration in the flask. This would lead to the calculated ammonia flux being higher than the real flux.

Leaving out the membrane eliminated the possibility of it fouling. However, there were still problems with the accumulation of foam, see Figure 49. This was however solved quite easily by adding 1 mL of anti-foaming agent. It is not clear if this foaming agent affected the result, besides reducing the foaming of the solution.

E.4 Conclusion

Even though there are clearly some errors in the measurement, it still indicates that high total flux and ammonia flux can be reached with vacuum stripping. Moreover, leaving out the membrane eliminated the possibility of fouling. Therefore, it would be interesting to look at vacuum stripping as a possible alternative for a solution with a presence of amphiphile or hydrophobic organics that can interact with the hydrophobic membrane of the VMS.